CO-DEFORMATION AND BONDING OF MULTI-COMPONENT BILLETS WITH APPLICATION TO Nb-Sn BASE SUPERCONDUCTOR PROCESSING

DISSERTATION

Presented in Partial Fulfillment of the Requirements for

The Degree Doctor of Philosophy in the Graduate

School of The Ohio State University

By

Xuan Peng

*****

The Ohio State University
2005

Dissertation Committee:	Approved by:
Professor Mike Sumption, Advisor	________________________
	Advisor
Professor Robert Wagoner, Advisor	Department of Materials Science and Engineering
Professor Katharine Flores	________________________
	Advisor
Professor Glenn Daehn	Department of Materials Science and Engineering

ABSTRACT

The standard procedure of the fabrication of low temperature superconductor precursors is the co-extrusion of composite materials and then co-drawing. These composites usually exhibit poor ductility and may not be readily formed into final small size, which limit the piece-length of commercialized superconductor wires. Defects including wire breakage and poor bonding between core and sleeve as well as between the individual filaments are the main problems for the manufacture. Hence, understanding the influence of the processing parameters on the co-extrusion and co-drawing of this kind of composite strands is an important subject. This project is focused on the bonding issues relating to the co-extrusion and co-drawing of this composite wires. The objective is to get a better understanding of interfacial bonding during the co-extrusion and co-drawing of the composites including the distributions of deformation, stress and temperature, and the generation process of interfacial bonding under different conditions which will be helpful for the parameter selection of the manufacture. Due to the high cost and limitation of empirical trial-and-error approaches, Finite Element Method (FEM) was used to simulate the co-deformation process to investigate the effects of die angle, area reduction, the core ratio and the variation of bonding between components on the deformed geometry, stress distribution in the product, and then

combine the FEM simulation with a Pressure Bonding Model to study the generation process of interfacial bonding between components during the drawing process. Co-drawing of differently assembled billets will be performed to verify the simulation results. Additionally, SEM, EDS and TEM observations and mechanical testing will be conducted to investigate the generated inter-component bonding after co-deformation. As a result, the relationship between drawing parameters and the generated inter-component bonding strength will be determined. Using the micrographic observation, the bonding mechanism during the co-drawing process has been proposed.

DEDICATE TO MY BELOVED FAMILY

ACKNOWLEDGMENTS

My time at The Ohio State University has been valuable and full of fun. I am sincerely grateful to a large number of people who have helped me throughout my study, research and daily life.

First of all, I would like to express my sincere appreciation to Prof. Sumption, Prof. Collings and Prof. Wagoner for their guidance, instruction through my thesis work and my related research. I have learned much from them in both technical and non-technical aspects of life.

I would also like to thank my family for supporting me to a higher education. My parents and my brother are always encouraging me. I owe great appreciation to my husband, Xiangnan Wang, who is always behind me and support me. His patience, understanding, encouragement and love helped me go through every obstacle and make my life here enjoyable and productive.

I owe thanks to Mr. Mike Tomsic for introducing me to Hyper Tech Research Inc. and giving me the chance to do experiments there. Thanks John Philips and Kevin F for helping me do the drawing experiments.

I would like to thank the cooperation, friendship from all the labmates in LASM.

Finally, I want to thank the support of staff members in Material Science Department. Lloyd Barnhart has been very helpful for mechanical tests. Henk Colijn and Cameron Begg taught me how to operate the SEM, FIB and TEM machines. Their assistance is very much appreciated.

VITA

August 4, 1971. . . . . .Born – Shuangfeng, Hunan, China

1992. . . . . B.S in Metal Forming
Northeastern University, Shenyang, China

1997. . . . . M.S in Metal Forming
University of Science and Technology Beijing, China

2002. . . . . M.S. in Materials Science and Engineering
The Ohio State University

1999 – Present. . . . . .Graduate Research Assistant
The Ohio State University.

PUBLICATIONS

Research Publications

1. Sumption, M.D., Peng, X., *et al.*, *Fabrication and Phase-transformation Issues in CTFF-MA Processed A15 Superconductor*, *Adv. Cryo. Eng.* 48B, 1057-1064 (2002).
2. Peng, X., Sumption, M. D. *et al*, *FEM study of hydrostatic extrusion and bonding of superconductor precursors*, *IEEE Trans. Appl. Supercond.* 13, 3434-3437 (2003).
3. Sumption, M.D., Peng, X., *et al.*, *Fabrication and properties of PIT Nb-Al and Nb-Sn based superconductors*, *IEEE Trans. Appl. Supercond.* 13, 3486 -3489 (2003).
4. Peng, X., Sumption, M. D. *et al*, *Finite Element Analysis of Extrusion of Multifilamentary Superconductor Precursor*, *Adv. Cryo. Eng.*, 50B, 425-432 (2004).
5. Sumption, M. D., Peng, X., *et al, Magnetization and deff in HEP Relevant RIT Type Nb3Sn Strands-Influence of Internal Barriers*, *Adv. Cryo. Eng.*, 50B, 836-843 (2004).

6. Sumption, M.D., Peng, X., *et al*., *Analysis of magnetization, AC loss, and deff for various internal-Sn based Nb3Sn multifilamentary strands with and without subelement splitting,* Cryogenics, 44(10), 711-725 (2004).
7. Peng, X., Sumption, M. D. *et al*,, *Finite Element Analysis of Drawing of Multifilamentary Wires*, to be published in *IEEE Trans. Appl. Supercond*
8. Peng, X., Sumption, M. D. *et al*,, *Microstructural Investigation of Internal-Tin Nb_3Sn Strands*, to be published in *IEEE Trans. Appl. Supercond*
9. Peng, X., Sumption, M. D. *et al*,, *Magnetization and d_{eff} in Multifilamentary Nb_3Sn Strands*, to be published in *IEEE Trans. Appl. Supercond*
10. Wu, X., Peng, X., et al, Ti and Sn Diffusion and Its Influence on Phase Formation in Internal –Tin Nb_3Sn Superconductor Strands, to be published in *IEEE Trans. Appl. Supercond*

FIELDS OF STUDY

Major Field: Materials Science and Engineering

TABLE OF CONTENTS

Page

Abstract. ii

Dedication. iv

Acknowledgments v

Vita vii

List of Tables. xi

List of Figures xii

LIST OF TABLES

Table Page

#.# Type title here . . . . ##

#.# Type title here . . . . ##

#.# Type title here . . . . ##

#.# Type title here . . . . ##

LIST OF FIGURES

Figure Page

#.# Type title here . . . . ##

#.# Type title here . . . . ##

#.# Type title here . . . . ##

#.# Type title here . . . . ##

LIST OF ABBREVIATIONS (IF NECESSARY)

α	alpha
$[\alpha]$	specific rotation
Ac	acetyl
br	broad (IR and NMR)
β	beta
n-Bu	*normal*-butyl
t-Bu	*tert*-butyl
Bz	benzoyl
°C	degrees Celsius
calcd	calculated
CSA	(1*S*)-(+)-10-camphorsulfonic acid
δ	chemical shift in parts per million downfield from tetramethylsilane
d	doublet (spectra); day(s)
DBU	1,8-diazabicyclo[5.4.0]undec-7-ene
DDQ	2,3-dichloro-5,6-dicyano-1,4-benzoquinone
DMAP	4-(*N*,*N*-dimethylamino)pyridine
DMF	*N,N*-dimethylformamide

DMSO	dimethylsulfoxide
eq.	equivalent
Et	ethyl
γ	gamma
g	gram(s)
h	hour(s)
IR	infrared
J	coupling constant in Hz (NMR)
k	kilo
KHMDS	potassium hexamethyldisilazide
L	liter(s)
LDA	lithium diisopropylamide
m	milli; multiplet (NMR)
μ	micro
M	moles per liter
Mc	chloromethylsulfonyl
Me	methyl
MHz	megahertz
min	minute(s)
mol	mole(s)
Ms	methanesulfonyl
MS	mass spectrometry; molecular sieves
m/z	mass to charge ratio (MS)

NaHMDS	sodium hexamethyldisilazide
NMO	4-methylmorpholine *N*-oxide
NMR	nuclear magnetic reasonance
p	para
Ph	phenyl
PMB	*p*-methoxybenzyl
PMP	*p*-methoxyphenyl
ppm	parts per million
py	pyridine
q	quartet (NMR)
rt	room temperature
s	singlet (NMR); second(s)
t	tertiary (tert)
t	triplet (NMR)
TBAF	tetrabutylammonium fluoride
TBAI	tetrabutylammonium iodide
TBS	*t*-butyldimethylsilyl
TES	triethylsilyl
Tf	trifluoromethanesulfonyl
THF	tetrahydrofuran
TLC	thin layer chromatography
TMS	trimethylsilyl

CHAPTER 1

1. INTRODUCTION

High temperature superconductors such as YBCO and BSSCO, as well as the recently discovered MgB_2, are the focus of wide study. Nevertheless, the low temperature superconductors remain the conductors of choice for all practical devices and the only ones made on a truly commercial basis. Of these, Nb_3Sn has the best high field performance. Research aim at improving their superconducting properties and manufacturing methods is ongoing. All practical low temperature superconductors are made, from a deformation and metallurgical point of view, with many similarities irrespective of whether the finished product is to be a mono-core precursor or a multi-core precursor. Typically, the mono-core precursor is fabricated through extrusion and subsequent drawing, and then re-stacked in preparation for a multi-core billet. The multi-core billet is then deformed to final size by extrusion and wire drawing. The various properties of the component materials, each having its own distinct mechanical characteristics, increase the difficulty of extruding and drawing the wire to the desired small diameters. Especially for the wire made through internal-Sn method, the internal Sn hinders the application of extrusion in the final deformation. The drawing of such a complicated multifilamentary wire intrigues big challenges for the manufacture. Fracture

is easy to occur which may be due to the non-homogeneous properties of each component during the forming process. Poor bonding between core and sleeve as well as between the individual filaments is another problem which is often encountered during manufacture. The adhesion of the filament-matrix interface is important during subsequent deformation. So far, a common feeling in the manufacture is that the bonding is critical for the drawing. A good bonding created may ensure a successful bonding in the next drawing. These problems relating to drawing are “intrinsic” to the processing route, and are typically addressed by carefully controlling a limited number of process related parameters. Hence, understanding the influence of the processing parameters on the co-extrusion and co-drawing of this kind of composite strands is an important subject. In fact, the study of the co-extrusion and co-drawing conditions which will enable proper plastic deformations of metallic composites to take place has interested many investigators [1, 2]. Alexander [3], Osakada [4] and Avitzur [5] conducted pioneering experiments on the hydrostatic extrusion of bi-metallic rods and proposed analytical models to predict the extrusion pressure and deformation patterns in the billets. Avitzur [6], Wu and Hsu [7] built analytical models for the conventional extrusion of three-layer composite rods. Lesik, Dyja [8], and Ragab [9] conducted drawing experiments on the bi-metallic rods, Muskaiski and Pilarczyk [10] built the finite element model for the co-drawing of bi-metallic materials. However, for the most part, little attention has been paid to the generation of bonding between the various components during the co-extrusion and co-drawing. Furthermore, most of these models were based on the upper-bound theorem which prevents initial interfacial condition from being included in the model and the final interfacial mechanics such as normal and shear stress at the interface could not be

evaluated. However, the level of bonding generated during co-extrusion and co-drawing is critical to the subsequent extrusion and drawing of the wire. Lugosi *et al* [11] showed through their experiments that the interfacial bond strength affected the deformation mode of billet, with weak bonds leading to earlier failures in the extrusion.

Based on the condition of superconductor manufacture, this project is focused on bonding issue relating to co-extrusion and co-drawing process. Experimental investigation on the real extrusion billet has been performed to confirm that perfect bonding could be obtained through proper extrusion. Then much work is focused on the co-drawing process. The objective of this project is to get an understanding of the generation process of interfacial bonding during drawing process, to identify the bonding mechanism and investigate the effect of bonding on the later co-deformation. Due to the high cost and limitation of empirical trial-and-error approaches, Finite Element Method (FEM) was used to simulate the co-deformation process to investigate the effects of die angle, area reduction, the core ratio and the variation of bonding between components on the deformed geometry, stress distribution in the product and the details in the interface, and then combine the FEM simulation with a modified pressure bonding model to study the generation process of interfacial bonding between components.

Co-drawing of differently assembled billets has been performed to verify the simulation results. Additionally, SEM, EDS and TEM observations and mechanical testing has been conducted to investigate the generated inter-component bonding after co-extrusion and co-drawing. As a result, the effect of drawing parameters on the generation of inter-component bonding strength and the influence of the interfacial bonding on the drawing conditions has been determined.

Chapter 2

2. Background Review

Future high field magnets stimulate the development of superconductors with good properties in the ever-increasing magnetic field (> 8 T). Until now, the High Energy Physics (HEP) superconductor has been Nb–Ti due to its reproducible critical current densities (J_c) in long lengths and its high ductility. Most of the commercial Nb–Ti wires were optimized for high J_c in the fields of 5 to 7 T at 4.2 K. However, if the field is up to 10 T even high, Nb-Ti conductors will not have the ability to carry current anymore and Nb–Ti was at its J_c limit and future higher field magnets would require superconductors with better high field properties. Presently, the best choice for this kind of superconductor is Nb_3Sn. Although Nb_3Sn has high strain sensitivity, and is brittle and difficult to handle, it has a higher upper critical field (H_{c2}) and critical temperature (T_c). Recently, Oxford Superconductor Technology (OST) reported that their Rod-In-Tube (RIT) type wires with Nb-7.5% Ta filaments and an unalloyed Sn source provided 12 tesla J_cs of 2800-3000A/mm^2 at 4.2K [12].Different designs of Nb_3Sn precursor strands have been developed to improve their fabricability and magnetic properties. Presently, three methods are primarily applied in the manufacture of Nb_3Sn wire: bronze, powder-in-tube (PIT) and internal-Sn methods. Each method has its own characteristics, but they face the

same challenge, which is how to improve the superconductivity properties while keeping long piece-length and low cost. Fracture is always a problem for the fabrication of complicated Nb_3Sn precursors that limits the piece-length of conductor. Poor bonding and the difference of the components are the main reasons which result in this fracture. Hence, understanding the bonding mechanism and the bonding generation during the co-deformation process, and the effect of bonding on the co-deformation process is the main goal of this project.

As a background review chapter, the fabrication methods of the Nb_3Sn superconductor precursors will be briefly introduced at the beginning of this chapter, and then literatures on the co-deformation and co-bonding process during co-extrusion and co-drawing will be reviewed. Then the goal of this project and the format of this document will be listed out.

2.1 Fabrication of Nb_3Sn superconductor precursors

2.1.1 Fabrication Methods

Nb_3Sn is a Type II superconductor that has the brittle A15 crystal structure, which indicates that this kind of conductor wire could not be deformed in the form of Nb_3Sn. As mentioned in the above, bronze, powder-in-tube (PIT) and internal Sn methods are the primarily used fabrication methods in the manufacture of Nb_3Sn wires. The common characteristic of these three methods is that Nb-Sn precursors are made at first, and then heat-treated to form Nb_3Sn which has superconductivity properties. These three methods

differ in their Sn sources, thereby differ in the properties of produced wires. Generally internal-Sn and PIT methods have produced wires with much higher J_c values than those by bronze method. The reason is that there is a larger fraction of non-Cu area (means high ratio of Nb and Sn) in PIT and Internal-Sn strands than that occurring in bronze wires, and thus more A15 phase formed after reaction. The following figures gave the schematic composition of the three methods.

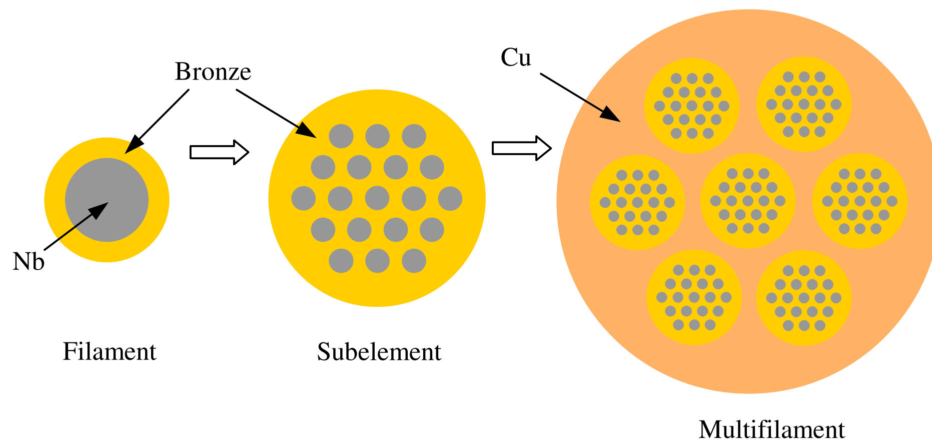

Figure 2.1 Schematic drawing of bronze process

Bronze method is the earlier used one. As shown in Figure 2.1, in the bronze process, Nb rod is inserted into a bronze tube firstly to form filament, then drawn to certain size for restacking to form a sublement wire, and then restacked to form the final multifilamentary composite wire, and the composite rod is extruded and drawn down to final size wire. Then the wire is heat treated to form Nb_3Sn. In this process, bronze work-hardens so quickly that the wires must be annealed after every few drawing passes. This excessive annealing makes the process labor-intensive, and may cause brittle phase Nb_3Sn formation which hinders further wire deformation. The Sn is from the bronze matrix directly, and the maximum available amount of Sn is limited by the maximum solubility of Sn in bronze. Now bronze with the maximum Sn of 8.6% in atomic percentage has been used to manufacture the Nb_3Sn conductor. The published best wires have J_c (4.2 K, 12 T) of 980 A/mm^2 [13].

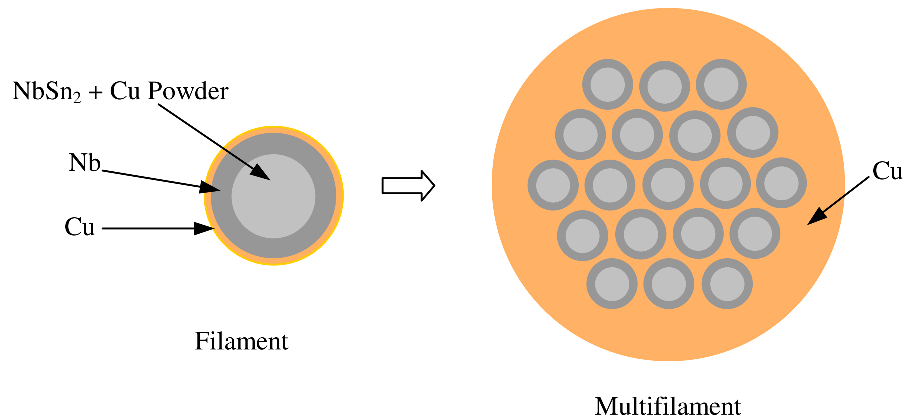

Figure 2.2 Schematic drawing of Power-In-Tube (PIT) process

Powder-in-tube (PIT) process has gained much attention in recent years. In this process, Nb tube assembled in a Cu tube is filled with various powders ($NbSn_2$, Nb_6Sn_5, Sn, Cu), and then drawn down to certain size for restacking (Figure 2.2). The restacked wire is then extruded or drawn down to the final size, and then heat-treated to form Nb_3Sn. In this process, it allows to choose powder constituents and their relative proportions freely.

Also, diffusion reaction of the wire at 675-700 °C for about 48h results in the formation of Nb_3Sn [14]. The shorter heat-treatment time saves the time and cost. The drawback of this method is that Nb tubes and special powders are expensive, making the cost greater than the other processing routes. So far, the reported best PIT wires have a J_c(4.2 K, 12 T) of about 2200 A/mm^2 [15].

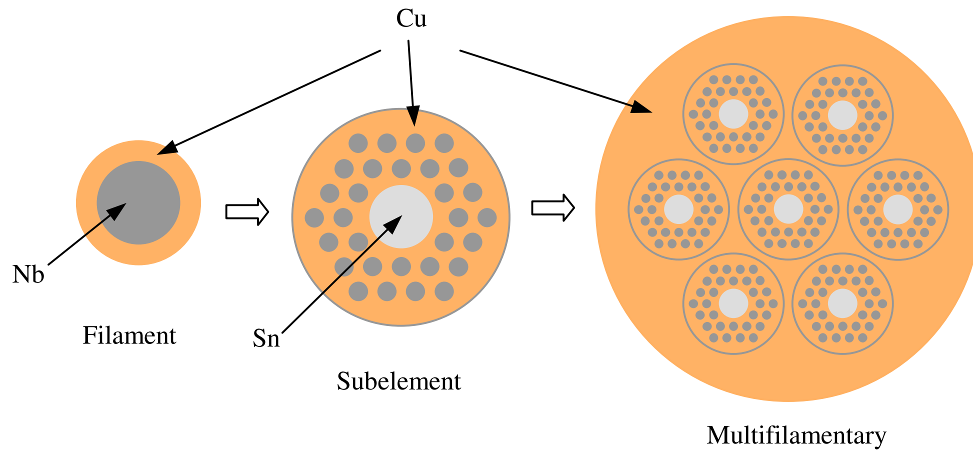

Figure 2.3 Schematic drawing of Internal-Sn process

Presently, the most common fabrication method for high J_c conductors is the internal-Sn process as shown in Figure 2.3. Typical commercial multifilamentary internal-Sn type Nb_3Sn precursor strands start with an assembly of Nb rods each jacketed with a Cu tube, individually drawn down to final size ready for restacking. These rods are then stacked to form a subelement billet, which is extruded to a suitable size for gun drilling. The third step is to gun drill the billet with a center hole and insert a Sn core into it. Finally, these subelements are restacked into a Cu can or a Cu can with an Nb barrier inside, and cold-drawn to finished size. In order to improve the strand's final properties, B_{c2} and J_c, some innovative approaches have been used including alloying the Nb with Ta, alloying the Sn with Cu, and dispersing NbTi alloy filaments in the subelements as a Ti source[16, 17]. Oxford Superconductor Technology (OST) reported that their wires with Nb-7.5% Ta filaments and an unalloyed Sn source provided 12 tesla J_cs of 2800-3000A/mm^2 at 4.2K [12]. In this approach, since the "internal tin" is added after extrusion but before the assembly of the subelement restack, the restacked multifilaments must be cold drawn instead of extruded to avoid the melting of Sn. This brings more challenges for the manufacturer due to the basic difference between drawing and extrusion processes. The internal-Sn process is advantageous comparing to the bronze process because it allows wire drawn to final size without intermediate anneals which saves time and labor. Also, the content of Nb and Sn is generally much higher, increasing the A15 cross-sectional area and thus raising $J_{c,non\text{-}Cu}$. The main advantage of internal-Sn over PIT is that the basic components are much cheaper, helping to keep the cost down. In this document, the focus is on the fabrication issues on making wires by internal-Sn method.

2.1.2 Fabrication Challenges

In recent years, significant efforts have been made in the development of high performance Nb_3Sn wires with smaller filament diameters. The High Energy Physics Division of the U.S. Department of Energy (DOE) initiated a national Nb_3Sn conductor development program aiming at developing strands with non-Cu J_c (4.2K, 12T) of 3000 A/mm^2 accompanied by an effective filament diameter (d_{eff}) of 40 μm or less [18]. In order to reach this objective, the direct way is to make multifilamentary wires with higher count number. However, the fracture during drawing and extrusion hinders the fabrication of such wires. Until now, it is believed that the big difference between the components in mechanical deformation properties, and the poor bonding between the components are the main reasons leading to the occurrence of fracture. In the Nb-Sn composite wire, the main components are Nb or Nb7.5%Ta, Cu, Sn. In fact, the co-drawing and co-extrusion processes are not only co-deformation processes but also bonding generation processes for the wires. Hence, to understand the mechanical properties of these components, the bonding mechanism and the effect of deformation parameters on the bonding generation are of great importance for improving the fabricability of this kind of composite wires.

2.1.3 Summary

Nb_3Sn wire has now become the best choice for high field magnets due to its good high field properties. Bronze, PIT and internal-Sn process are the mainly applied methods to fabricate the Nb3Sn precursor wires, and they have their own characteristics. Bronze is the earlier used one, and the bronze wire has good ductility, but the limited source of Sn hinders the improvement of J_c. PIT wire could obtain the high J_c, but the cost is much higher comparing with the other methods. As a result, the internal-Sn process has become a promising method for fabricating this kind of wires. Various design of internal-Sn wires enable the reach of high J_c. However, the internal-Sn faces more challenges in fabrication especially in co-drawing of the final complicated multifilamentary wires. Poor bonding and improper matching of each component are still the main problems disturbing the manufacturer of Nb_3Sn precursors. Hence, the investigation in these two facets is very helpful for increasing the piece-length of the superconductor wires.

2.2 Area Reduction of Bi-metallic and Multi-metallic Composite Wire

Besides metallic superconductors, more and more metallic compounds consisting of two or more metals are also often required by industry for reasons of economy or because composites can achieve mechanical or thermal properties that can’t be obtained with single material. Their applications range from increased strength-to-weight ratio, improved corrosion resistance to high-temperature field [19]. For example, Aluminum-

clad steel wire combines the strength of steel with the electrical conductivity and corrosion resistivity of aluminum [20]. For metallic superconductor wires, the superconductor core clad with copper combines the superconductivity at cryogenic temperatures with assurance against failure when a local rise in resistance or temperature occurs [21].

Extrusion and drawing are necessary to fabricate such wire products. When drawing or extruding wires, the required deformation is accomplished by pulling or pushing the wire through a fixed, conical die, hereby reducing the diameter through plastic deformation. The conditions imposed by the different directional forces determine the basic differences between drawing and extrusion. In extrusion, the general state of compressive stress with one elongate strain results in the highest plasticity of the extruded metal, thereby larger pass area reductions could be allowed. While there exists tensile stress state along the drawing direction in the drawing process due to the pulling force at the die exit, which limits the pass area reduction in order to avoid the breakage in the wire. Hence, extrusion would be safer for fabricating wires. However, they face similar challenges in performing a successful process since the billet goes through similar conical dies and deforms into smaller size wire. The selection of appropriate dies and processing parameters are very important, and it is dependent on the billet formula including materials, wire size and so on. In fact, numerous investigations have been carried out to improve the application of drawing and extrusion on the manufacture of bi- and multi-metallic composite rods or wires in the past few decades.

2.2.1 Forming Process

Generally, the metallic composites are composed of two or more different materials, each material having its own distinctive mechanical characteristics, which increases the difficulties for the manufacture of small size wires, for example, fracture often occurs due to the non-uniform deformation of the different components in the drawing of composite superconductor precursors. This is also the reason why only a limited number of bi- and multi-metallic components were produced commercially though the number of combinations of metals that can be co-deformed is large [22]. Hence, the study of the forming condition, which will enable sound plastic deformations of metallic composites to take place, has spurred the interest of many investigators.

Eilman[23], Given [24], Pilarczyk[8], Avitzur[25-27], Osakada[4], Yamaguchi and Matsushita *et al* [28] all conducted pioneering experiments on the drawing and extrusion of bi-metallic rods. Alexander [3], Avitzur[5, 29-31], Osakada[4] and Nagy[32] *et al* proposed analytical models to predict forming forces and different deformation patterns of the billet during the process. Pilarczyk[10], Pacheco and Alexander *et al*[33] analyzed the detailed mechanics in the billet by using Finite Element Method. When the metallic composite billets goes through the conical dies, non-uniform stresses and strains are produced because of the different elastic and plastic properties of the components, which increases the complexity of the forming process. From both of the experimental and analytical work, it has been shown that the following parameters are important to the successful co-deformation of metallic composite rods through conical dies:

1) Area reduction, r%

2) Semi-cone die angle, α

3) Land length of the die, L

4) Friction between the billet and the die

5) Size ratio of the core and filaments

6) Strength difference between the components

7) Bond strength at the interface between the components

8) Filament assembly for multi-filamentary billets.

In their analysis of the extrusion of bi-metallic rods with hard cores, Osakada *et al*[4] identified three possible modes of deformation. Uniform deformation was referred to the products in which both deformed to the same reduction without failure. Cladding occurred when the clad material was much softer than the core. In this case, no deformation of the core occurred and the softer material deformed to cover the harder one. In the third situation, the harder core fractured by tensile necking. Their analysis and experiments showed that uniform deformation occurred at low die angles and the core fracture was due to the tension in the center at higher extrusion ratios. They got the limit of extrusion ratio as about 3.6 for a die included-angle of 45°. This critical extrusion ratio increased as the die angle decreased, which was because of the uniform deformation at low die angles. Later on, Story *et al*[27] observed a new deformation mode in their hydrostatic extrusion experiments of bi-metal rods, wave-type failure, which was the incipient necking of core and like “Sausage”. The proper combinations of process variables may result in a region where successful extrusions were expected. Some important conclusions were drawn from their experiments: The relative size of core was

an important parameter for the choice of other variables; the range of acceptable reductions in area tended to decrease with increasing die semi-cone angle; the strength ratio was very sensitive, a slight increase in strength ratio, 25-50 percent, significantly reduced the size of the safe or successful zone; increasing receiver pressure increased the size of the safe zone.

Zoerner *et al*[34] developed three different interface bond conditions, lubricated, intermediate and metallurgical bond, and investigated the effect of the bond conditions on the extrusion process. They found that the largest zone of sound flow occurred when the core and clad was metallurgically bonded and the decrease in bond strength restricted the range of semi-cone angles and area reductions which could be used to obtain sound flow. For the lubricated core/sleeve interface billets, no sound flow was observed. Subsequently, Lugosi *et al*[11] did more experiments for identifying the importance of the interfacial bond strength on the soundness of aluminum-core copper-clad composites. In their experiments, the interfacial bond strength did influence the deformation mode of the billet, and the weak bond led to an earlier failure of the billet. But when the extrusion ratio was high enough, it had no appreciable effect on the process. Furthermore, severe fluctuations of extrusion pressure were observed to associate with billets with low interfacial bond strength. This phenomenon was attributed to the faster extrusion of aluminum core comparing to the copper sheath which intermittently sticks to the die and acts as a die orifice. They also found a clean, degreased interface was enough to obtain a sound, uniform product when using a proper set of extrusion parameters, but as for the bond quality, they found an extrusion ratio of 19.1 was still insufficient to produce a strong, metallurgical bond between the components in the as-extruded product.

Oliver and Nix [35] investigated the effect of strain hardening in extrusion of axisymmetric bi-component rods. Their experiment results showed that when the core hardened more rapidly than the sleeve, the rod began to deform non-uniformly, and this caused the core to fail. But failure did not occur when the sleeve materials work-hardened a little rapidly than the core. Hence, when assembling materials for co-extrusion, the strain-hardening rates of each material needed to be considered. These parameters should be selected such that the strength ratios of core to sleeve stay within the values that produce successful extrusion.

Eil'man [23] pointed out that the cross-section-area ratios of the bimetal components should be constant under constant drawing conditions. Any accumulation of shell or core metal would result in the defects in the wire, even lead to the core or sleeve fracture. Rasp and Paweiski [36] applied the linear mixing law for the bimetallic billet and estimated the drawing force by the aid of elementary plasticity theory. Lesik and Dyja [8] measured the microhardness on the cross section of drawn steel wire clad with copper and confirmed the nonuniform stress-strain state in the joint of different materials. Ragab [9] and his co-workers explored some of the unusual effects of lubrication when drawing a steel wire clad with soft copper by using both force equilibrium equations as well as experimental measurement of drawing force. The reduction in the die-billet interfacial friction (due to lubrication) has been found to lead to an increase in the drawing force and radial pressures on the coating and core which enhances the coating-core interlayer friction conditions. This finding is very interesting, but needs to be tested in other metallic combinations and other lubricant.

The above experiments were all for the different types of copper-aluminum and steel-copper alloys, but in fact the superconductor precursor wire is an enlarging family manufactured by extrusion and drawing due to its widening application. All the superconductor wires are extruded or drawn to the final small size depending on the type of superconductors. Due to the complication of the wires, the companies and researchers are trying to increase the piece-length by trying different technologies. Fiorentino and his co-workers[37] from Battelle conducted the earlier experimental investigations in using hydrostatic extrusion. They tried to confirm the feasibility of this new method as a promising forming technology for the mono- and multi-filamentary superconductor precursor wires including the manufacture cost and the superconductivity properties. Alterovitz[38], Chen *et al*[39] studied the process for multi-filamentary Nb-Ti and Nb-Sn wires. They found that the products had a more uniform cross section after hydrostatic extrusion, and the diameter of the filaments could be up to 0.75 μm which was difficult for the conventional methods. Xu and his co-workers[40] applied the cold hydrostatic extrusion on the manufacture of internal tin processed multi-filamentary wires. They defined the appropriate extrusion parameters for a perfect product with a homogeneous distribution of Nb filaments and Sn cores without any swelling and sweating defects: for die angles of 45-50°C, the extrusion ratio was less than 4. When the extrusion ratio was above 4, the temperature of the billets rose to above 200°C, and the tiny cracks appeared in the sleeve because of the high inner pressure of the Sn core and its melting. These experiments indicated the importance of the temperature rise during the hydrostatic extrusion which was often neglected in most work. In Oxford Instruments, Superconducting Technology (OI-ST), they are trying to improve the fabricability of their

internal-Sn billets through different ways. Rods of NaCl as fillers were used to replace the Sn, and hot extrusion was applied to develop internal-Sn conductors with good interfacial bonding. The good interfacial bonding enables the successful drawing down to the final small size.

The above reviewed experimental methods consisted of varying some of the parameters of the system, and determining whether the extrusion or drawing thus produced would be sound or whether defects would occur. But because the co-deformation of such composites is a very complex process, and the limited experimental data just represented some special cases and were incomplete. For new materials, a huge amount of work must be repeated, which is a time-consuming and high cost attempt for the understanding of the whole process. Hence, theoretical investigation has been used to analyze the process which ranged from simple, semi-empirical approaches, to complex upper bound analysis and finite element method.

To obtain simple estimates of the extrusion pressure for extruding composite billets, Alexander and Hartley [3] extended the analyses developed for homogeneous materials to the composite rod. For a composite billet consisting of a cylindrical core surrounded by an external sheath, which have the volume fraction A_C and A_S respectively, the required extrusion pressure is[3, 41]

$$P = P_C \cdot A_C + P_S \cdot A_S$$

Where, P_C, P_S are the extrusion pressures for the core and sleeve separately at the same extrusion condition. Their experimental data agreed with the above-calculated values

within the accuracy of the measurements. This simple analysis assumed the deformation was uniform, and it provides an empirical estimate on the choice of extrusion pressure. The similar formula could be applied in the co-drawing of bi-metallic wires.

Avitzur and his co-workers [5, 29, 30, 42] applied the upper bound theorem to study the bi-metal co-extrusion and co-drawing process with the objective of determining ranges for area reduction, die angle and core volume fractions over which sound products were obtained, i.e., there was no failure of the core or clad. Their analysis was based on the assumption of spherical and toroidal velocity fields in the core and sleeve respectively. Also, a perfect bond between the sleeve and core, and constant flow stresses for the materials were postulated. They concluded that in general, fracture of the harder constituent was more likely than that of the softer one, whether the arrangement was hard-core soft clad or soft-core hard clad. The higher the ratio of the yield strength of the harder constituent to that of the soft one, the smaller was the range of safe parameters. Figure 2.4 is the typical graphs showing the criterion for the prevention of core facture during extrusion and drawing when the values of friction, bond strength and extrusion ratio were specified, and no front and back tension was applied. Core fracture was expected below each respective curve, indicating the core fracture occurred for higher values of core strength, and it was deterred by smaller die angle.

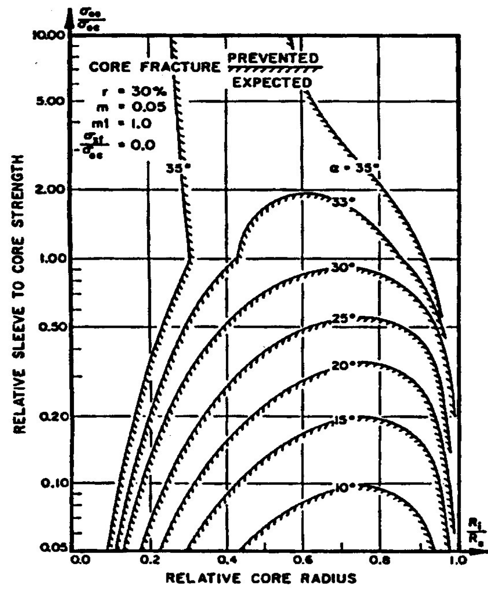

(a) Co-extrusion (b) Co-drawing

Figure 2.4 Criterion for core fracture in bi-metal co-deformation

Realizing that the assumption of velocity fields used in the previous upper bound method had not necessarily reflected the flow characteristics peculiar to the composite billet, Tokuno and Ikeda[43] constructed a kinematically admissible velocity field for the extrusion of Pb-5%Sb clad aluminum rods on the basis of observations of actual material flow to refine their model and got more accurate results which agreed well with their experiment results. Their analysis showed that the increase in the flow stress ratio, the die angle and die friction promoted non-promotional flow irrespectively of whether the core material was softer or harder than the sleeve material, which led to the non-uniform deformation in the product. This work did improve the accuracy of the analysis, but much more experimental work was necessary for the construction of the velocity field.

Nagy [32] examined the drawing of a bimetallic wire consisting of a weak sleeve and a comparatively strong core. He applied the Upper Bound Method and analyzed the reasons why shaving happened. He pointed out the back stress is helpful for eliminating the shaving and small area reductions were undesirable from the viewpoint of shaving. Muskaiski and Pilarczyk [10] *et al* simulated the drawing of steel wire clad with copper billet by using Forge-2 software, and checked the thickness change of copper sheath. Their results show that the copper sheath deforms more serious than that of steel core which is related to their difference in deformability.

Pacheco and Alexander[33] investigated the mechanics of Copper-covered aluminum rod during extrusion using finite element method. They assumed the materials were rigid-plastic and no relative movement occurring at the interface. They predicted the interface shape between the clad and core and the boundaries between the rigid and deforming regions, and identified that the boundaries between the rigid and deforming regions

differed from the assumed spherical shapes, which was in a good agreement with Sliwa's experimental results[2]. At last, they introduced a constant friction at the interface into their model, and assumed the friction factor was 1.0 (full bond) or 0 (no friction). Their results suggested that the fracture of sheath material was more likely when the core fraction was large and the friction at the sheath/core interface was low.

Scrinivasan and Hartley [44]used the FEM program IFDEPSA to simulate the extrusion process, and their billets were also Cu-clad Al-core rods. They investigated the development of stresses in the deformation zone under different processing conditions of die angle, extrusion ratio and volume fraction of the core. But large extrusion ratios were not used in his work because of the limitation of the program itself. Dehghani[45] refined the model by using ABAQUS which is improved in the treatment of the seriously distorted elements. He investigated the distribution of the residual stresses in the products with the change of the process variables. In these two models, the process was assumed isothermal and strain rate independent, materials were assumed to be elastoplastic and obey the Von-Mises yield criterion, and a perfect bonding between the components was considered. They drew the similar conclusions that lower die angles in general promoted a more uniform metal flow and lower residual stress magnitude, and lower area reductions led to less compressive stress state in the center of billet where central burst favored, and too large area reductions caused the high possibility of surface cracks.

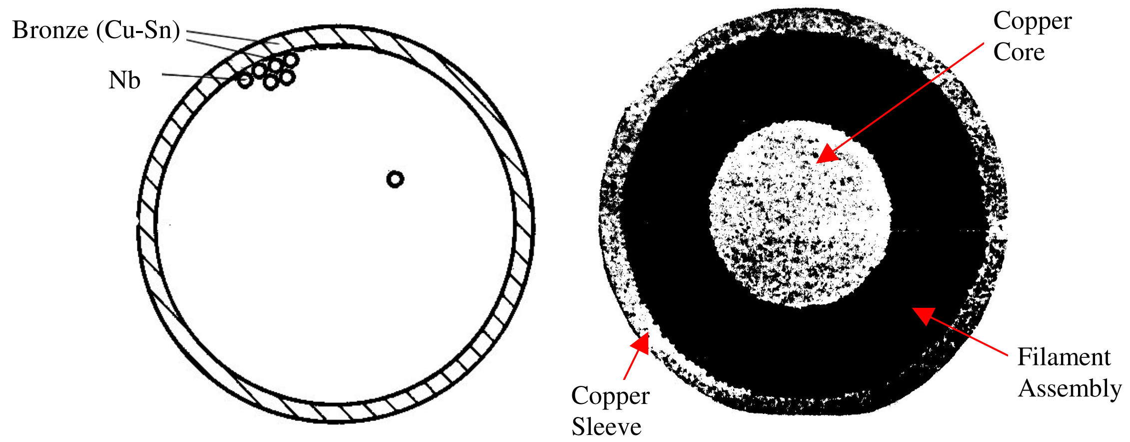

(a) Bronze processed Nb_3Sn (b) Cross section of NbTi SSC

Figure 2.5 Multi-component billet assembly

As for the theoretical analysis of multi-component billets, Very little work was published. Generally the multi-component billets are the assemblies of mono strands and multifilamentary superconductors exemplify this category. Figure 2.5 shows the typical assemblies for multi-filamentary superconductors, and their difference is whether there is copper stabilizer in the center. Avitzur and his co-workers[6, 46, 47] extended their upper bound model to this case. They simplified the structure as tri-metal as shown in Figure 2.5 (b), and devised the criterion for the prevention of filament breaks. The billet included the core, the outer sheath and the intermediate sleeve, where the intermediate sleeve was the filament assembly. Predominant failure modes of the studied multi-filamentary wire were initiated at the region of the filament assembly. Failure usually started either with the breakage of a single filament or a group of them. Sound flow would occur only if all three components experience identical elongation, which meant that each component would experience reduction in area identical to the global reduction in area. Any other combination of reductions led to fracture. They considered the effect of strength difference, size ratio and pass reduction, and assumed a perfect bond between the components. Through the analysis, they got the safe regions for the process as shown in Figure 2.6. This figure told us the importance of the distribution of the stabilizer copper between the core and sleeve for the formability of such billets: if all the copper is in the core or in the sleeve, any die angle is permitted at the given conditions, but if the filament assembly was intermediate, the die angle should be below the low section of the loop, which indicated that the small die angles were preferred.

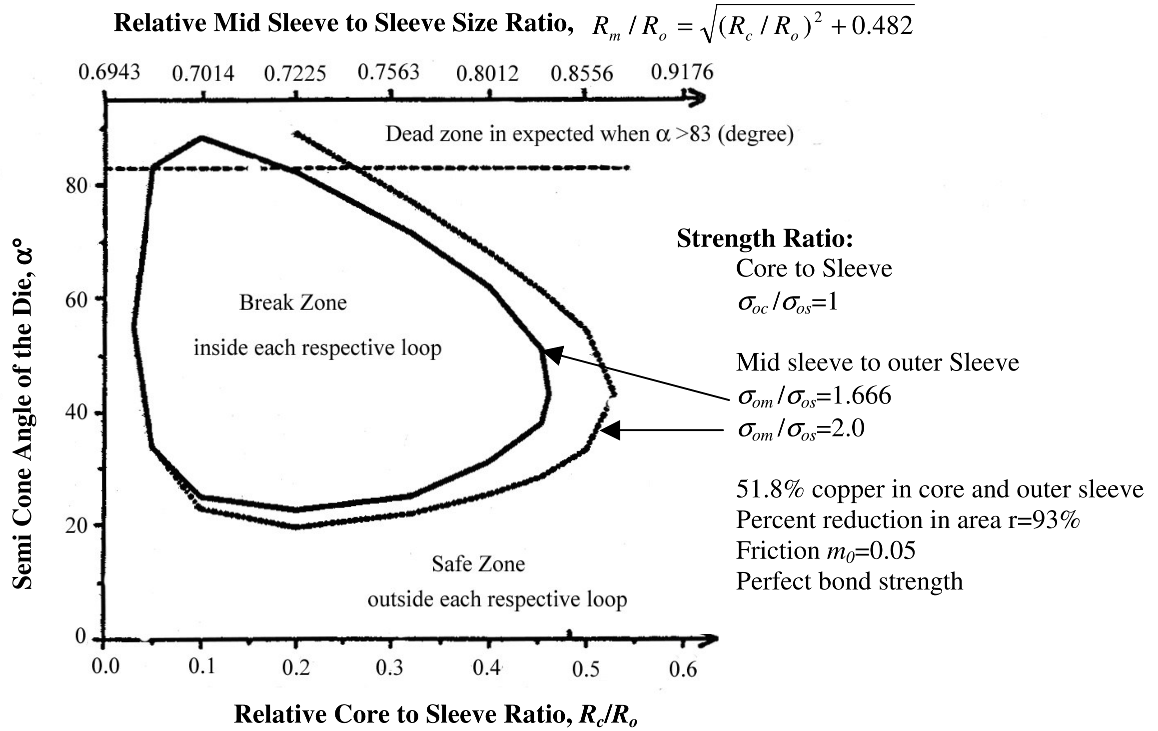

Figure 2.6 Tri-metal Fracture Criteria for extrusion

2.2.2 Bonding Generation

Extrusion and drawing have been used to produce the high quality bi-metallic or multi-metallic products[19, 21]. For these products, a metallurgical bond between the different components is advantageous or necessary. For example, the weak bond between the superconductor core and copper clad will deteriorate the stabilizer function of the copper and lead to the failure of the superconductor when a local rise in resistance or temperature occurs.[20, 22] The poor bonding between the components hinders the successful co-deformation in the following steps [48]. However, most of the published work focuses on the study of forming condition which would result in a successful co-deformation without fracture, and very little attention was paid to the bonding process during the co-extrusion and co-drawing process.

Avitzur and his co-workers[22] proposed that the metallurgical interfacial bonding through co-deformation process could be achieved through pressure bonding. For the assembled billet, no contact is forced on the sleeve and core. Moreover, the surfaces of the core and the sleeve are not perfectly cylindrical, rather, they are undulant surface. During the co-deformation process, the initial actual contact between the matching surfaces to be bonded is confined to a few crests only, composing only a fraction of the apparent area. With the processing of extrusion or drawing, those crests experience high local pressure and are therefore crushed. Through these plastic deformations, virgin surfaces are exposed to one another, and the metallurgical bond forms instantaneously across these surfaces. Considering this process, Sliwa *et al*[49-51] and Montmitonnet[52]

summarized that the general requirements for a satisfactory bond between components in a combined deformation of different materials were as follows: sufficient pressure (compressive stress in the deformation zone); sufficient increase in surface area during the deformation; limited degree of in homogeneity of the flow in the deformation zone. Bay[53, 54] also showed that the adherence force of the cold-formed metals increased with the amount of strain or rather the proportion of the clean surface created by deformation. Hence, the degree of deformation and geometry of the die play the most important part in forming sufficient bond between components during the co-deformation [50, 55]. Avitzur and his co-workers got a perfect bond by co-drawing a copper-clad iron core rod up to 85% reduction in area [22]. However, Osakada, Limb, *et al*[4] didn't obtain good-welding products when they used various die angles, as 30°, 45°, 90°, and extrusion ratios, as 2.5, 2.9, 3.6, 4.0, 4.5 respectively for the hydrostatic extrusion of Cu-core Al-clad rods, although the copper core appeared to be fixed tightly to the aluminum sleeve. Hartley *et al*[56] measured the core/sleeve interfacial strength of copper-clad aluminum rods produced by hydrostatic co-extrusion. Their results showed the interfacial shear strength as a function of the extrusion ratio and die angle. They concluded that the interface strength exhibited a minimum at a particular extrusion ratio and the change in die angle alone did not reveal any significance in the variation of the interfacial strength. But from the value of the interfacial strength, it appeared that the components were not bonded strongly, possibly it's due to the low extrusion ratio. In fact, Lugosi[11] once pointed out that an extrusion ratio of 19.1 was still insufficient to produce a metallurgical bond for clean and degreased interfaces. Hence, it seems that the investigators' conclusion about the minimum value at a particular extrusion ratio was based on

insufficient evidence. Furthermore, it would be more convinced if the investigators use the microscopy technology to analyze the bonding area corresponding to the interfacial shear strength values.

In the pressure bonding process, the surface state is a very important factor for a strong bond[53, 54, 57-62]. The cleaner the surfaces are in the interface, the easier it is to produce a metallurgical bond. But the real surfaces of the materials are not ideally clean, and they are often covered with oxide layers [51, 63, 64]. The question arises as to whether these oxide layers will prevent the two metals from bonding: this depends on the nature of metals and on the rheology of their oxides. Cave[65] has shown that, when rolling together copper and aluminum sheets (the oxides of which are fragile), the oxide layers were broken into small platelets, through which "clean" metals came into contact, ensuring a strong metallic bond. But if the oxides could stand the high strains without being broken, they would prevent direct metallic contact and hence weaken the adherence between the two metals [52]. Therefore, one of the constraints on the nature of the metals must concern the rheology of the oxide layers formed, i.e. metals with fragile oxides should be chosen for this kind of bonding.

Temperature serves the important function of increasing the mobility of atoms, and it affects the plasticity and diffusivity[66]. The high temperature often raises the complexity of the bonding process. When the temperature is up to 0.4~0.8 T_m (where T_m is the melting temperature of the lower melting-point materials), the diffusion mechanism begins to work in the bonding process[66-68]. Nakasuji *et al*[69] heated the Ti-clad Cu rods to 800°C, then hydrostatically extruded them from 77mm to 40mm in diameter. They measured the interfacial shear strength up to 170 MPa, which indicated a good bond

obtained in this case. The investigators ascribed this strong bonding to the diffusion process at the interface, and they also observed the inter-diffusion of various elements through the interface. However, Loewenstein and Tuffin [70] pointed out that the diffusion occurring in co-extrusion was limited by the very short time of extrusion process and the rapid cooling of the extruded section. It appears that whether the diffusion occurs or not depends on the temperature, the properties of the materials and the extrusion velocity. Therefore, it's important to study the metallurgical characteristics of the bond in the co-extrusion for the identification of bonding mechanism.

2.2.3 Summary

Through both the experimental and theoretical investigation, the effects of the main process variables on the co-drawing and co-extrusion processes can be summarized: lower die angles promote a more uniform metal flow; Low interfacial strength between the components lead to the occurrence of defects; The fraction of core to sleeve affects the process significantly depending on the strength ratio of the core to the sleeve; Critical area reduction exists for the sound products at certain extrusion or drawing condition such as die geometry and materials, and the effect of area reduction associates with the assembly method of the materials.

The finite element method and upper bound theorem have been used as theoretical tools to study the effect of varying process variables and predict which kind of parametric combination could avoid the defects during co-drawing and co-extrusion process. But in the upper bound method, as summarized in above section, materials exhibited no

variation of flow stress with temperature or strain rate and the assumption of velocity fields was unreliable. All these characteristics suggest its limitations on application. Hence, the finite element method is considered as a more effective approach. In the published references, FEM was used to predict the distribution of stresses, strains in the deformation zone and residual stresses after deformation in the co-extrusion and co-drawing of bi-metal. However, some improvements are necessary for the more comprehensive understanding of the process. As indicated in the experiments that the interfacial bond between the sleeve and core was an important variable for the co-deformation process, the input of this variable to the FEM model is necessary. In addition, the attempt to extend the FEM model for bi-metal to multi-metal composite is very meaningful for the successful drawing and extrusion of the complex multi-filamentary wires.

The limited references gave us the rough ideas that area reduction, die geometry, temperature, presence and thickness of oxide layers are the important factors for the metallurgical bonding during the co-deformation. This process involves the application of pressure by die, the increase of the true area of contact between the materials and possible diffusion when the temperature is high enough. However, how these factors affect the bonding process and bond quality has not been fully investigated. Moreover, no published work on bonding during co-drawing process indicates the importance of this investigation.

To understand the nature of the bond formation during the co-deformation, it is necessary to understand the distribution of stresses and strains and temperature within the materials and their resulting deformation behavior. But until this understanding is developed, the

design of co-deformation bonding process will continue to be trial and error and will remain problematic. So it is necessary to incorporate the bonding criteria along with the mechanics of co-deformation bonding.

2.3 Objective and Format of this Document

This thesis focuses on the fabrication of internal-Sn type wires, and the objective is to get a better understanding of interfacial bonding generation under different drawing and extrusion conditions and the effect of interfacial bonding on the drawing and extrusion process.

Chapter 2 is a background review one, the main fabrication methods of Nb_3Sn superconductor precursors was introduced at the beginning and then literatures on the co-deformation and co-bonding process during co-extrusion and co-drawing was reviewed.

Chapter 3 is focused on the literature review of interfacial bonding. Basics of solid-state bonding were introduced and literature on the characterization of interfacial bonding was reviewed.

In chapter 4, the bonding generation during the co-extrusion has been investigated by using SEM and STEM observation. A properly designed extrusion schedule could creates a perfect bonding between the components in a very complicated subelements.

In chapter 5, various drawing experiments have been done, and the interfacial characteristics have been analyzed by using SEM observation. Co-drawing bonding mechanism was proposed.

In chapter 6, based on the experimental schedule, FEM simulation was used to simulate the multiple drawing process, and the interfacial mechanic properties was investigated. A pressure bonding model was modified to calculate the bonding strength created in the interface. Finally, a bonding stress test was designed to test the bonding strength in the drawn billet.

In chapter 7, based on the FEM simulation, the effect of the drawing processing parameters on the deformation process was analyzed.

Chapter 8 summarizes the findings of this thesis and concludes this documents.

Chapter 3

3. Literature Review in Solid State Bonding

Solid state bonding is a joining process where two materials could be coalesced at temperature essentially below the melting point of the base materials being joined, without the addition of brazing filler metal. Basically these processes include cold pressure bonding, diffusion bonding, explosion welding, friction welding and ultrasonic welding. In all of these processes, time, temperature and pressure individually or in combination produce coalescence of the base metal without significant melting of the base metals. The Welding Handbook [71] and Wallach's [72] brief review gave a complete explanation of solid-state joining.

3.1 Main Solid State Bonding Processes and its Application

As its name suggests, the solid state bonding occurs without the presence of liquid or vapor phases. It is usually applied to the materials to be joined: at low temperature to avoid unwanted phase transformation; of very dissimilar nature for which process involving fusion often are not viable since brittle compounds may form; in applications

for which joint design precludes fusion welding; at high rates and for multi-component joining in one operation.

3.1.1 Diffusion Bonding

Diffusion bonding produces welds by the application of pressure at elevated temperature with no macroscopic deformation or relative motion of the component. The applied pressure is set above the level needed to ensure essentially intimate surface contact but below the level that would cause macroscopic deformation. The temperature is generally below the melting point of the joined materials. Figure 3.1 shows the stages during diffusion bonding. At the first stage, deformation of the contacting asperities occurs primarily by yielding and by creep deformation mechanism to produce intimate contact over a large fraction of the interfacial area. During the second stage, diffusion becomes more important than deformation, and many voids disappear as grain boundary diffusion of atoms continues. Simultaneously, the interfacial grain boundary migrates to an equilibrium configuration away from the original weld interface, leaving many of the remaining voids within the grains. In the third stage, the remaining voids are eliminated by volume diffusion of atoms to the voids surface. In this process, temperature and pressure are the most influential variables. Temperature determines the rate of diffusion that governs void elimination, and the pressure promotes the larger area of contact. It is also necessary to ensure that the oxide layer does not constitute a barrier to atom migration and the formation of intermetallic compounds must be controlled. This technique is particularly suitable for joining metals which are difficult to be welded by

conventional fusion welding such as Ti and its alloy, and joining of large areas in one operation.

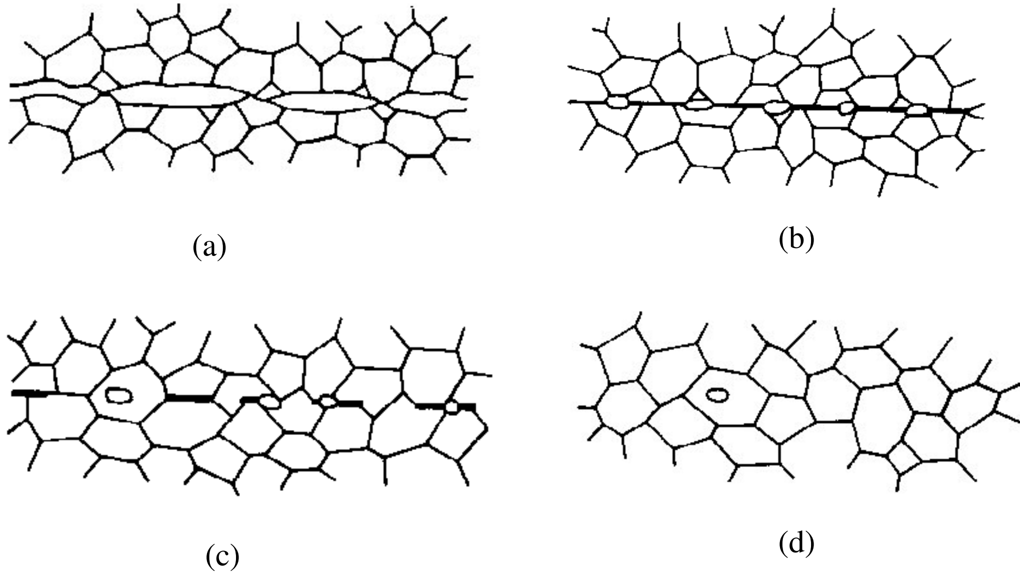

Figure 3.1 Stages during Diffusion Bonding

3.1.2 Explosive Bonding

Explosive bonding is accomplished by high velocity impact of the components to be welded with the control of detonation. Figure 3.2 shows the typical arrangement for explosive bonding. The explosive in granular form is distributed uniformly over the top surface of the prime component. The detonation controls the explosion. The explosion accelerates the metal to a speed at which a metallic bond will form between the components when they collide. The kinetic energy of motion is converted to heat at the joint interface. The high pressure generated at the interface due to the collision causes the coalescence and welding. The process is most commonly applied to the cladding of plates with dissimilar metals.

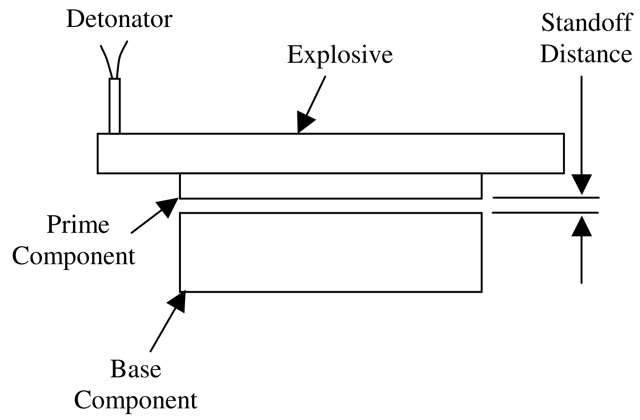

Figure 3.2 Arrangement for Explosive Bonding

3.1.3 Friction Bonding

In friction bonding, the relative rotation of one material surface against another under axial load is used to generate frictional heat, to remove surface contaminants and to produce bonding. In the simplest arrangement as shown in Figure 3.3, one component is rotated around its axis while the other is held stationary. When the appropriate rotational speed is reached, the two components are brought together and an axial force is applied. Rubbing at the interface heats the parts locally and softens the materials, thereby upsetting starts. In this process, the weld is characterized by a narrow heat-affected zone, the presence of plastically deformed materials around the weld, and the absence of fusion zone. Friction welding is usually considered when at least one of the components has axial symmetry.

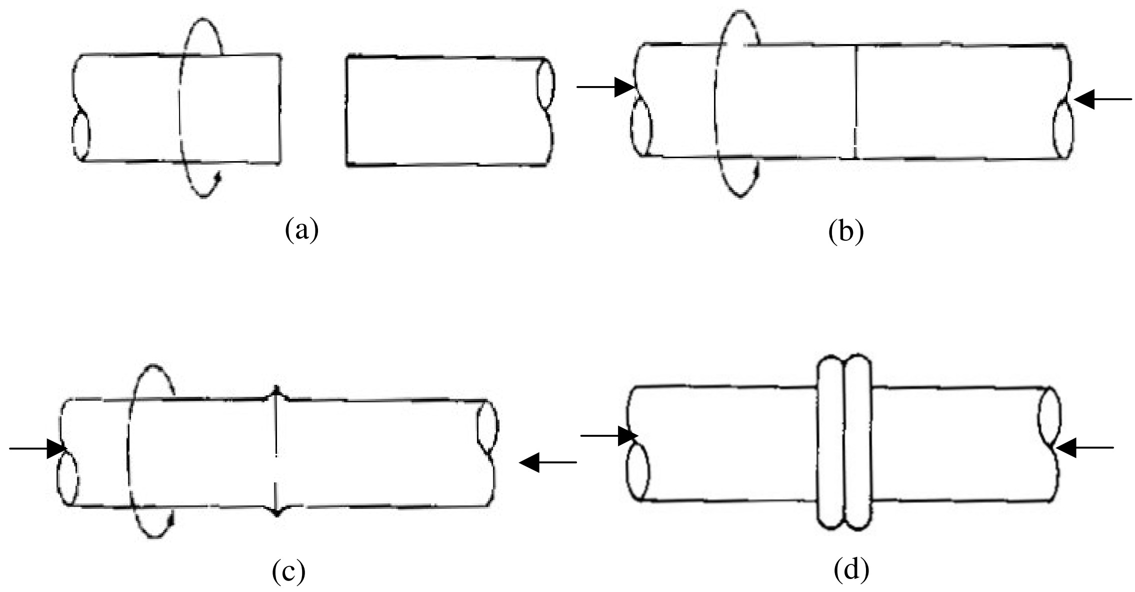

Figure 3.3 Basic Steps in Friction Welding

3.1.4 Ultrasonic Bonding

Ultrasonic bonding produces welds by the application of high frequency vibratory energy while the components are held together under pressure. Figure 3.4 illustrates the typical ultrasonic welding system. The ultrasonic vibration is generated in the transducer and transmitted to the component through the sonotrode tip. Frequency normally ranges from 10000 to 60000 Hz. Simply saying, the combination of a static clamping normal force and a high-frequency oscillating shear force causes coalescence at joint interfaces. The process has been used extensively in the electronic, aerospace industries. It is used to produce lap joints between metal sheets or foils, between wires or ribbons and flat surfaces.

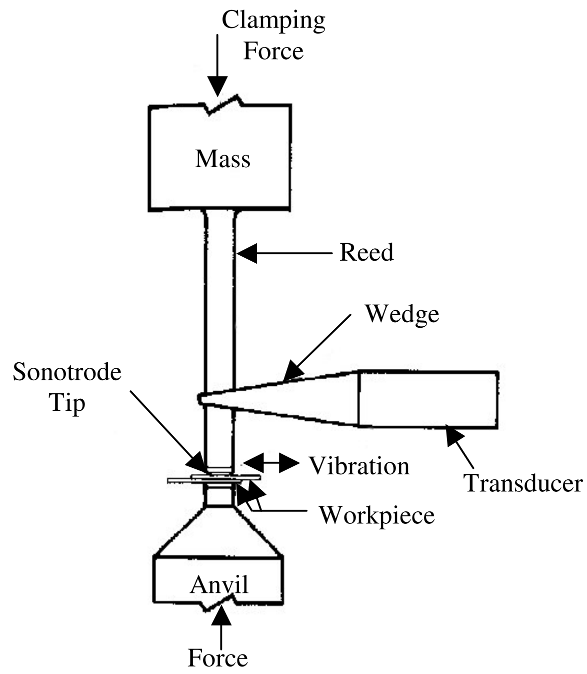

Figure 3.4 Typical Ultrasonic Bonding System

3.1.5 Cold Pressure Bonding

In cold pressure bonding, pressure is used at room temperature to produce coalescence of materials with substantial deformation at the joint. The plastic deformation causes the generation of a new, clean surface at the joint surface, which in turn promotes solid state bonding when the two surfaces are close enough to each other. A characteristic of this process is the absence of heat, either applied externally or generated by the welding process itself. The process has been extensively used to join dissimilar metals in numerous applications including the welding of aluminum wire stock. Rolling bonding is a typical cold pressure bonding process used in the manufacture of metal laminates [73]. The rolls applied sufficient pressure on the rolled plates to cause deformation at the faying surfaces. The bonding created by passing through the conical dies such as drawing or extrusion is also explained as the cold pressure bonding by a few researchers [22]. The pressure applied by the die promotes the coalescence of two components.

3.2 Characterization of Interfacial Bonding

As mentioned in the above sections, two or more materials are combined to obtain enhanced performance, which is influenced by the level of bonding. Recent investigations show that the interfacial bonding strength has profound influence on the failure of dissimilar materials. Good bonding is essential for the metal matrix to effectively distribute the load borne by the composite. Without excellent matrix-to-

filament bonding, decohesion of the fiber-matrix interface occurs during deformation, leading to poor load transfer and consequently failure. This becomes a serious problem occurring in the drawing of complicated wires such as the multifilamentary superconductor precursors. Hence, the importance of interfacial properties in composites spurs the intensive research interests in both experimental, micromechanical characterization of the interface and investigation of the factors affecting the bonding.

In experiments, microscopic observation such as Scanning Electron Microscopy (SEM) and Transmission Electron Microscopy (TEM) are the main tools to investigate interfacial behaviors at atomic level [66, 67, 74]. The measurement of interfacial bonding strength is critical for the evaluation of strength, durability and performance of such new materials. Different kinds of mechanical tests have been designed to measure the interfacial bonding strength in the composites, thereby to design the bonding parameter. As two kinds of materials are used in bonding, bonding strength measurements are more complicated than the traditional strength measurements for homogeneous materials. There are currently no standards or specifications for testing, but a lot of researchers designed a series of tests corresponding to the types of joining. For the cladding and plate components, peel testing and lap-shear testing are commonly used [75]. As shown in Figure 3.5, the peel test has been in use to measure the load necessary to peel the layer apart. The sample is held in a fixture that rotates during the test to ensure that the layer being peeled is always perpendicular to the peel axis. The load to peel the layers is recorded and normalized to give a peel strength in load/unit length. In the lap-shear test, the specimen is prepared as that shown in the schematic diagram of Figure 3.6. A slot is machined from opposite sides of the sample to the bond line. The distance between the

two slots must be selected so that the failure is by shear rather than tensile failure of one of the materials. Comparing these two tests, the fabrication of a lap-shear test specimen is more difficult. Hence peel test is more generally used for the plate or cladding materials.

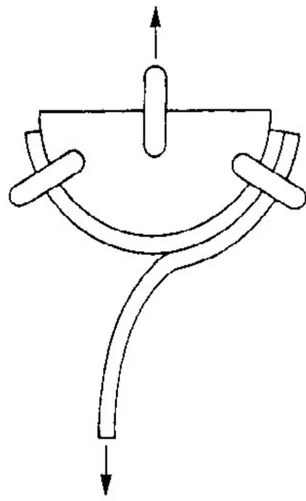

Figure 3.5 Schematic diagram showing the geometry of peel test

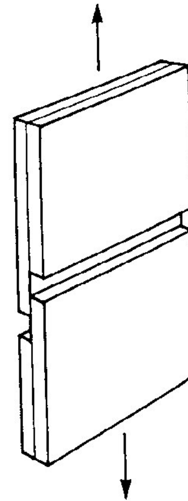

Figure 3.6 Schematic diagram showing the geometry of lap-shear test

For round materials like cladding wires or tubes and fibers, other kinds of tests have been used [76]. Pull-out test (Figure 3.7(a)) is usually used to assess the adhesion of fibers

embedded in adhesive or polymer resin. The force required to pull the embedded fiber from the resin is used to define adhesion strength. Opposite to the pull-out test, another test called push-in test is used to measure the adhesion strength as well. As shown in Figure 3.7(b), the force required to push the fiber debonding from the resin matrix is used to define the bonding strength. In both of these tests, different specimen geometries are used and a shear force is applied to the interface. When the interfacial debonding occurs, the interfacial shear strength is then calculated based on the ultimate shear load and the debond area.

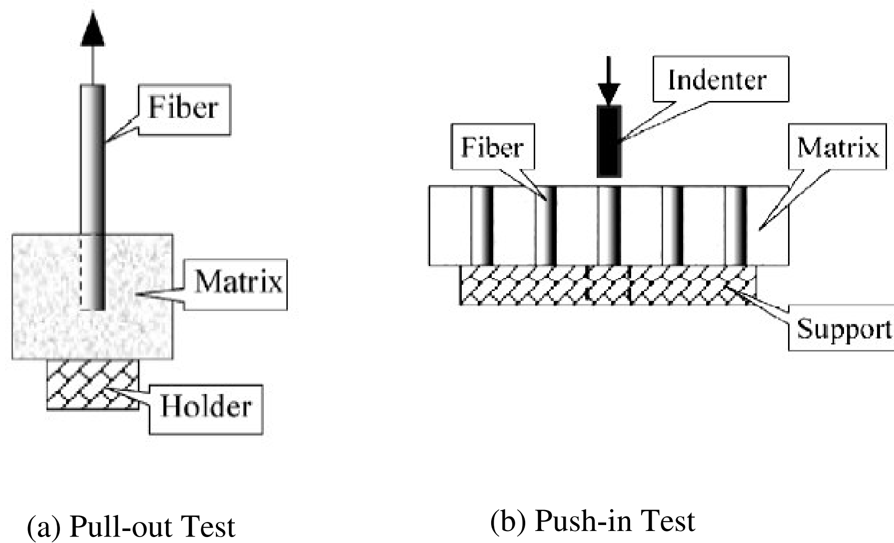

(a) Pull-out Test (b) Push-in Test

Figure 3.7 Schematic drawing of tests for interfacial shear

The three-point bend test [77] is another method for evaluating the bonding level as shown in Figure 3.8. The force required to de-bond the cladding layer is indicative of the level of bonding. Li and his co-workers used the small punch test to evaluate the diffusion-bonded W/Ta interface. Figure 3.9 (b) shows the schematic drawing of this test. The bonded sample was sliced into thin disks and then accepted the test. After exerting

certain force, fracture occurs in the specimen as shown in Figure 3.9 (a). This phenomenon indicates the perfect bonding formed in the W/Ta interface. These tests could be used to evaluate if the interface is bonded, but it is impossible to quantify how much bonding has been created.

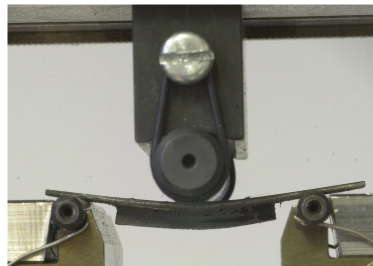

Figure 3.8 Three-point Bend Test

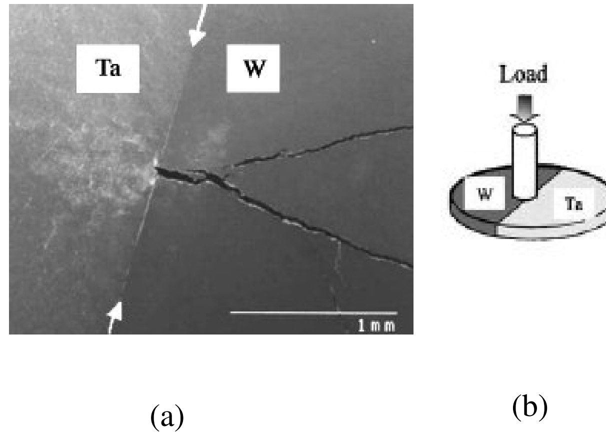

(a) (b)

Figure 3.9 Small Punch Test

Based on the above mentioned, we know solid state bonding process is complicated: the principal factors affecting the strength of joining are the chemical composition of the metals, the creation of virgin surfaces, the presence and thickness of oxide films, temperature, pressure and degree of strain at the interface. Therefore, its investigation involves different aspects such as mechanical, thermal and material science. Generally,

the optimum bonding conditions have been determined by experimental method, which naturally requires numerous experiments. It would be advantageous to apply the numerical method to predict the bonding process in advance so as to save experiments and time. In this area, a lot of attempts have been done corresponding to different kinds of bonding techniques.

Takahashi and Nishiguchi [78], Guo and Ridley [79] all developed numerical models to predict the diffusion bonding process and optimize the bonding conditions. They considered diffusion bonding as the intimate contact process of clean uneven surfaces, and assumed that diffusion bonding is a complete void elimination from the bond line, and no plastic deformation occurring in the process. In fact, the creep plastic deformation is even more dominant than diffusional mechanism as bonding pressure is high. Later on, Takahashi and Nishiguchi [80] enhanced their model by relating the interfacial region with the bulk material using Finite Element Method. They defined the surface ridge pattern, and assumed the initial contact material as viscoplastic. In their FEM model, they neglected diffusion and assumed the interfaces are free of oxide layer. Their assumptions limit their model to the bonding process with high vacuum and high temperature. Lee and his co-workers [81] involved the presence of surface irregularities, oxides and the formation of intermetallics into their model, and assumed the dispersed oxide as particles in the matrix. Hence the interfacial bonding becomes the bonding of matrix/particle, particle/particle, matrix/matrix. Their model was only based on the qualitative explanation, and no quantitative result was obtained.

During friction bonding, the components to be joined are forced to rub each other, and the frictional heat generated at the rubbing interface softens the nearby material. After

certain time, the rubbing is terminated and the bond is produced by solid-state bonding between hot materials. Hence, a combination of thermal and plastic deformation effects is needed to be considered in order to simulate the friction bonding process effectively. Most of the earlier numerical investigation work was focused on the thermal aspects in the friction bonding process and analytical solutions were proposed based on different assumptions [81, 82]. Francis and Craine [83] assumed the softened material as a Newtonian fluid of large viscosity and simulated the frictional stage. Later on, Sluzalec [84] applied a coupled thermo-mechanical FEM model to completely characterize a typical friction bonding process of transient, large deformation and high temperature operation. Kallgren and his co-workers [85] developed an FEM model to simulate the material flow as well as thermal expansion during the friction stir welding process. Moal and Massoni [86] developed a thermo-mechanical FEM model on the inertia friction welding of two similar parts and displayed the evolution of welding zone and temperature. All these FEM models could predict the final deformation shape and temperature distribution. Unfortunately, no bonding criterion has been proposed so far.

For the numerical investigation of explosive bonding, a complete thermal-mechanical process was considered. Oberg and his co-workers [87] proposed a finite difference model to simulate the deformation patterns in macro-scale weld formation, hump formation and jet formation. Pressure, temperature, strain rate and internal energy distribution are all graphically presented from this mode. Unfortunately, they could not investigate the wave generation in the explosive bonding due to the excessive mesh distortion at the interface. Kornev and Yakovlev [88] developed the model of wave formation under explosive welding in terms of the dynamical stability loss of an

elastoplastic layer under constant loading. Their calculation results show that there exist conditions under which wave formation may occur. Later in 2000, Hermant applied finite element method in the modeling of explosive welding. He simulated the transition of interface from planar to wavy which agrees well with experimental observation.

For ultrasonic bonding, very limited work on numerical calculation could be located. Yang and his co-workers [89] calculated the temperature field in the joint of polythene, which was produced by ultrasonic welding, by using the theory of energy transmission in a viscoelastic body. Doumanidis and Gao [90] implemented the spot ultrasonic bonding of thin metal foil in their laboratory, and developed a dynamic, elastoplastic, three-dimensional FEM model to simulate the process so as to select and optimize the process parameters.

With regard to pressure bonding, the most recent and comprehensive analysis is that from Bay [53, 57, 61, 73, 91]. He developed a theoretical model to predict the bonding strength corresponding to certain bonding conditions. The bond formation and subsequent bond strength are controlled by the extent of deformation. Bay's theory quantifies the bond strength in terms of the surface exposure and normal pressure at the bonding surface. He proposed two basic bonding mechanisms occurring in the pressure bonding of metals whose surfaces are scratch-brushed before joint plastic deformation. One is the fracture of the brittle cover layer formed by scratch-brushing, extrusion of base metal through the cracks, buildup of real contact, and coalescing with the base metal of the opposite surface. The other is the fracture of the contaminant film and thin oxide layer. His group has done a series of experiments to verify his model, which shows the high agreement between the model and experimental results.

3.3 Summary

Five typical solid state bonding processes have been reviewed in this section starting from the introduction of concepts and their applications, then summarizing the characterization of the interfacial properties and measurement of interfacial bonding strength, and finally reviewing the progresses in the numerical investigations of the different bonding processes. Solid state bonding is a complicated process which referring to mechanical, thermal and materials sciences, and they are commonly used in industry. The selection of welding parameters is still mostly based on the trial-and-error experimental study. Although a lot of attempts on numerical investigation have been taken to simulate different kinds of bonding process, no any bonding criteria has been established yet. Moreover, very few published work is focused on the bonding generation in the co-extrusion or co-drawing, and the bonding mechanism in these processes has not been fully clear, and the relationship between the bonding strength and the technology parameters have not been established.

CHAPTER 4

4. Bonding Generation during Co-extrusion of Subelements

In the fabrication of superconductor precursors, as the basic stacking units in a final multifilamentary wire, the quality of subelments is of great importance for the subsequent successful drawing of multifilamentary wires. Subelements are also complicatedly constructed, in which the center is Cu replacing Sn in the extrusion process to avoid the melting of Sn, the intermediate layer is the assembly of monofilaments which are Nb rods each jacketed with a Cu layer, and the outside is Cu for stabilization. This composite wire is composed of many components each having different deformation properties, and all the components are handly assembled as a start. Through proper extrusion, a fully interfacial-bonded subelement wire with uniformly distributed and less distorted filaments is desired for subsequent operations. Poor bonding between core and sleeve as well as between the individual filaments may increase the difficulty in forming and result in the decohesion of the filament-matrix interface during subsequent deformation. Hence, proper billet design and selection of optimized extrusion schedules are very important for the achievement of final long piece-lengths and the improved superconducting properties. This chapter is focused on the extrusion process of subelement wires, and we need to answer if well-bonded subelement wires could be produced through our specially handled

extrusion process and how to characterize the interfacial bonding in this certain conditions. In this chapter, the construction of subelements was introduced and the bonding created in the subelements during co-extrusion was examined and characterized.

4.1 Experimental Procedure

4. 1.1 Subelement Construction

For the subelement construction, a bunch of designs were attempted in different companies [15-17]. The basic principle is to guarantee the ratio of Nb to Sn is Stoichiometric, 3:1. The outside Cu worked as a stabilization, and the inside Cu speeds the diffusion reaction of Nb and Sn. Figure 4.1 shows the three typical designs in the manufacture of subelements. Due to their similarity in the construction, EG3 in figure 4.1 (c) was used to identify the interfacial bonding. EG3 was assembled and drawn for Supergenics LLC at Hyper Tech Research Inc. It had three Ta splits within the subelements, 283 monofilaments being formed by cladding Nb rods with Cu tube for a Nb/Cu ratio of 65/35, and a few hundreds of Cu rods in the center to replace the Sn. All the filaments, Cu rods and splits were cleaned following a special procedure to remove the interfacial contaminants, and then were assembled in a Cu can with an outer diameter of 2”. This assembly was sealed in the open end and then was hot isostatically pressed

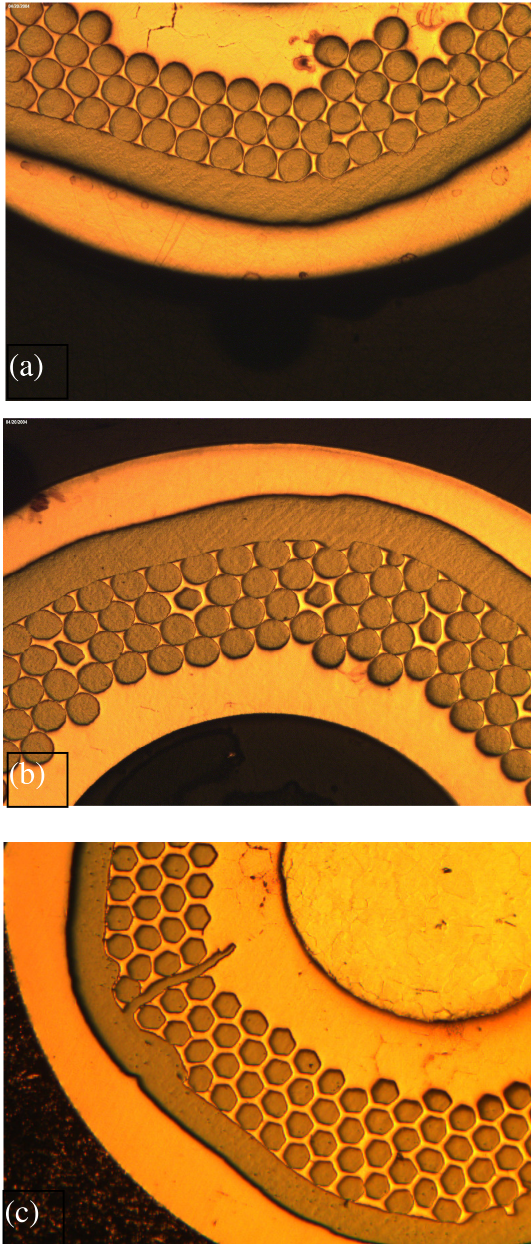

Figure 4.1 Cross section of typical subelement

(HIP) at 600 °C at 28000-30000 psi. Figure 4.2 shows the billet after the HIP process. This billet was then sent to Nu-Tech for extrusion. The billets were extruded to 0.5” at one pass, thereby the pass area reduction is about 93.75%. The extrusion temperature is 600 °C. Figure 4.1 (c) shows the 0.5” cross-section of this extruded subelement, where the Sn rod has been inserted after the gun-drilling of the central Cu. From this optical image, the shapes of the monofilaments inside are pretty good and the interfaces between Cu and Cu, and between Cu and Nb seem well bonded.

Figure 4.2 The subelement billet ready for extrusion

4.1.2 FIB Technology for Underlying Interface Observation and Sample Preparation

In order to investigate the interfacial bonding between the components in the billet, Focused Ion Beam (FIB) technique was used. It combines a scanning electron microscope (SEM) with thermal emission tip for high resolution imaging and a focused ion beam (FIB) with gallium metal ion beam source for nanoscale cutting. Figure 4.3 shows the FEI Strata FIB Microscope DB235, a dual beam SEM/FIB system, used in this experiment. The ion beam column is arranged 52° away from the electron beam. Therefore, nanoscale cutting of structures using focused ion beam could be performed while simultaneously monitoring the progress using SEM. Additionally, the fresh cutting surface could be observed through the rotation of the beam or the sample so that we could investigate the interfacial bonding characteristic through this technique. In this experiment, the extruded subelement wires have been mounted in a conductive base, and the cross-sections have been polished. The cutting is along the axial direction of the wire, hence the fresh interface could be observed under the high resolution microscope.

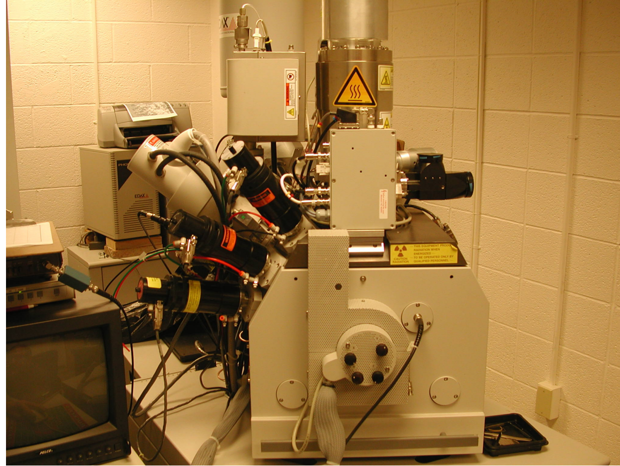

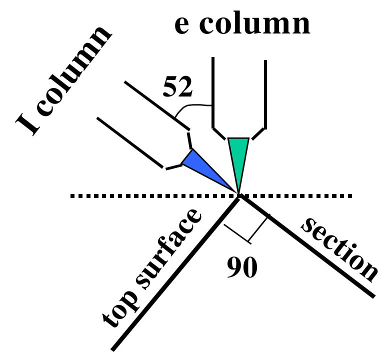

Figure 4.3 FEI Strata FIB Microscope DB235 System with the arranging of electron and ion beam

The cuttings in the longitudinal direction along the typical interfaces such as the interface between Nb and Cu, and between Cu to Cu were performed. Figure 4.4 shows the position where the cut was carried out in the interface between the Nb barrier and outer Cu layer of sample EG3. In this experiment, for each specimen a 1 μm-thick Pt strap was deposited to protect the area of interest. Following this deposition, the preparation utilized 20000 pA Ga ion beams for the initial trench cuts followed by 5000 and 1000 pA cuts to define the membrane as shown in Figure 4.5. Polishing of the specimen was accomplished using 300 and 100 pA Ga ion beams. The final polishing was performed while the specimen was tilted 1.2° into the Ga ion beam to flatten and thin the membrane further. The polished surface could be observed under the high resolution I-beam or e-beam mode directly by rotating the beam direction or sample. From the direct look, no any gap or holes were observed at the interface. We could make a preliminary conclusion that the bonding had been created at the interface. In order to observe the interfacial bonding details, this lifted-out thin membrane was taken out for further observation by transmission electronic microscopic (TEM).

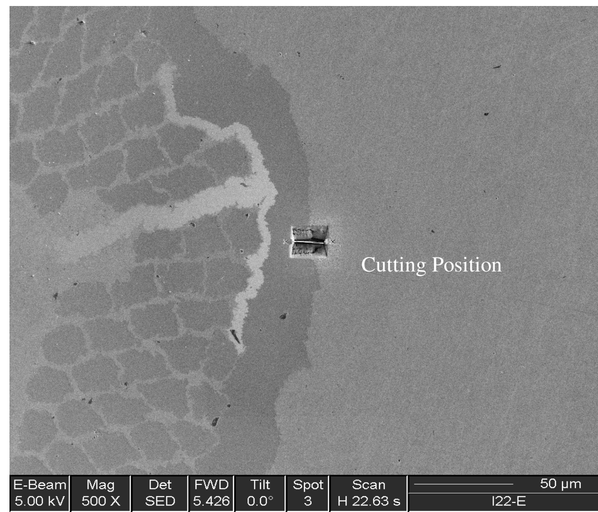

Figure 4.4 Secondary Electron image showing the cutting Position.

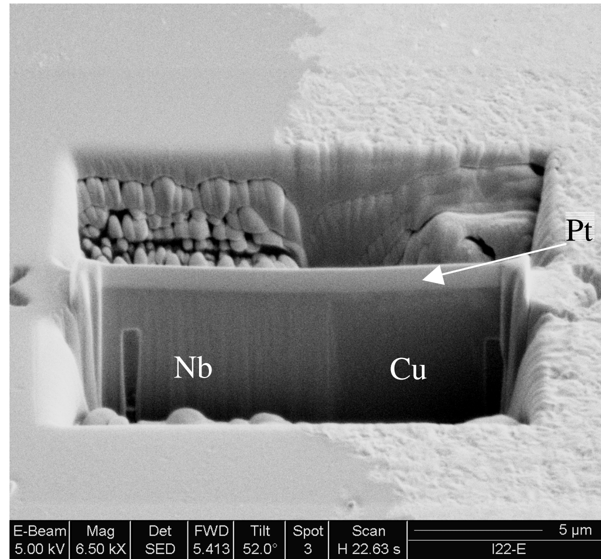

Figure 4.5 Cross section of the FIB milling sample.

4.1.3 STEM Observations of Interfacial Characteristics

An FEI Tecnai TF20 was used in this experiment to probe the Nb-Cu interface. This instrument performs high-resolution micro-analysis and scanning transmission electronic microscopic (STEM) imaging. It is optimized for nano-analysis of materials using energy-dispersive x-ray spectrometry (EDXS), and has a low system background in EDXS in combination with a very small beam size (size of the probe <0.3nm). All the peaks relating to the element are quantified during these measurements (as compared to the single peak capability of the usual EDX-SEM). Hence EDXS attached with STEM provides a more accurate determination of composition over a tiny area.

4.2 Results and Discussion

4. 2.1 Microscopic Characteristics at the Interfaces

According to the close-up images of the subelement's cross sections shown in Figure 3.1, the filaments appear to be well bonded. Figure 4.6 is the high resolution images of the fresh interfaces (cutting surfaces) after FIB cutting. The filaments were perfectly bonded to each other through Cu to Cu interfaces, and the Nb center was also well bonded with the Cu sheath in the individual filaments.

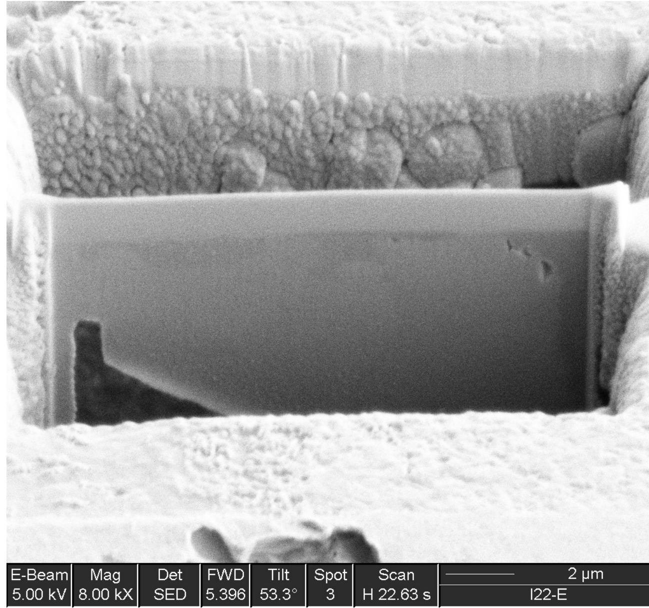

Nb-Cu-Nb interfaces in HP7, HP11

Figure 4.6 The interfaces under FIB

In order to further analyze these bonded interfaces, the lift-out interface samples were observed under the STEM. Figure 4.7 is the STEM image of the interface between the Nb barrier and Cu sleeve in billet EG3. AB is a characteristic line crossing the interface, all the points at an interval of 0.1 μm along this line being analyzed using the composition profile function in Technai TF20. Figure 4.8, a plot of the composition variation along line AB, indicates that Nb and Cu have formed a diffusion couple separated by an approximate 400nm diffusion layer that formed during the HIP and subsequent hot extrusion. This composition analysis confirmed that the Nb barrier had become metallurgically bonded to the Cu sleeve in the subelements during those processes. The similar results were obtained in the interface between Nb and Cu in the filaments. This well bonded subelement ensures success of the next steps: continued drawing of the subelements or drawing of the restacked multifilamentary assembly.

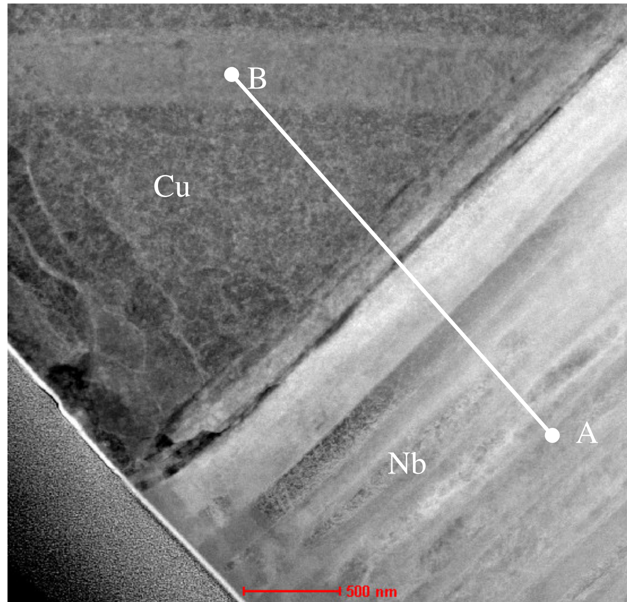

Figure 4.7 The interface between Nb barrier and Cu sleeve under STEM.

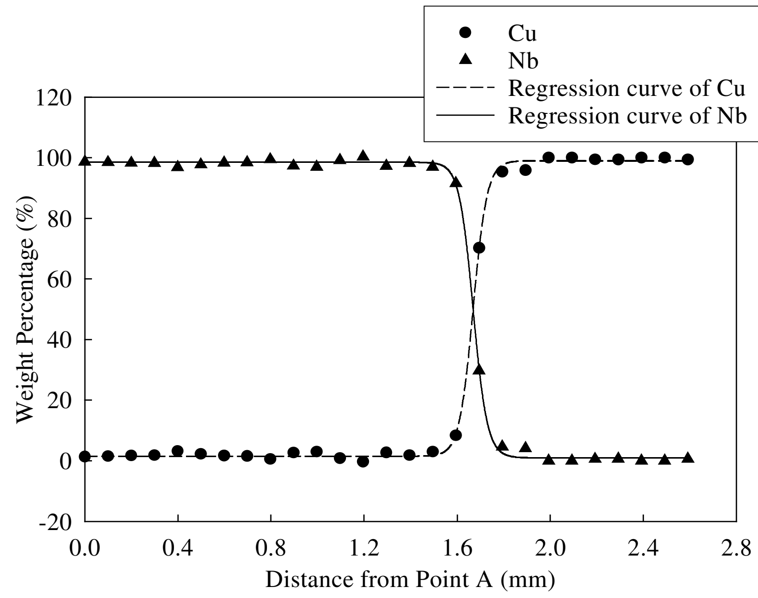

Figure 4.8 Composition profile along line AB.

4.3 Summary

The fabrication of typical internal-Sn subelement strands was reviewed in this chapter, and the bonding generation during the deformation was observed. FIB was used to cut into the sample to show the fresh interfaces, and also to observe the interfaces in the high resolution. This direct observation shows the perfect bonding generated between the filaments and between the components in the filaments. STEM was used to identify the composition variation across the interfaces and to further describe the characteristics of interfaces. A 40 μm diffusion layer formed during the HIP, and subsequent hot extrusion, which confirmed that perfectly bonded subelements could be obtained by proper handling and extrusion. These fully bonded subelements are helpful for the subsequent drawing of restack strands.

CHAPTER 5

5. Investigation of Bonding Mechanism in Co-drawing

Through extrusion, a well bonded subelement wire could be obtained. Generally, this wire is then to be gun-drilled in the center to remove the central Cu, and Sn rod is inserted into the central hole. Thus a subelement involving Sn has been made. Due to the low melting point of Sn, cold drawing is the only viable method to reduce this wire and its restacked wire to small sizes. In the restacked multifilamentary wire, the lack of bonding between the different components increases the difficulty of drawing down to small wire sizes. In the experiments, if the subelements bond well with one another, the billet works as a whole and thereby has better drawability. But what are the main factors influencing the bonding generation and how does the bonding generate? Until now, no work has been published on the bonding creation during the co-drawing process. However the bonding plays very important role in the co-drawing of different component. In this chapter, different kinds of wires, including real internal-Sn multifilamentary conductors, simple Nb-Cu bimetallic wire and the restacked Nb-Cu multifilamentary wire, were drawn, and their interfacial characteristics were investigated by using microscopic techniques. Based on the microscopic observation, the bonding

mechanism during co-drawing process was proposed and the corresponding theoretical evaluation method was discussed.

5.1 Experimentation

5.1.1 Sample Preparation

Looking at the restacked wire (shown in Figure 5.1), the bonding problem is mainly in the lack of bonding between the Cu sheaths of the subelements, between the outer Cu can and the Cu sheaths of subelements, and between the Nb barrier and Cu sheaths if barrier is inserted inside the outer Cu can. In order to investigate the basic bonding characteristics during the co-drawing process, we started with the co-drawing of a bimetallic rod, Nb rod cladded with Cu layer, which is called monofilament. When this wire was drawn to certain size, it was hexed and then cut into short pieces to be ready for restacking. Then the seven pieces were cleaned and restacked into a Cu can, thus a 7-restack billet was accomplished. The bonding between the Cu sheaths of the mono filaments and between the Cu can and the Cu sheath of mono filament, and the bonding between Cu and Nb in the filament have been investigated. Figure 5.2 summarizes the fabrication routes in this experiment. All the drawing experiments were done using a draw bench. Drawing oil was used as the lubricant to reduce the friction. The series of dies used in this drawing are carbide die with half die angle of 6 degrees. Drawing speed used was 75 mm/s.

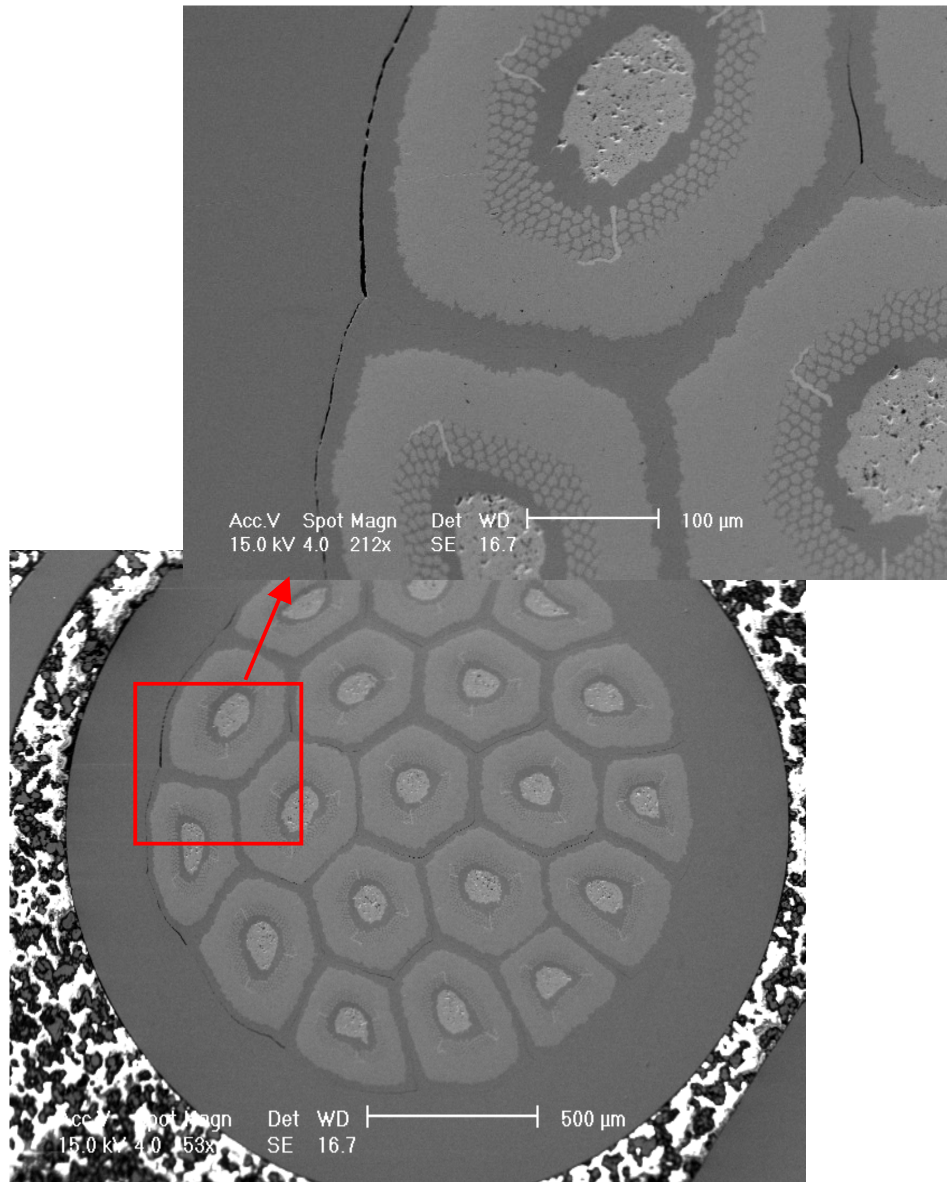

Figure 5.1 Cross-section of 19 restack wire showing the lack of bonding between the components.

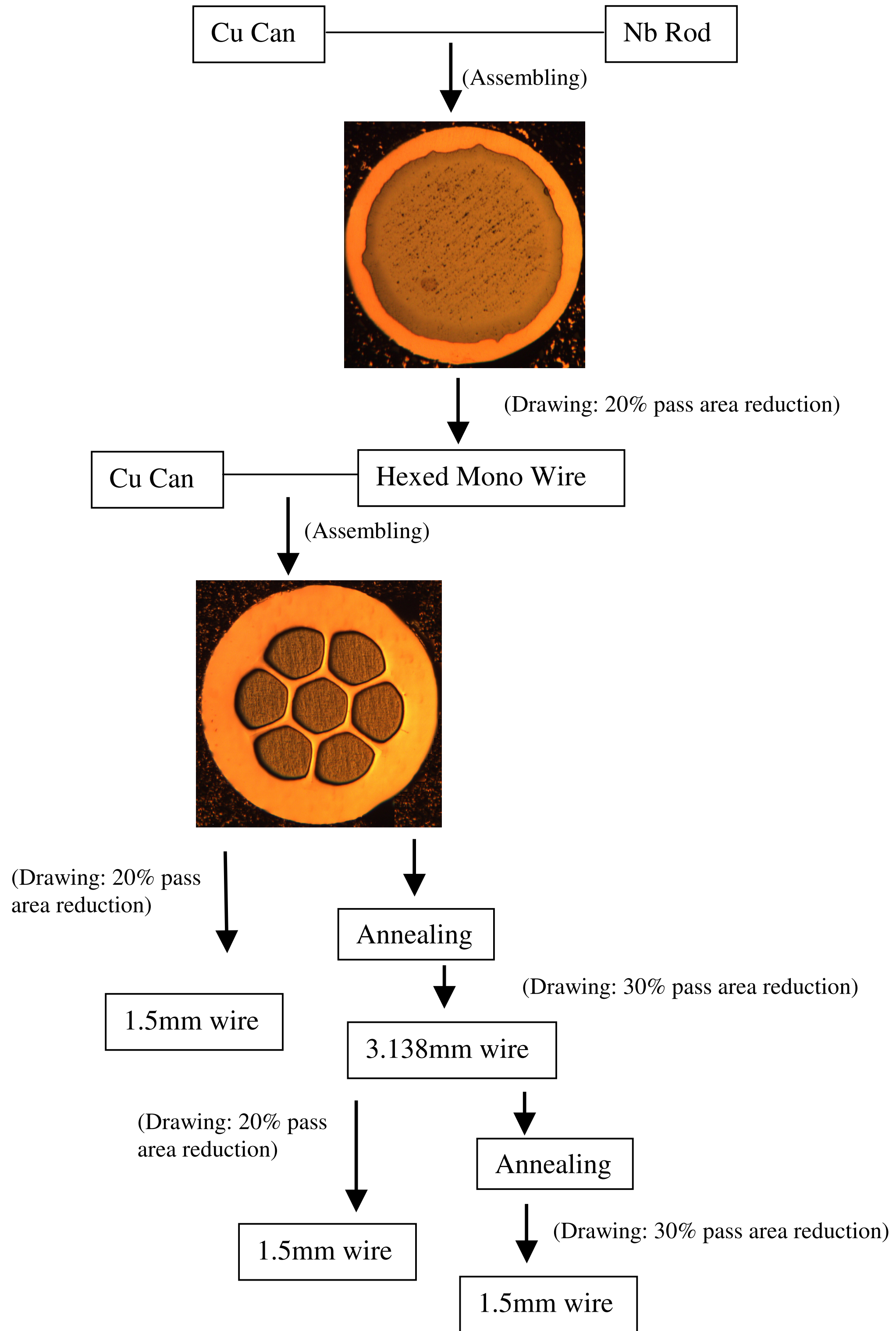

Figure 5.2 Fabrication Routes of Nb-Cu Composite

Specifically in this experiment, the starting Nb rod is annealed and has a diameter of 1/4", and the Cu tube is fully hardened and its outsider diameter (OD) is 3/8" and its thickness is 0.020". At the beginning, the Cu tube was drawn down to the size to fit for the internal Nb rod. The diameter of the assembled mono wire is about 7.29mm. This assemble wire was then drawn down to smaller sizes through a series of dies with different sizes. The following drawing schedule was realized:

ϕ7.29mm →ϕ6.561mm →ϕ5.904mm →ϕ5.314mm →ϕ4.732mm →ϕ4.304mm →ϕ3.874mm →ϕ3.486mm →ϕ3.138mm →ϕ2.824mm →ϕ2.541mm →ϕ2.287mm →ϕ2.058mm →ϕ1.853mm →ϕ1.667mm →ϕ1.5mm →ϕ1.35mm →ϕ1.094mm →ϕ0.984mm →ϕ0.886mm.

A part of the wire with diameter of 1.853mm was saved for the next restack. The mono wire was hexed through a hex die with point-to-point distance of 0.076", and then was cut into seven pieces and restacked into a Cu tube with outside diameter of 7.25mm and thickness of about 1.0mm. The 7-restacked wire was separated into two batches, one was directly drawn down to small sizes and the other one was annealed under 850 °C for 2 hours to improve its drawability. These two restacked wires were drawn down to smaller sizes by different schedules as follows:

Restack I

ϕ7.29mm →ϕ6.561mm →ϕ5.904mm →ϕ5.314mm →ϕ4.732mm →ϕ4.304mm →ϕ3.874mm →ϕ3.486mm →ϕ3.138mm →ϕ2.824mm →ϕ2.541mm →ϕ2.287mm →ϕ2.058mm →ϕ1.853mm →ϕ1.667mm →ϕ1.5mm. The pass area reduction is around 20%.

Restack II

ϕ7.29mm →ϕ5.904mm →ϕ5.041mm →ϕ4.304mm →ϕ3.675mm →ϕ3.138mm →ϕ2.824mm →ϕ2.541mm →ϕ2.287mm →ϕ2.058mm →ϕ1.853mm →ϕ1.667mm →ϕ1.5mm. The area reduction of the first few passes is around 30%, and then changed to 20% due to the occurrence of fracture. In order to keep the 30% pass area reduction, the wire with diameter of 3.138mm from Restack II, which is at the beginning of fracture, was annealed for the second time to increase its drawability. The annealed wire was continued with 30% area reduction following this schedule:

Restack III

ϕ3.138mm →ϕ2.679mm →ϕ2.287mm →ϕ1.953mm →ϕ1.667mm →ϕ1.5mm.

Prior to the assembly of mono wire and restacked wire, all the component wires must be thoroughly cleaned in order to be free of oxide and other surface defects. The cleaning procedure includes degreasing, acid etching, rinsing in water, and then in acetone and methanol. The clean surfaces lead to the easier bonding between the components. In this experiments, the pass area reduction and total deformation are the variables for determining the bonding characteristics. Different samples were picked up for the microscopic observation and bonding test to study the effect of deformation and pass area reduction on the bonding generation and the bonding mechanism during the co-drawing.

5.1.2 Interfacial Observation

Optical Microscopy and Scanning Electron Microscopy (SEM) are the main techniques to be used to observe the interfacial properties. Also, Focused Ion Beam (FIB) technique was used to cut into the Cu-Cu, Cu-Nb interfaces to show the fresh interface under high resolution SEM attaching with FIB. Based on the above drawn wires, four groups of samples were selected and compared. The first group is the Nb-Cu bimetallic wires. Three sizes of wire were selected to show the bonding between Nb and Cu: 6.561mm, 1.5mm, 0.886mm. The total area reductions that these wires experienced are 19%, 95.8%, 98.5% respectively. Figure 5.3 shows interfaces in these wires with different area reduction. Firstly, Nb rod was just mechanically assembled in the Cu tube, and they are lack of bonding even after the first pass. Through the continuous drawing, the wire was reduced to smaller sizes and the components got gradually bonded. In size of 1.5mm wire, most area in the interface was partially bonded as shown in figure 5.3 (b), with cavities existing at the interface. If looking at the even smaller size wires, these cavities disappear and smooth boundary line is there as shown in figure 5.3 (c). The joint boundary is wave-shaped.

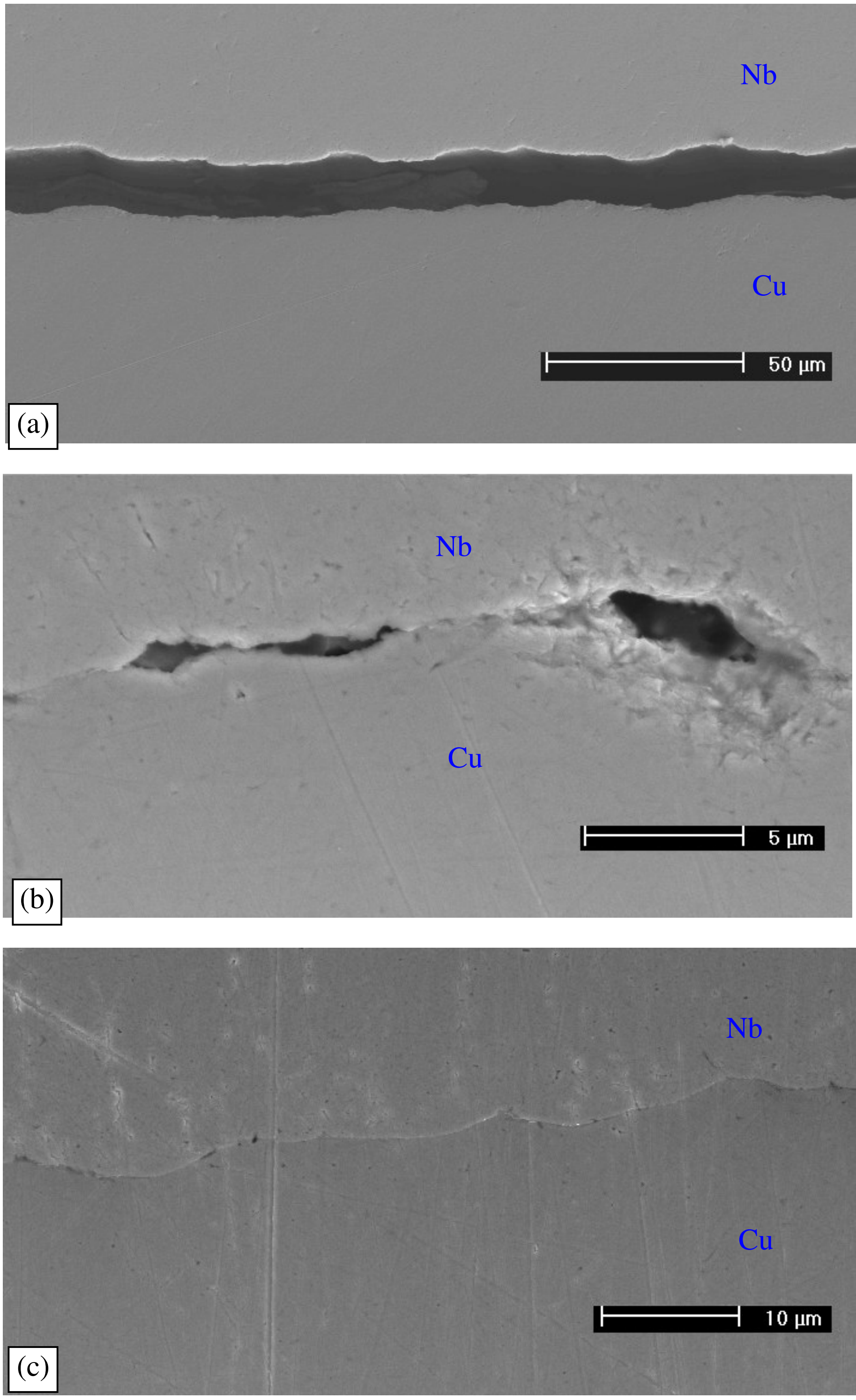

Figure 5.3 Bonding in the bi-metallic wire

The second group is Restack I which is the 7-restacked wire without annealing before drawn. Lower pass area reductions were used for this wire due to its relative lower drawability. The pass area reduction is about 20%. Two sizes of wire were selected: 1.853mm and 1.5mm, and their total area reductions are up to 93.5% and 95.8% respectively. In the assembled wire, all the components are lack of bonding as that in the monofilamentary wire. Moreover, in its component, the drawn mono rods, the Nb and Cu are also lack of bonding as we see in the bimetallic wire. Figure 5.4 shows the interfaces in the selected wires. In the 1.5mm wire, as a whole, the components have been bonded with each other. However, if taking a close-up observation, Nb is still not metallurgically bonded to the Cu in the monofilaments, and the bonding of Cu-Cu has not been formed in everywhere. From these observations, we know that the bonding between Cu and Cu is easier to generate than those between Nb and Cu. This agrees well with the results from the standard pressure bonding that the metal with higher melting temperature is more difficult to get bonded that that with lower temperature. FIB was used to cut into the interface to observe the fresh interface. Figure 5.5 shows the Nb-Cu and Cu-Cu interfaces in the 1.5mm wire under FIB. Good bonding was observed in these interfaces.

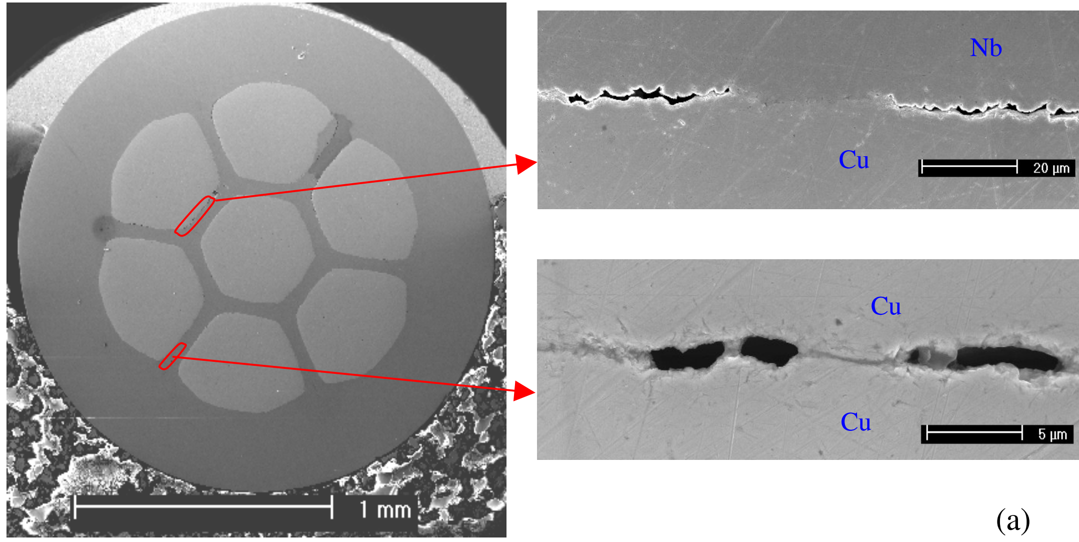

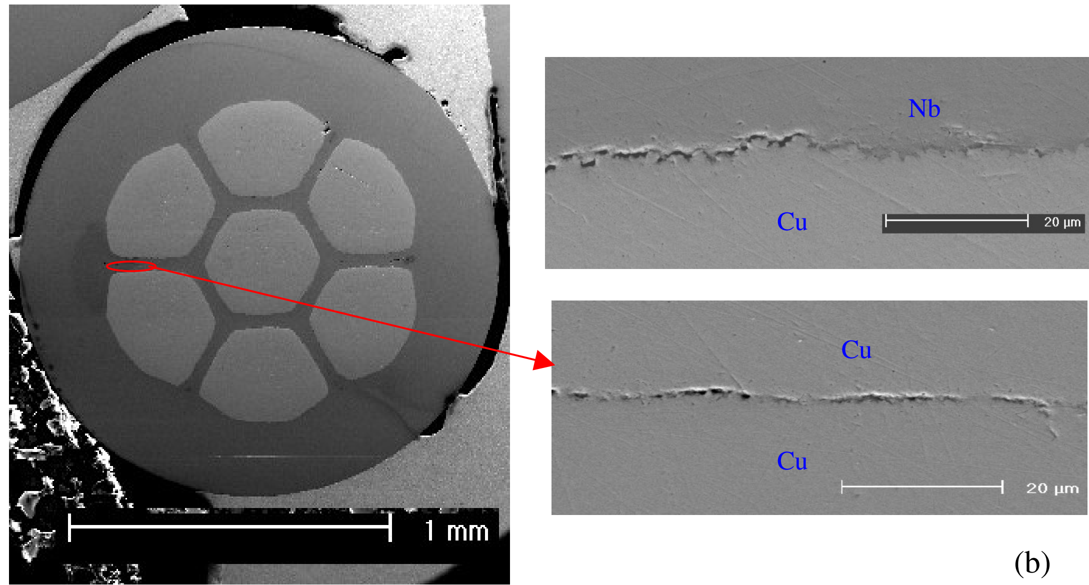

Figure 5.4 Bonding in the unannealed restack wire

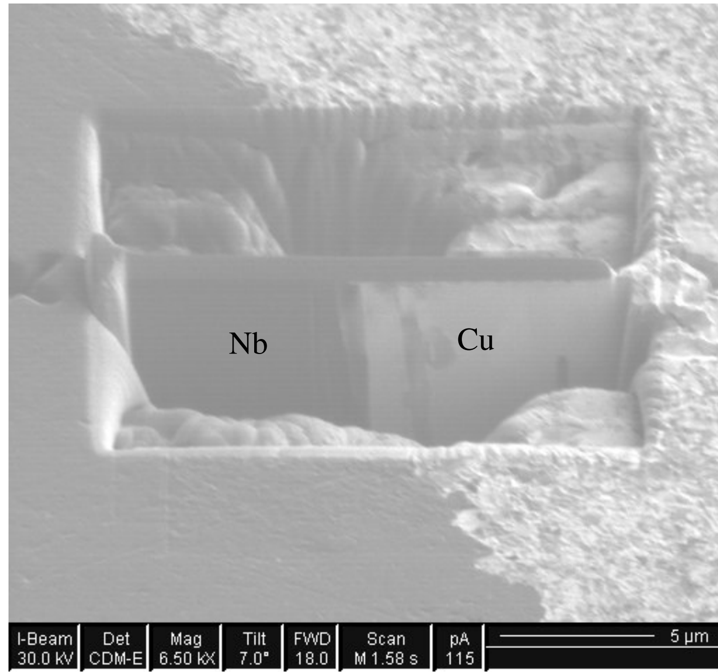

Figure 5.5 Bonding in the unannealed restack wire

The third group is Restack II which is the 7-restacked wire consisting of monofilaments annealed under 850 °C for 2 hours, which results in the increase of the pass area reduction of the first few passes until the breakage. Figure 5.6 shows the cross-section of 1.5mm wire and its interfaces. In the monofilaments, metallurgical bonds form between Nb and Cu, but there still lacks bonding between Cu and Cu. Comparing with the unannealed wire, the Cu-Cu bonding condition is even worse in the annealed case. This is due to the heavy oxide in the external surface of Cu formed in the annealing. We did not etch the monofilament but just regularly cleaned it before restacking. This oxide layer hindered the bonding creation during the drawing process. Higher area reduction might be better for the bonding. Hence we picked up a short piece at size of 3.138mm and annealed it, then use the 30% pass area reduction to draw it, which is our fourth group. As a result, perfect bonds between Cu and Cu, and between Cu and Nb have been created. Figure 4.7 shows the cross section of 1.5mm wire and the close-up look of the interfaces. Through these series of experiments, we got a brief idea that the pass area reduction is important for the bonding generation and larger area reduction leads to stronger bonding. Surface quality is another important factor influencing the interfacial bonding. The oxide in the interface hampers the bonding. Effective cleaning including etching and rinsing is a necessary step for the components before assembly.

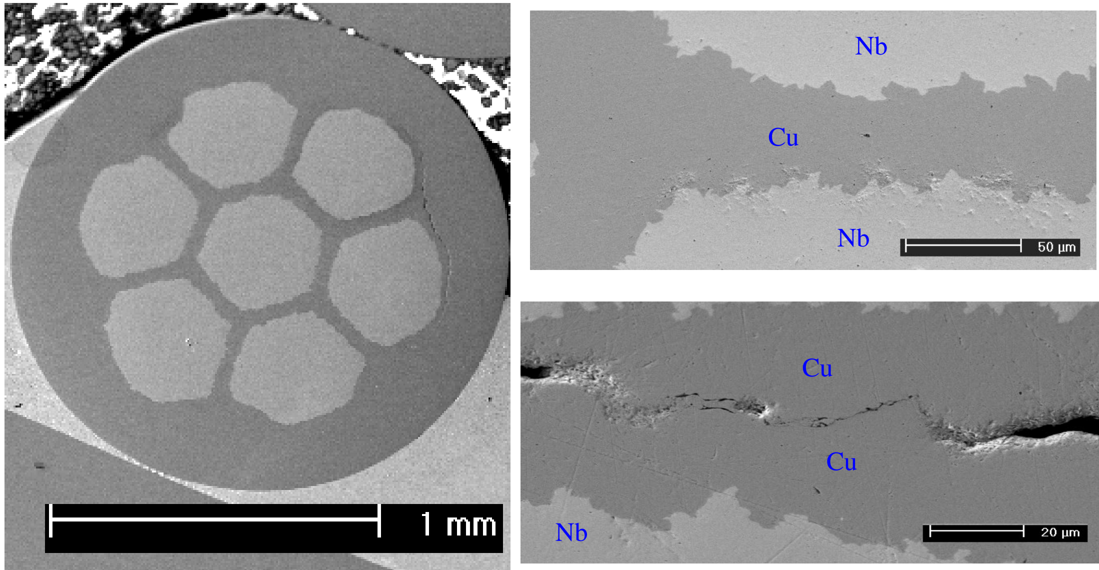

Figure 5.6 Bonding in the annealed restack wire

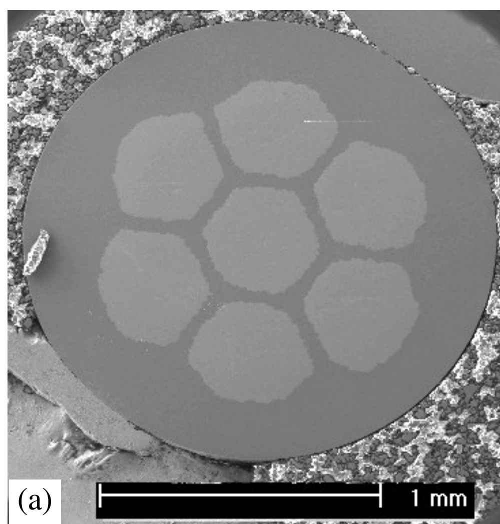

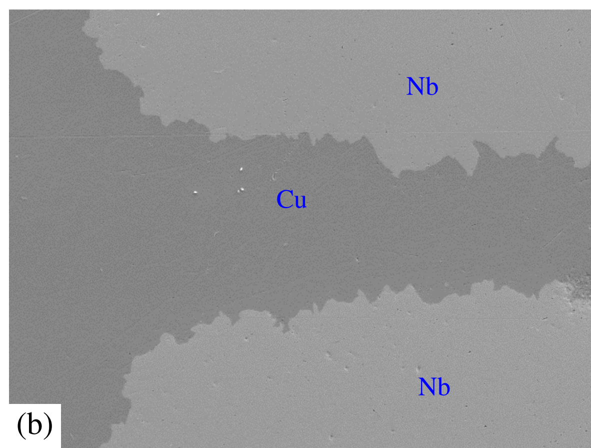

Figure 5.7 Bonding in the annealed restack wire

5.1.3 Interfacial Bonding Strength Test

The microscopic observation confirms that bonding could be created through co-drawing. But how much bonding could be created and how the drawing processing parameters affect the bonding generation are still questions in our mind. In this section, a special push-out bonding test was designed to evaluate the interfacial bonding strength between the inside component with the outside one through modifying the push-in testing in identifying the adhesion between the fiber and its resin matrix. Figure 5.8 shows the schematic drawing of this test. The samples were cut into slices, and both cross-sections of the slice were polished by sand paper. The cross-sectional area of the core component was measured before the testing. A force parallel to the axis is applied to push the inside component out. This test was conducted on a standard MTS Tensile Test Machine. The shear load was recorded as a function of crosshead travel. Figure 5.9 shows the typical curve recorded in this test, which is the change of load with the travel distance of the crosshead. The maximum force, $F_{\max}$, was the force to start separating the internal component from the external sleeve, which was used to calculate the bonding strength, the shear strength of interface following this equation:

$$\tau = \frac{F_{\max}}{2\pi \cdot r \cdot l}$$

Where τ is the bonding strength, r is the diameter of the internal component, l is the contact length between the internal and external component, and $F_{\max}$ is the maximum force for starting debonding. The speed of the crosshead is 0.02 mm/s.

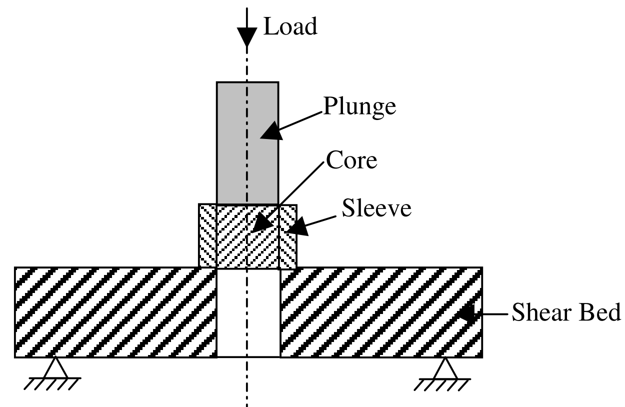

Figure 5.8 Schematic drawing of the Push-in Test for measuring the bonding Strength Between two Components

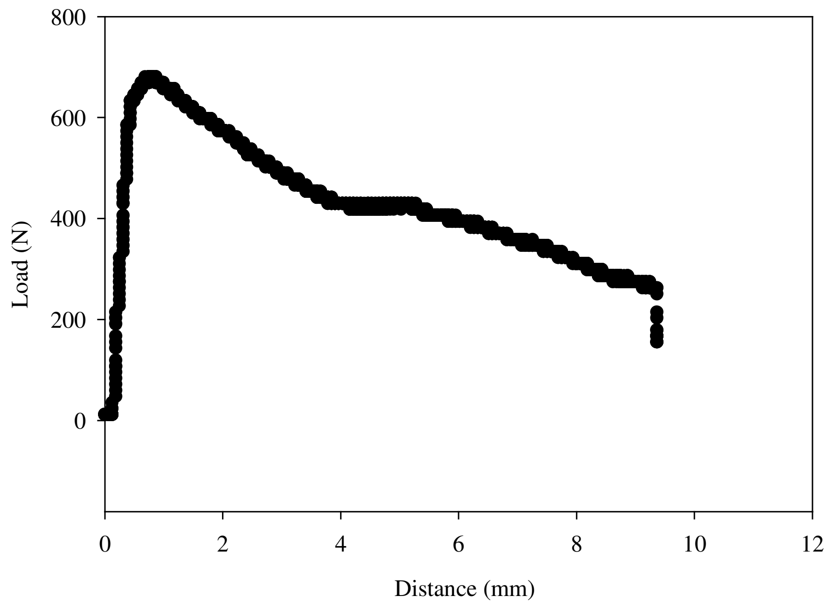

Figure 5.9 Typical Bonding Test Curve

Table 5.1 and Figure 5.10 show the test information for the Nb-Cu mono wires with different sizes. All these data shows that the wires experiencing higher deformation have stronger bonding although their pass area reduction is almost the same, 20%. With higher deformation, the exposed fresh surfaces will be larger which improve the possibility of bonding. However, the measured bonding strength is not high enough to confirm that there exists metallurgical bonding between the Nb and Cu in the monofilament which is due to the lower pass deformation and thereby the lower pressure exerted on the interface.

Diameter (mm)	Length (mm)	Total Area reduction (%)	Force (N)	Bonding Strength (MPa)
4.732	3	57.87	704.83	18.4
3.874	2	71.76	621.21	29.7
3.138	2	81.47	680.94	40.4
1.853	2	92.82	633.15	60.6
1.5	1.5	95.77	406.14	68.6

Table 5.1 Bonding strength in the Nb-Cu monofilaments

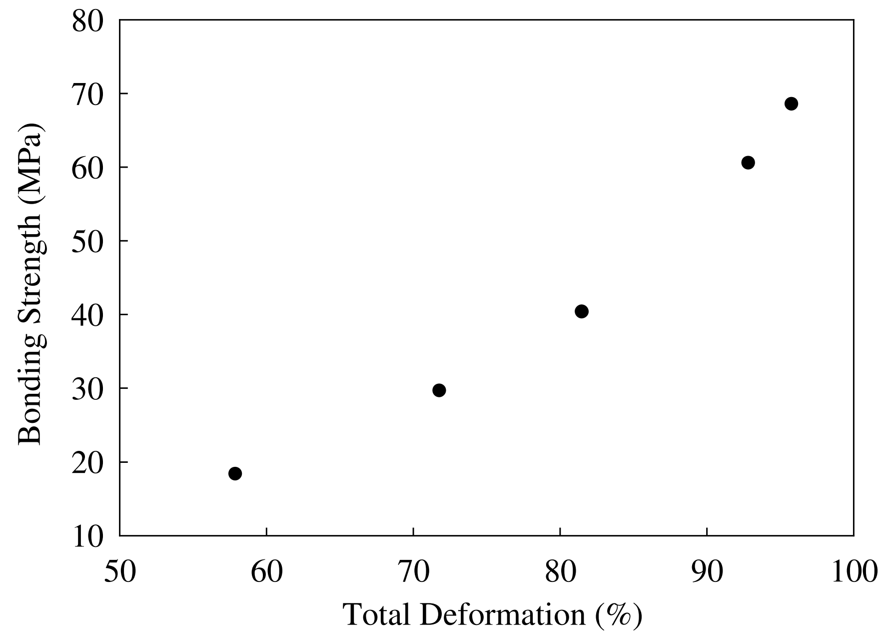

Figure 5.10 Nb-Cu Bonding Strength changes with total deformation in the monofilaments

This test has also been used to evaluate the bonding created in the restacked wire. Since the monofilaments in the restacked one are too small to find proper ram to push it out, only the bonding between the outer sleeve and the inside filaments was measured which is similar to that for the monofilament. Table 5.2 and Figure 5.11 shows the bonding strength of interface between Cu to Cu in the drawn restacked wires. It shows the rising trend with the increase of the total deformation although it does not indicate a perfect bonding through the drawing. Moreover, for the third group, the bonding strength increases very rapidly which shows that the area reduction is very important for the bonding creation.

Wire Diameter (mm)	Measured Bonding Strength (MPa)		
	Restack I	Restack II	Restack III
5.904	8.53	6.72	
4.304	24.5	28.4	
3.138	42.5	44.3	
2.287	52.9	54.2	86.3
1.667	71.2	68.2	103.6
1.5	81.3	75.9	114.8

Table 5.2 Cu-Cu Bonding strength in the restack wires

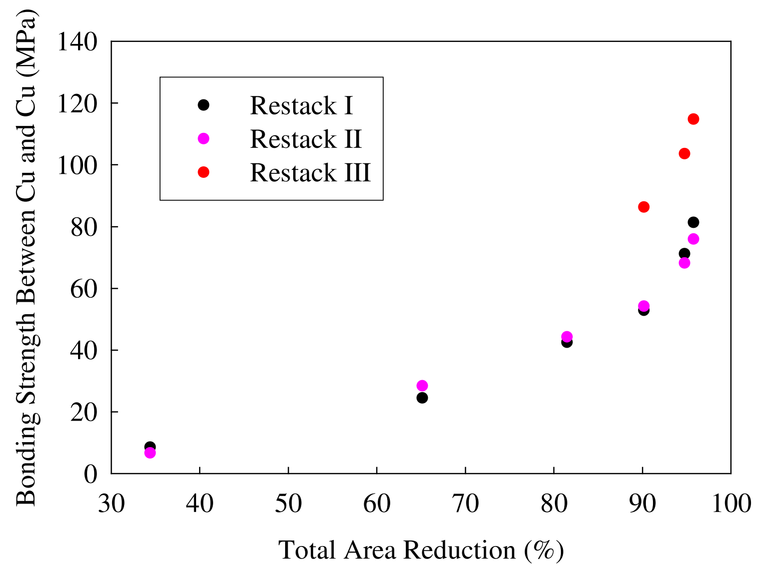

Figure 5.11 Cu-Cu Bonding Strength changes with total deformation in the restacked wires

5.2 Theoretical Evaluation of Interfacial Bonding Generated during Co-drawing

From the above images and bonding test, we know that the components could be fully or partially bonded during co-drawing. With the high deformation and high pass area reduction, the bonding state would be improved. In this section, a theoretical evaluation of this bond strength will be calculated by modifying the rules proposed by N. Bay for pressure bonding.

5.2.1 Description of Bonding Mechanism in Co-drawing

From the previous sections, we have already noticed that the bonding during co-drawing process is gradually generated. After restacking, the different components have just been mechanically assembled together. The surfaces of the components are originally not flat and straight but wave-like and undulant. When the assembled wire goes through the conical die, the components deform independently at first and the wire is lengthened, thereby new external area is created which is possibly only the stretching of surface oxide and contaminant layer. Hence, no any bonding is created in the first few passes. With the continuous drawing, when the deformation is enough to break up the thin contaminant and oxide layer on the interface, the virgin surface of the metals exposes to each other. At this time, if the pressure exerted by the die is large enough, the naked fresh surfaces will be close enough to be atomically bonded, thus metallurgical bonding occurs. Hence, the bonding occurring in the co-drawing process is a kind of pressure bonding. Pressure and

the exposed virgin surfaces are important factors for the creation of bonding. Figure 5.9 and Figure 5.12 are the close-up images of the Cu-Nb and Cu-Cu interface in the restacked wire respectively showing the partially bonded interfaces.

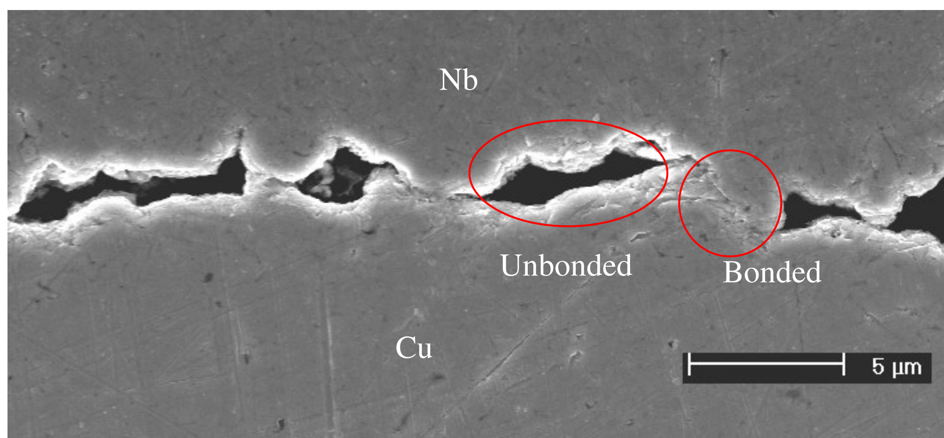

Figure 5.12 Interfacial Bonding

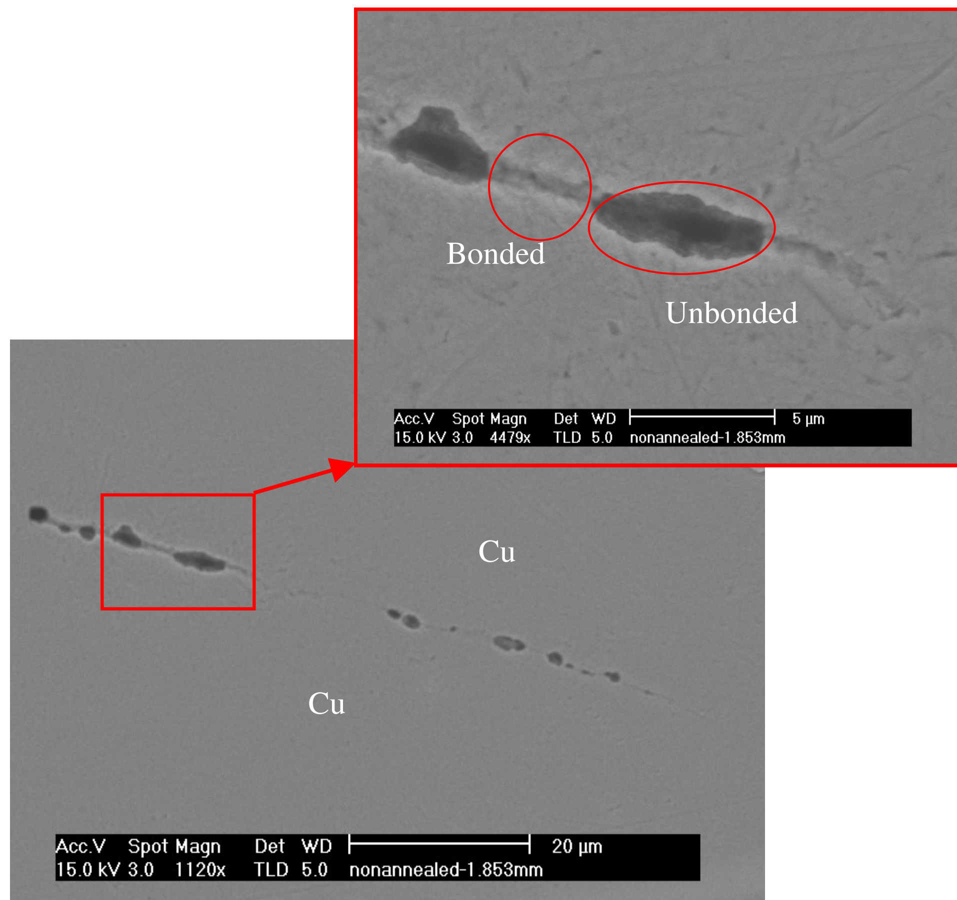

Figure 5.13 Interfacial Bonding

5.2.2 Theoretical Evaluation of Bonding generated in Co-drawing

As a kind of pressure bonding, the bond strength can be increased through an increase of true contact area in the co-drawing bonding process. The bond strength is essentially a summation of the adhesion strengths of interfacial grains. Interface impurities such as oxides, contamination layers, and foreign particles greatly affect the bond strength. During the drawing process, the sheared materials at the interface are highly stressed, atomically clean, and therefore very reactive. The heavy deformation during drawing process breaks up any oxide layer which may have formed in the time interval between cleaning and billet assembly and thereby creates new atomically clean surfaces. From previous standard pressure bonding experiments investigation, there exists a threshold surface exposure, $Y' = (A' - A_0)/A'$, which is necessary to break the thin oxide layer. In this expression, A_0 is the interfacial area before deformation, and A' is the area corresponding to the threshold surface exposure. From their results, the threshold surface exposure of Cu to Cu is about 44%. Unfortunately no data could be located for the threshold surface exposure of Nb. Based on our bonding test results shown in the previous section in this chapter, the bonding stress is about 29MPa when the deformation is about 71.76%, after which the bonding strength increases more obviously. Hence, we assumed a threshold of starting bonding of , which is corresponding to the threshold surface exposure of 46.8%. This threshold surface exposure indicates that a corresponding threshold of deformation is needed to initiate bonding, below which no bonding occurs. Pressure is another basic parameter of importance in the formation of

bonding during co-drawing. Pressure primarily increases the development of bonding above threshold deformation.

In order to estimate the bond strength created during co-drawing, Bay's pressure welding model [54] was modified and applied. In this case, the component materials are assumed to be cleaned before assembly, but slightly contaminated or oxidized afterwards. Then the metal-to-metal contact will be intermittent within the contact regimes generating the true bonding force. Figure 5.12 and 5.13 shows the real intermittent bonds formed during the co-drawing process. Figure 5.14 is the schematic outline of the bonding mechanism. Based on this bonding mechanism, we define the interfacial bonding strength as the apparent bonding stress, which is the stress required to separate the two surfaces, namely the unit force, F, in the whole apparent area, A_a.

$$S_{\mathrm{BF}} = F / A_a \qquad (5.1)$$

Where S_{BF} is the apparent bonding strength which we are interested in.

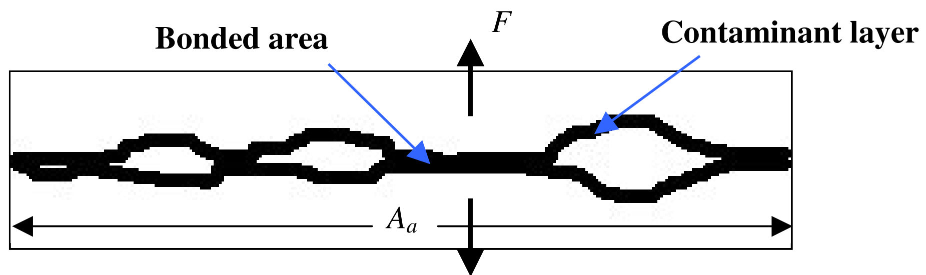

Figure 5.14 Schematic outline of co-drawing bonding

However, the bonding is gradually created during the drawing process. Usually only partial surface has been actually bonded in certain conditions while the left surface has not. Hence, we could rewrite the expression of the required force, *F*, for separating the two surfaces as:

$$F = S_{\mathrm{BF}} \cdot A_a = S_{\mathrm{BFT}} \cdot A_t \qquad (5.1)$$

Where S_{BF} is the apparent bonding stress, S_{BFT} is the true bonding strength of real contact surfaces which is almost equal to the applied normal pressure N [92], A_a is the apparent area after deformation, A_t is the actually contacted area which is expressed as the following:

$$A_t = A_a - A' \qquad (5.2)$$

Where A' is the area corresponding to the threshold deformation. Thus, we could calculate the apparent bonding stress.

In the co-drawing process, the deformation area is also the bonding area which is in the die area as shown in Figure 5.12. The wire is drawn through the conical die and plastic deformation occurs which creates newly fresh area at the interface. The die exerts normal pressure on the wire and thereby the interfaces, which is the main parameter to develop the bonding. Hence, the normal pressure at the interface and the deformation are necessary to be known for the evaluation of bonding. However, these two parameters are all dependent on the drawing parameters such as area reduction, die angle, the lubricant conditions and material itself which is complicated. Moreover, the distribution of the normal pressure and deformation along the deformation area is non-uniform. In this document, finite element method (FEM) has been used to investigate the mechanic conditions during the co-drawing process, which will be described in the following

chapter. Then the rules defined in this chapter will be combined with the mechanics to calculate the bonding strength corresponding to different drawing parameters.

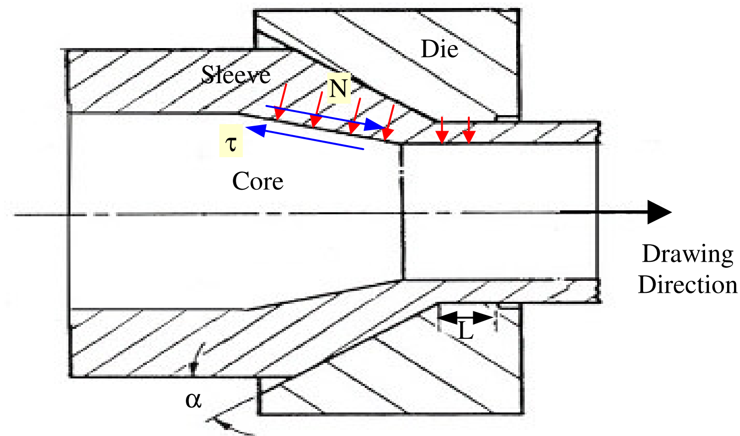

Figure 5.15 Schematic outline of co-drawing

5.3 Summary

The bonding creation during the co-drawing process of the bi- and multi-component wires has been investigated in the chapter. The bonding process during the co-drawing

process is a kind of pressure bonding. During the drawing process, the thin oxide and contaminant layer on the contacted interfaces was broken at first due to the deformation, which leads to that the virgin surface of the metal was exposed to each other directly. When a high enough pressure was exerted on them, the two virgin surfaces will push to each other and creates the bonding. Area reduction is a crucial factor for the creation of interfacial bonds during co-drawing. A larger area reduction results in the increasing of normal pressure on the interface which promotes the interfacial bonding. Surface conditions are also important for the creation of bonding. An effectively cleaned interface is helpful for the bonding.

CHAPTER 6

6. Theoretical Investigation of Bonding during Co-drawing

Pressure and original contact area are the most important factors for the creation of bonding during co-drawing of composite. All these factors are dependent on the drawing process parameters including die configuration, pass area reduction and lubricant condition, and the material itself including the mechanical properties of the components and the assembly ratio of each component. Due to the influence of all these factors on interfacial bonding creation, modeling of deformation behavior and stress state within the conical deformation is essential for the co-drawing bonding. Models have been well established for predicting drawing force even stresses distribution in regular drawing of single material rod. However, no attention has been paid to the bonding during co-drawing. Due to the geometrical constraint imposed by the die, it is obvious that the pressure exerted on the materials and the deformation vary with the position within the conical deformation zone. This pressure exerted by the die is transferred from the outer surface to the internal interface to enable the interfacial bonding between two contacted surfaces. This is a very complicated problem relating to material science, mechanic and even thermal science. It’s impossible to use the classic theoretical method such as slab, upper bound method to investigate such details as interface mechanics. Hence, in this work, finite element method (FEM) has been used to investigate the interfacial mechanics

corresponding to various drawing parameters and material assembly. In this chapter, starting with the mechanical properties of the materials relating to the superconductor precursor wire manufacture, then the drawing of bi-metal and multifilamentary wire was focused on, and the development of bonding during co-drawing of bi-metal and multifilamentary was examined by FEM and the and the bonding strength was evaluated by using the modified N. Bay model, which was used in evaluation of the regular pressure bonding.

6.1 Materials Properties

In the manufacture of superconductor precursors, Nb and Cu are the main materials whose characteristics mainly influence the fabrication process. Hence, to understand their mechanical properties is very important for the manufacture. In our application, Cu is fully hardened and Nb is annealed. Two kinds of mechanical test have been taken to investigate their properties: tensile test and Vicker's hardness (HV) measurement. Figure 6.1 and Figure 6.2 are the flow stress curves of Cu and Nb measured by the tensile tests. Cu is fully hardened, and it arrives at the fluctuation value very soon after applying tensile force. For Nb, its hardening route follows the below power law:

$$\sigma = 409.44\varepsilon^{0.248} + 116.1$$

Referring to the drawing process, the HV hardness was measured to show the influence of reduction on the variation of mechanical properties. Figure 6.3 shows the variation of

hardness of Cu and Nb in the drawing process of mono-filament. The horizontal axis is the total area reduction, which is defined as:

$$r\% = \frac{A_0 - A_1}{A_0}$$

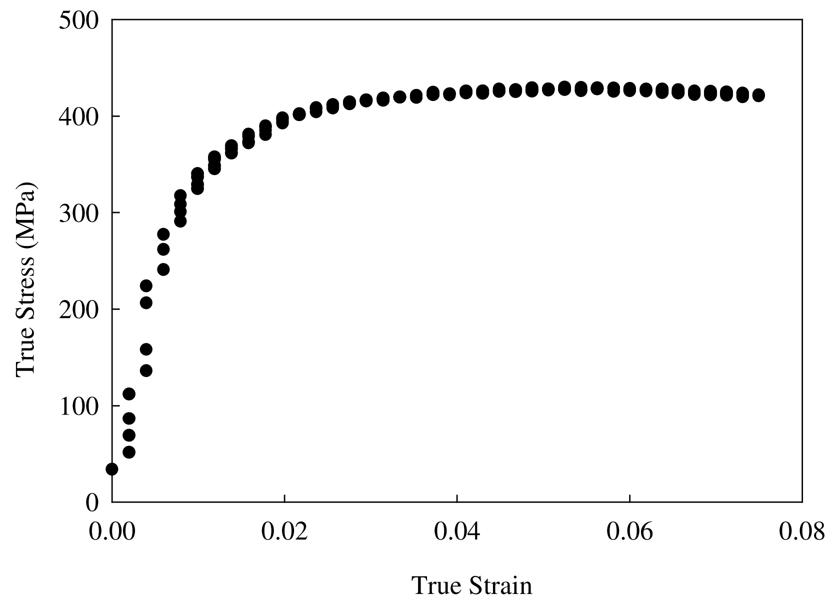

Figure 6.1 Flow stress curve of fully hardened Cu

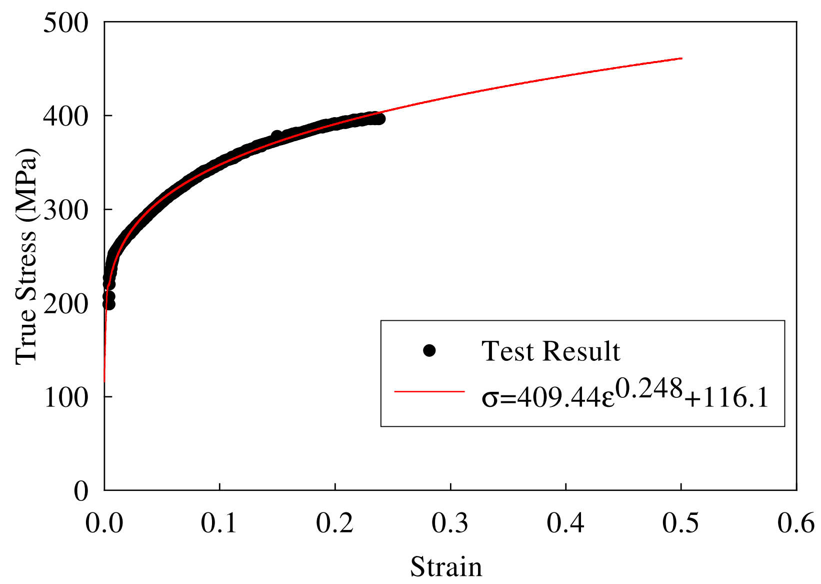

Figure 6.2 Flow stress curve of Nb7.5%Ta

Where $r\%$ is the area reduction, A_0 is the initial cross-section area of the billet, A_1 is the cross-section area of the wire after each pass. Along this drawing schedule, the pass area reduction is about 20%. The hardness is the average value of a few points along the radial direction as shown in Figure 6.4. The distribution of hardness presented in the sleeve of Cu indicates no significant change within the drawing process where its hardness is around 110, and its flow stress is around 425 MPa. The annealed Nb-7.5%Ta hardens very quickly after experiencing a high deformation of 90%. This characteristic brings a big challenge for the drawing of small size wires up to which a significant deformation is always needed. The high strength increases the required drawing force which will lead to the fracture of the weaker material.

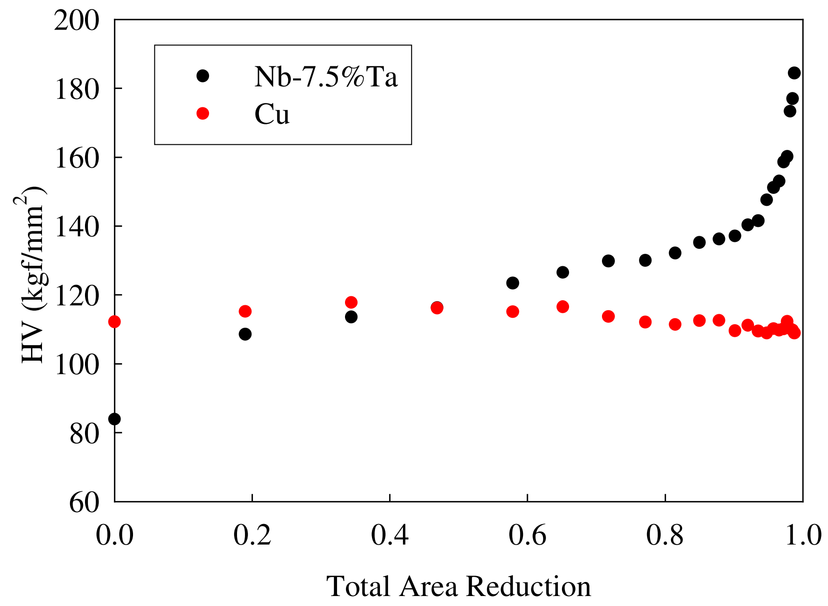

Figure 6.3 Hardness Variation in the drawing process

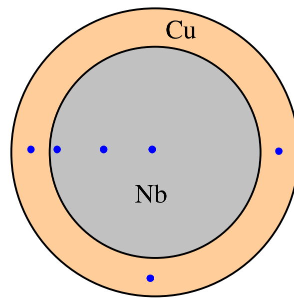

Figure 6.4 Position of Hardness Measurement

6.2 Determination of Friction Coefficient between Billet and Die

The friction can be measured directly or calculated indirectly from the data recorded during drawing process. In this work, it is evaluated by using the slab method. Commercial AWG 6 pure copper wires (has >99.95% Cu) were chosen in this experiment. The diameter of the testing wire is 4.085mm, then this wire was drawn down to 0.5mm by a series of conical carbide die sets, the pass area reduction is 10%. The drawing oil was used as the lubricant, and the load cell was installed to record the drawing force at each pass. Figure 6.5 shows the drawing force at each pass.

Based on the drawing force, slab method, also called the free body equilibrium approach, was used to calculate the friction coefficient under this condition. This method was originally developed to calculate stresses and loads by integrating the differential equation of equilibrium under a simplified stress state. For the drawing of a round rod or wire, generally cylindrical symmetry was postulated and the material was assumed to comply with the Von-Mises yield criterion. In this derivation, the friction between wire and die surface was included and was assumed to follow the Coulomb friction law. What is different from the classic slab method is that the drawing stress required to overcome the shear deformation is also included in this work referring to Altan's book. The final expression for the relative drawing stress is as follows:

$$\frac{\sigma_d}{\bar{\sigma}} = \frac{k}{1+k} \cdot \left[1 - \left(\frac{R_o}{R_f} \right)^{2(1+k)} \right] + \frac{4}{3\sqrt{3}} \cdot \tan\alpha \qquad (2)$$

where $k = \dfrac{\mu \cdot \cot\alpha + 1}{\mu \cdot \tan\alpha - 1}$, σ_d is the drawing stress, $\bar{\sigma}$ is the average flow stress of the drawn material at the die entrance and die exit, R_o, R_f are the radius of wire at the die entrance and die exit respectively, α is the semi-angle of the dies, μ is friction coefficient at the interface between die and wire.

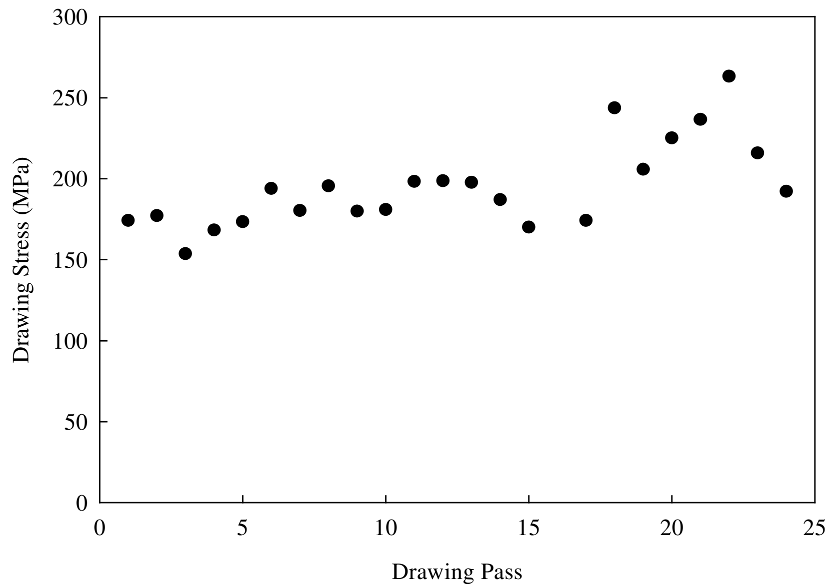

Figure 6.5 Drawing stress for each pass

Following the above equation, the friction coefficient for each pass could be calculated. Figure 6.6 is the results. The friction coefficient is around 0.13, which was used in the later FEM modeling.

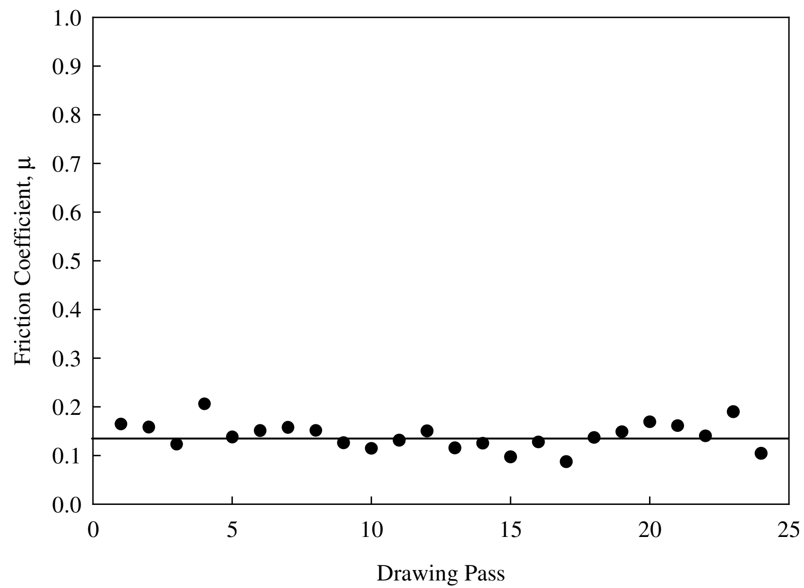

Figure 5.6 Evaluation of Friction Coefficient

6.3 Interfacial Bonding Creation in the Monofilament

6.3.1 FEM model description

The monofilament consisted of an outer Cu sleeve and an inner Nb core. In our model of drawing through a conical die, the billet materials were assumed to be elasto-plastic and to obey the standard Von-Mises plasticity theory with isotropic hardening. Their flow stresses follow the curves plotted in Figure 6.1 and Figure 6.2. The die, which is generally made of high strength steel and much stiffer than the billet, was assumed to be a rigid body. Taking advantage of the cylindrical symmetry of the problem, a two-dimensional, axi-symmetric finite element mesh system was constructed. Four-node, bilinear and quadrilateral axi-symmetric elements were used. Figure 6.7 shows the finite-element mesh of a single-pass drawing as a basis for the multi-pass drawing procedure. The wire movement is achieved by incremental application of the displacement to the wire's front section. For purpose of the numerical analysis, only a short representative part of the wire is taken as the domain of interest that was accordingly discretized by finite elements.

The analysis in this model is composed of two parts. First is the mechanical calculation to compute the stress and strain during the co-drawing process. This is then coupled to a model of heat transfer during the deformation. 90% of the plastic work was assumed to heat the materials, with 10% lost to the environment. Standard ABAQUS program was used in this work to do the simulation.

In this model, the pass area reduction, the die angle, and the ratio of core were pre-selected as the forming parameters. The friction between the billet and the die and between the sleeve and core is assumed to satisfy the Coulomb friction law; the friction coefficient of billet/die interface is from the previous calculation, 0.13, and that of core/sleeve is assumed to be 0.2. Corresponding to the experiments in the previous chapter, multi-pass drawing process was simulated, which was modeled according to the scheme shown in figure 6.8. To ensure objectivity of the computation, the steady state in the drawing process must be achieved at every pass. Besides this, the elastic recovery of the drawn wire after the complete removal of the drawing force between two successive passes has to be properly considered. In this model, the die was removed after drawing a sufficient long part of the modeled wire through the first die, thus allowing the relaxation of stresses due to elastic unloading. With the stress state relaxed, the wire was drawn through the next die. Again when a sufficient length of the modeled wire was drawn through this die, the die was removed and the procedure proceeds in the same manner.

The basic die schedule follows the experimental schedule of mono-filament in chapter 4. Pass area reduction is about 20%, the die angle is 12° and the core ratio is about 75% as shown in figure 6.9. From the bonding test, it seems that the bonding started from the 4.732 mm pass, and thereafter the bonding stress increases with the following drawing. Hence, we assume that the bonding start at this pass, which indicates the threshold bonding of Nb and Cu. In this simulation, our objective is to evaluate the effect of drawing parameters on the bonding process, hence we start from the starting point of bonding, and after 4.732mm, the pass area reduction was changed to about 10%, 30% and 35% to investigate the influence of area reduction. Besides changing the area reduction,

die angle was changed to 20° and 30°. Also, the core ratio was changed from 75% to 60%, the multiple pass drawing was repeated to investigate the effect of core ratio. Figure 6.9 summarized the main drawing schedule simulated in this work. This simulation was aimed at determining the influence of the above-mentioned parameters on the development of bonding in the bi-metallic wire drawing. In order to simulate the multiple passes, restart technique in ABAQUS was used to remain the geometric and stress, strain state of the previous step, and restart the new step from the previous step.

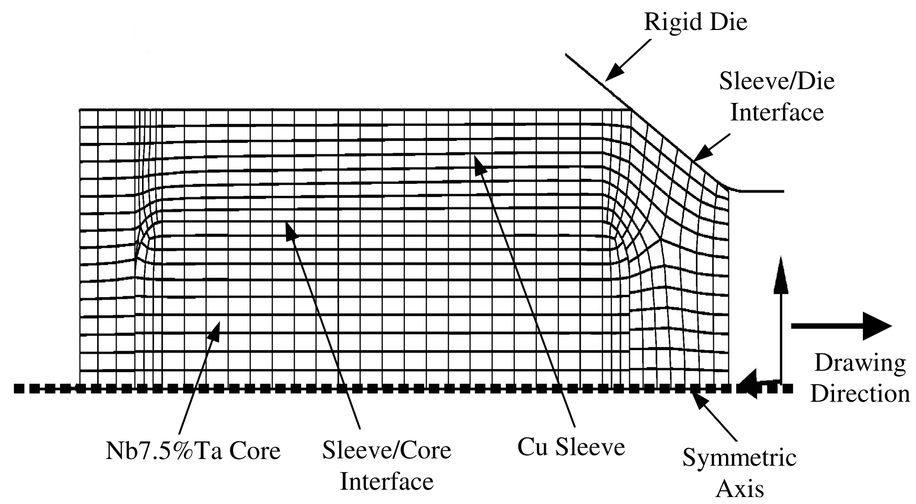

Figure 6.7 Axi-symmetric FEM model of a single-pass drawing Monofilament

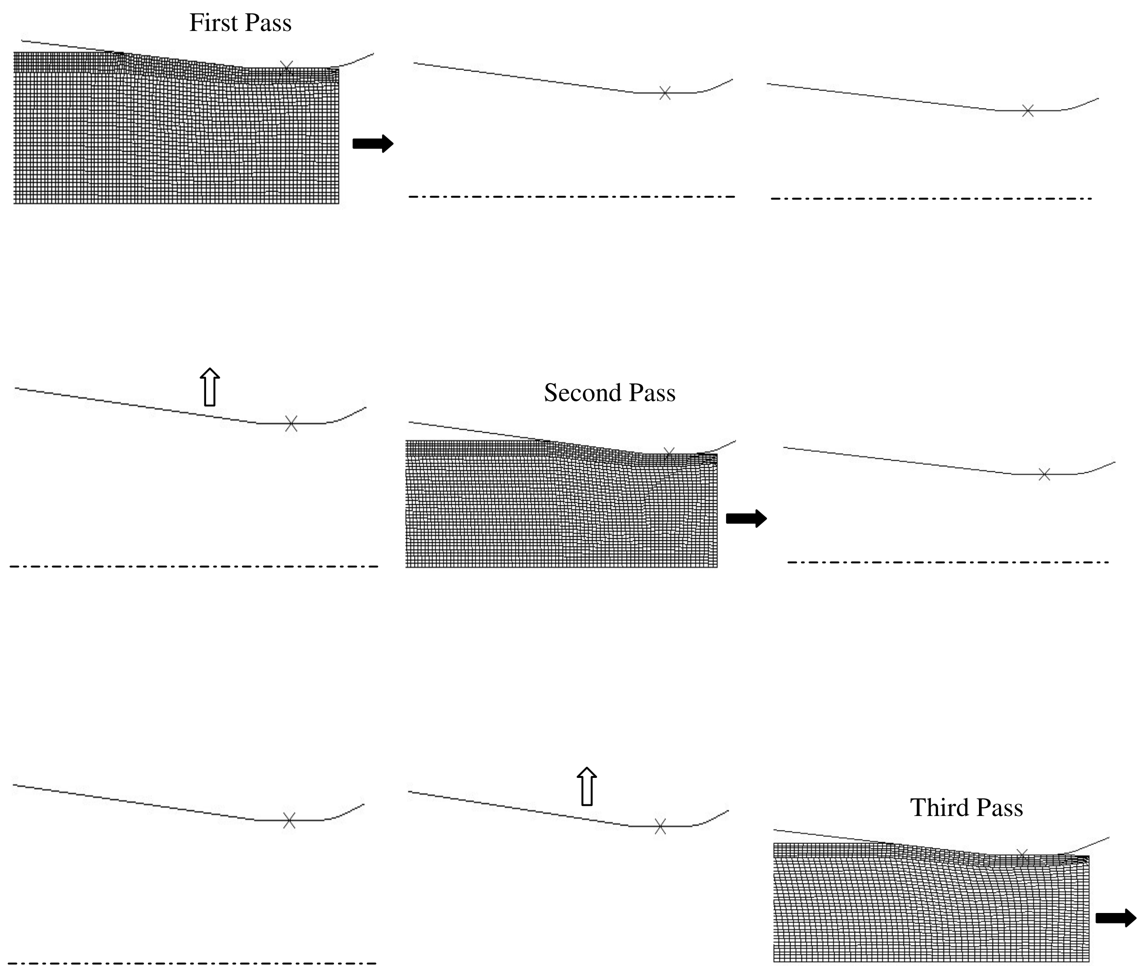

Figure 6.8 Simulation scheme for the multi-pass wire drawing

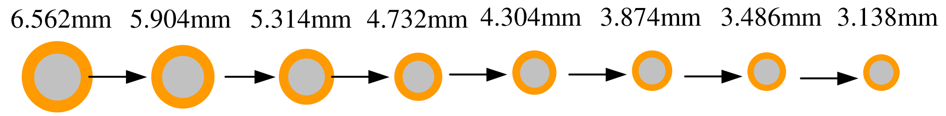

(a) 8 Pass drawing of Nb-Cu billet

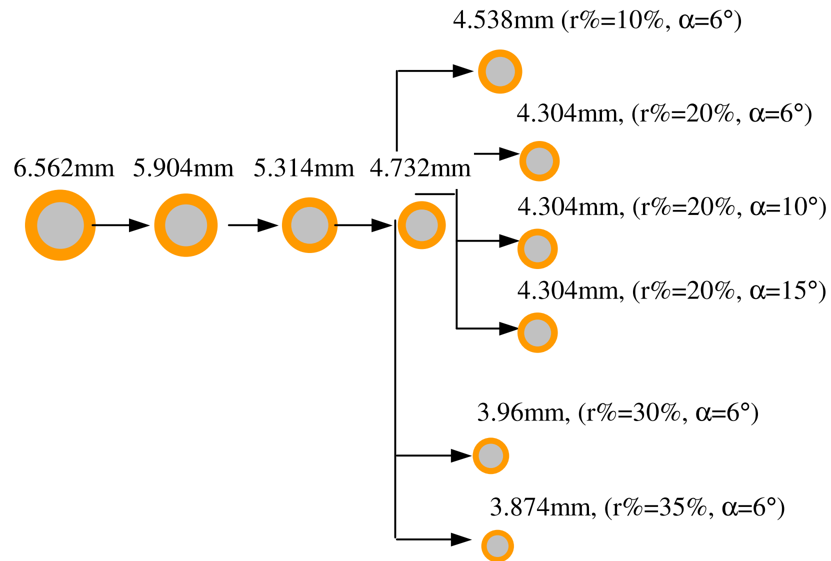

(b) Various drawing parameters

Figure 6.9 Layout of Drawing Schedule in the FEM model

6.3.2 Pressure Distribution at the interface

Initially, during co-drawing, the actual contact between the surfaces to be bonded is confined to a few crests at the surfaces, composing only a fraction of the apparent area. As the drawing proceeds, these crests experience high local pressure, become crushed, and thereby tend to bond across these surfaces. Sufficient pressure in the deformation zone, clean surfaces and sufficient newly created surface during the deformation are required for a satisfactory bond between components during the co-deformation. Figure 6.10 records the normal pressure along the core/sleeve interface under the deformation zone during the multi-pass drawing. The distribution of the normal pressure at the core/sleeve interface in the deformation area is not uniform, and peak values are at the die entrance and die exit. This trend is similar to the distribution of normal pressure on the die surface which is very harmful for the die life. Although the area reduction and die angle are the same in these multiple drawing passes, the distributions of the normal pressure are different. With the ongoing of drawing, the materials work-hardens leading to the increase of the required drawing force. As a result, the normal pressure at the interface also increases.

Figure 6.11 and 6.12 show the change of normal pressure at the core/sleeve interface against changes of die angle and extrusion ratio. Smaller die angles and higher area reductions result in higher normal pressure on the interface, and are thereby more

effective for the inter-component bonding. Obviously, the area reduction is more critical for the higher normal pressure in the interface.

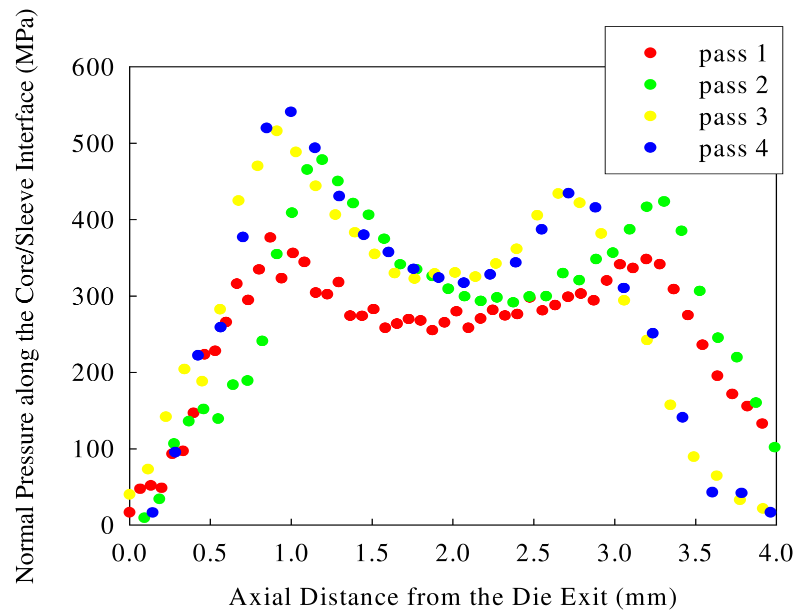

Figure 6.10 Effect of drawing passes on the normal pressure at the core/sleeve interface.

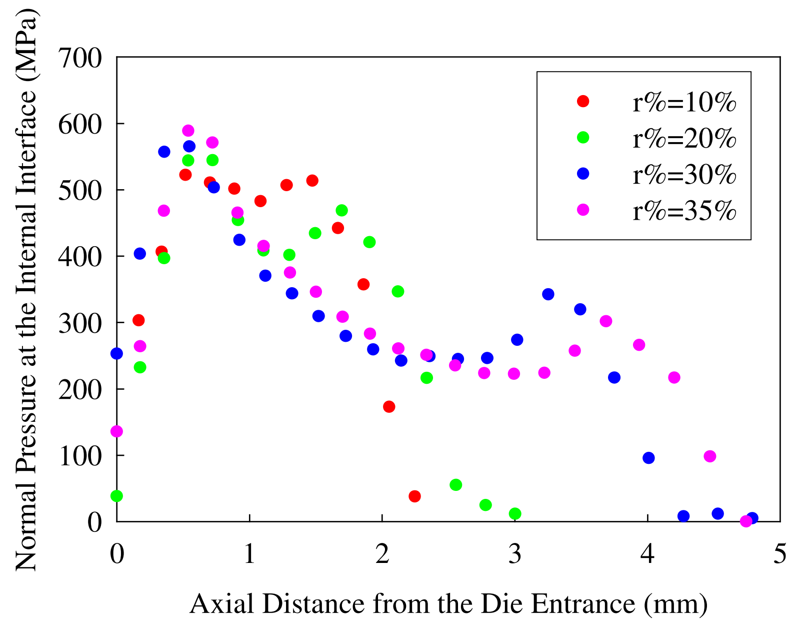

Figure 6.11 Effect of area reduction on the normal pressure at the core/sleeve interface.

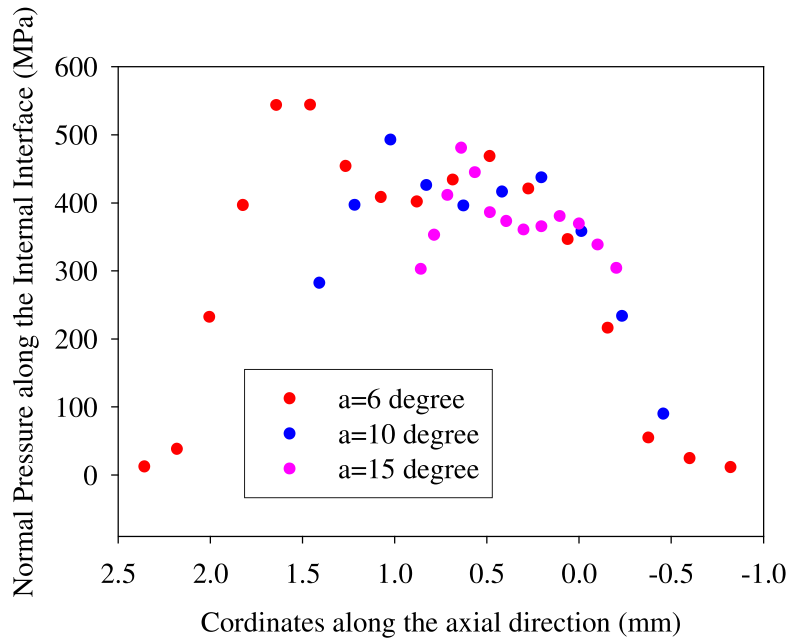

Figure 6.12 Effect of die angle on the normal pressure at the core/sleeve interface.

Figure 6.13 shows the influence of core ratio on the normal pressure. The thicker sleeve results in the lower normal pressure on the interface. The reason is that a thinner sleeve is easy to transfer the force from the die to the interface.

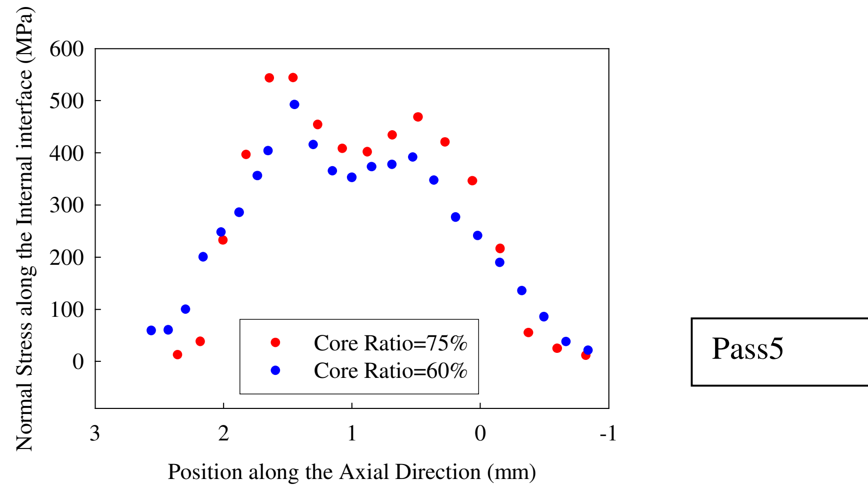

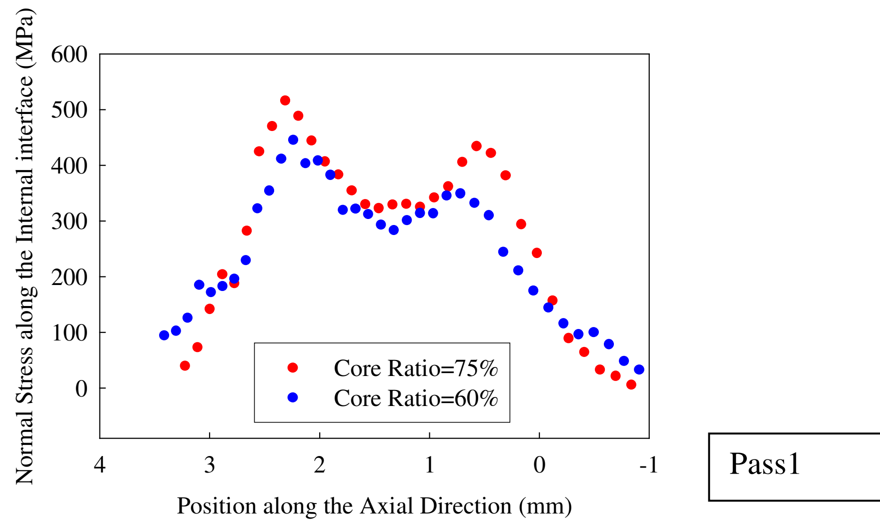

Figure 6.13 Effect of core ratio on the normal pressure at the core/sleeve interface.

6.3.3 Deformation Distribution

Deformation is another critical factor influencing the bonding process in the co-drawing process. For different materials, certain deformation exists for initiating the bonding which is called the threshold deformation. Based on the experimental results in the previous chapter, Nb-Cu bonding initiates at about the total area reduction is about 57%, and Cu-Cu bonding initiates at about 40%. During the drawing process, the deformation is non-uniform in the deformation area due to the profile of the conical die. In order to calculate the expanding of the core/sleeve interface, the profile of the interface under the deformation zone was recorded. Figure 6.14 and 6.15 show the interface profiles with different area reduction and die angle for the 5th pass.

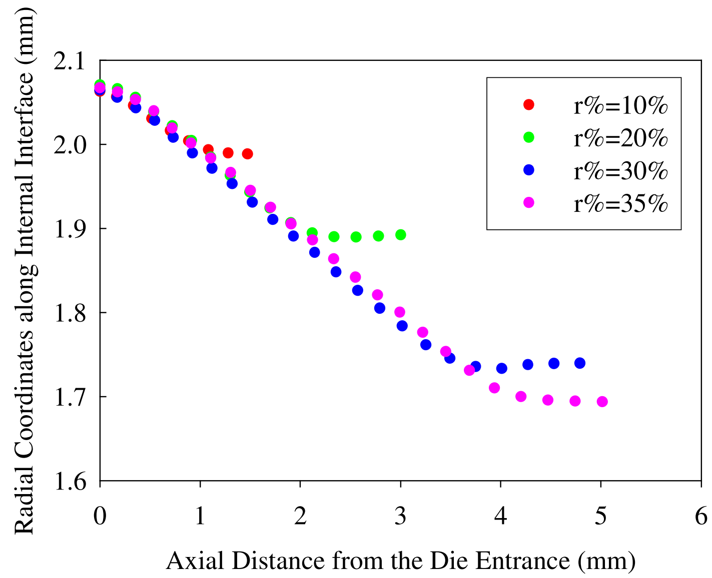

Figure 6.14 Profile of the Core/sleeve interfaces at different area reductions.

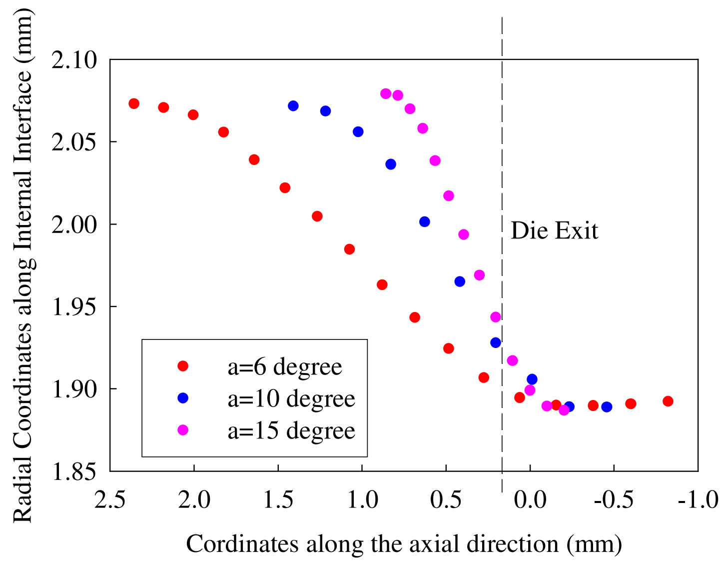

Figure 6.15 Profile of the Core/sleeve interfaces at different area reductions.

6.3.3 Estimation of Bonding Strength

Following the equation 4.1 and replacing the true bonding stress with the normal pressure at the interface, and the below equation was obtained:

$$S_{\mathrm{BF}} = S_{\mathrm{BFT}} \cdot \frac{A_t}{A_a} = N \cdot (1 - \frac{A'}{A_a}) \qquad (6.1)$$

Where S_{BF} is the apparent bonding stress which is what we calculate, N is the normal pressure, A' is the area corresponding to the threshold deformation and A_a is the apparent contact area. Recognizing that the distribution of the normal pressure and deformation along the deformation area is non-uniform, the bond strength at each position is calculated and its maximum value is defined as the bond strength created in the process. Figure 6.16 shows the effect of area reduction and die angle on the created bond strength. Bonding is more responsive to area reduction than to die angle. An increase of area reduction and reduction of die angle lead to stronger interfacial bonding while the effect of die angle is smaller.

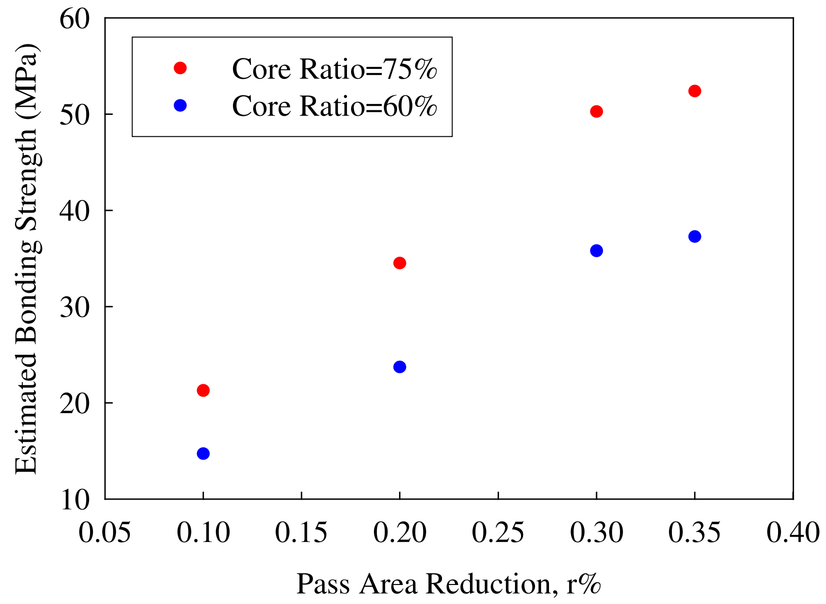

Figure 6.16 Core/sleeve interfacial bond strength as a function of area reduction, r% and core ratio

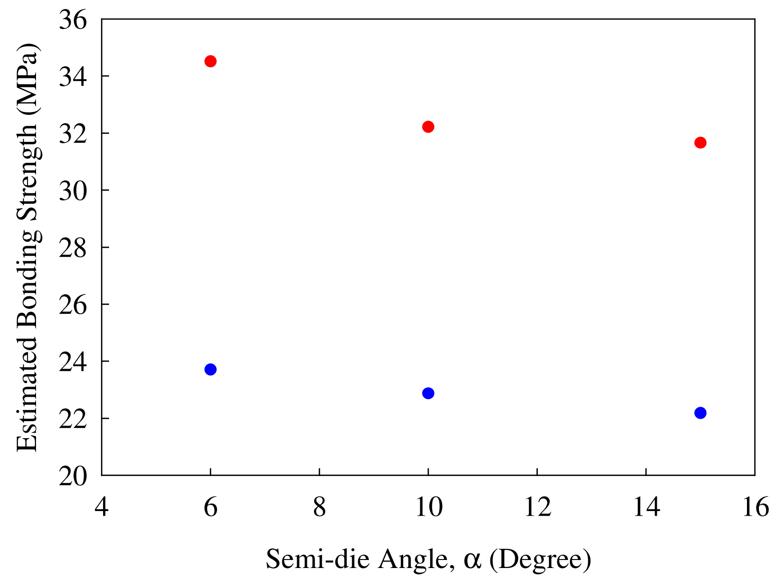

Figure 6.17 Core/sleeve interfacial bond strength as a function of semi-die angle, α and core ratio.

6.3.4 Temperature Distribution

From the calculated field of plastic strain and temperature, the plastic deformation is most severe near the surface of the billet and the peak temperature observed depends on the drawing parameters. Temperature rise, ΔT, is due to the plastic deformation and friction heating. The heating resulting from the work of deformation causes almost uniform temperature rise on the cross section of drawn product, while the friction heat leads to the temperature rise in the surface layer of the deformed material. The influence of drawing parameters on peak temperature is shown in Figure 6.18 and 6.19. The increase of area ratio causes a greater ΔT, while the die angle has little effect on the ΔT. This data shows that the peak temperature, occurring in the regular drawing process where the drawing speed is low, is pretty low. However, for the multi-pass drawing process, if the heating is accumulated from the previous passes, the temperature will be high enough to create reaction in the billet. In our experiments, we try to cool down the billet before going through the next pass to avoid the unwanted reaction. As for every single pass, the temperature rise may not be high enough to affect the bonding condition.

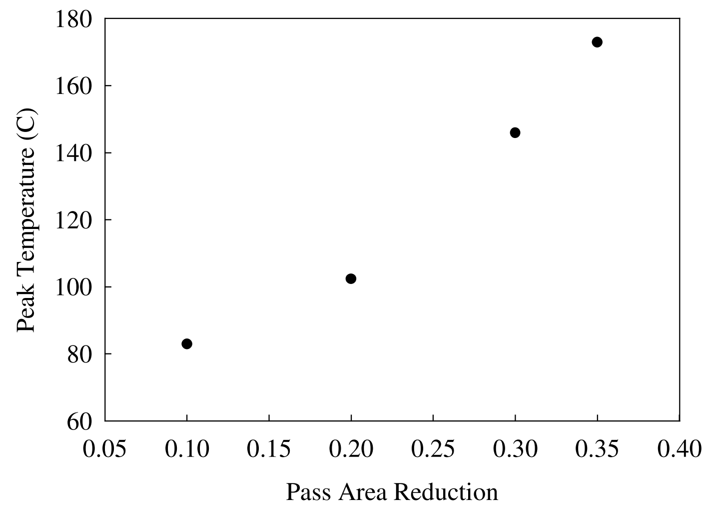

Figure 6.18 Effect of pass area reduction on the maximal temperature in the billet

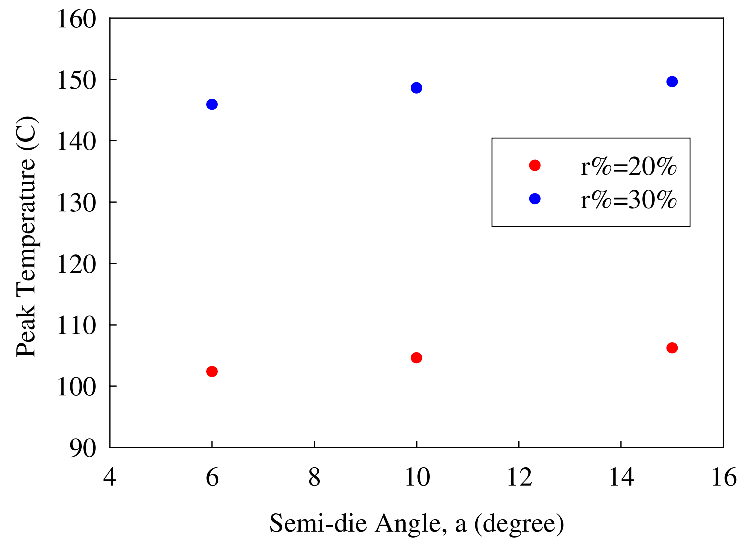

Figure 6.19 Effect of die angles on the maximal temperature in the billet

6.4 Interfacial Bonding Creation in the Multifilaments

6.4.1 FEM model description

As shown in the experiments, the composite billet consisted of an outer Cu can and 7 inner Cu/Nb mono rods. The inner 7 rods were restacked in a configuration as shown in Figure 5.9 consisting of 6 hexagonal monofilaments around 1 hexagonal filament sheathed in a Cu can. The hexagonal arrangement is closely packed. The constituent materials were assumed to be elasto-plastic and to obey the standard Von-Mises plasticity theory with isotropic hardening. In this model, the assembled billet has been assumed to be annealed before drawing to improve their drawability. Following the model of monofilament, the die, was assumed to be a rigid body. A three-dimensional finite model was constructed. Eight-node, trilinear displacement and temperature solid elements were used. Due to the symmetry of the billet structure, only half of the finite-element mesh and the boundary conditions used in this calculation need to be shown in Figure 6.10. The friction between the billet and the die and between monofilaments is assumed to satisfy the Coulomb friction law. In the filaments, the Nb core is assumed to be perfectly bonded to the Cu sleeve.

In this simulation, the pre-selected parameters in the modeling of monofilaments, area reduction, die angle and core ratio, are still the main factors. This simulation was aimed at investigating the stress, strain distribution during co-drawing process, and determining

the influence of different processing parameters and assembly on the development of interfacial bonding as well as the temperature rise within the billet during co-drawing.

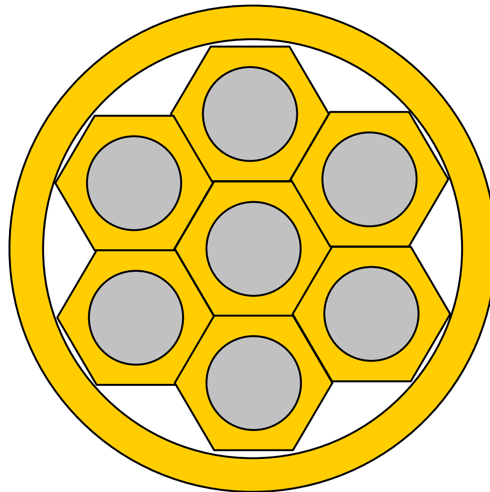

Figure 6.10 Cross-section configurations of the billet

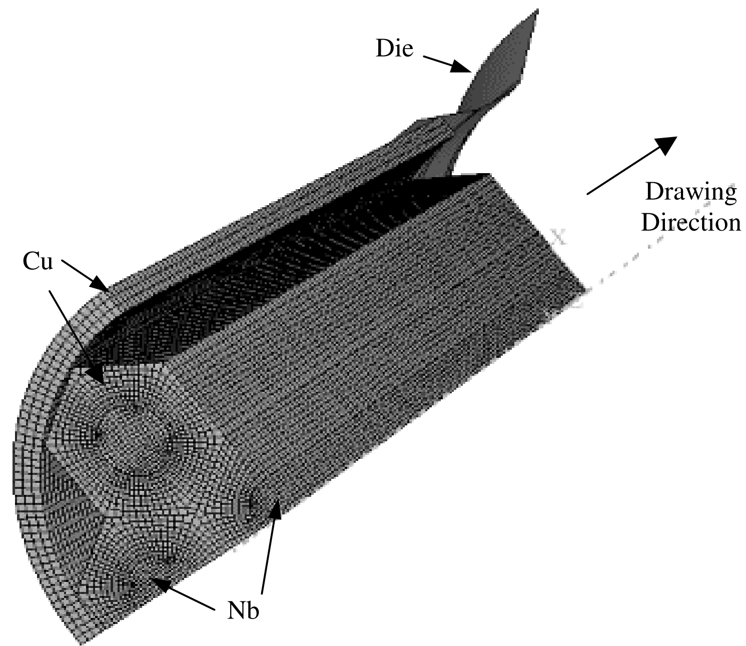

Figure 6.11 3D FEM model of drawing 7 restack precursors.

CHAPTER 7

7. Effect of Main Parameters on the Co-drawing process

In the drawing of monofilament and multifilament, the different mechanical properties create challenges for the successful drawing. Usually the softer component undergoes higher reduction in area and elongates more than the harder component. Thus, the harder one is subjected to tensile stress which will result in the ductile fracture when the tensile stress is above its fracture strength. Moreover, the whole wire hardens with the accumulation of deformation which leads to the increase of the required drawing force to pull it through the die. When the drawing force is increased to be greater than that to deform or break the weaker material already through the dies, the fracture will occur at the die exit side, which is called tensile failure. When wire breaks occur, the drawing process stops and significant downtime occurs and the piece-length of wire is limited. These defects are caused by a combination of factors. Breaks can be attributed to either materials defects, where inclusions are introduced during the casting or rolling stage, or to the defects in the wire drawing process itself, tensile failure and central burst being the common. The proper combination of drawing process parameters and proper die designs may delay or avoid this occurrence, which spurs a lot of interest in the research and manufacture. But most of the work are focus ed on the drawing of fine mono-metallic

wire, and no complete work on the drawing of multi-component material. In this chapter, the effect of the main drawing parameters on the drawing process were analyzed based on the finite element modeling (FEM) results from the previous chapter.

7.1 Drawing Force

The estimation of drawing force is significant from a very practical point of view. If the magnitude of this stress is bigger than the yield stress of the drawing material, then the drawn wire will neck and result in breakage. In the previous FEM modeling of the multi-pass drawing, the drawing force at each pass could be extracted. It is based on the die reaction force from the FEM model, divided by the reduced cross-sectional area of the wire at the die exit. Figure 7.1 shows the change of drawing stresses with the drawing time for the multiple passes of drawing the wire down to 4.732 mm where the drawing speed is about 75 mm/s. In order to validate the finite element models, the drawing forces were recorded in the drawing experiments. The forces were collected by a load cell being attached to the die during the first few passes, which was converted to stresses by dividing it by the cross-sectional area of the drawn wire. Figure 7.2 is the recorded drawing stress curves in the experiments, where the points were recorded every one second. Both sets of curves indicate the steady state of drawing process since the billet stays still in the die. Comparing the values obtained in the experiments and the FEM simulation, being shown in table 7.1, there is very little difference between the experimental and FEM simulation results, which indicates the validation of the FEM simulation in this documents.

	Drawing Stresses (MPa)		
	Pass 2	Pass 3	Pass 4
Experiment	162	202	251
FEM Model	168	213	249
Difference	3.57%	5.42%	0.8%

Table 7.1 Drawing stresses Recorded in the experiments and FEM modeling

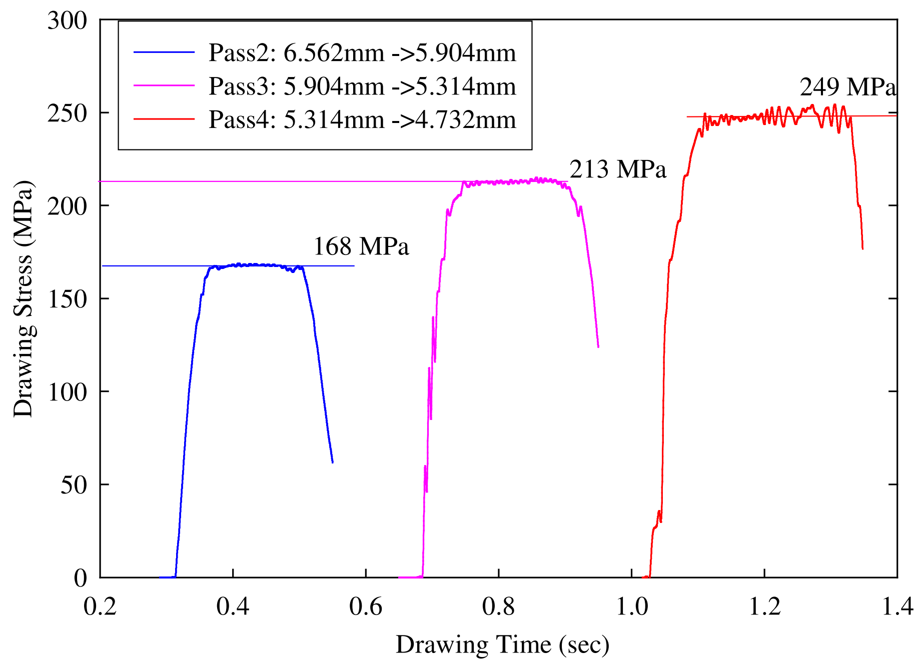

Figure 7.1 Drawing stress curves for different passes by FEM modeling

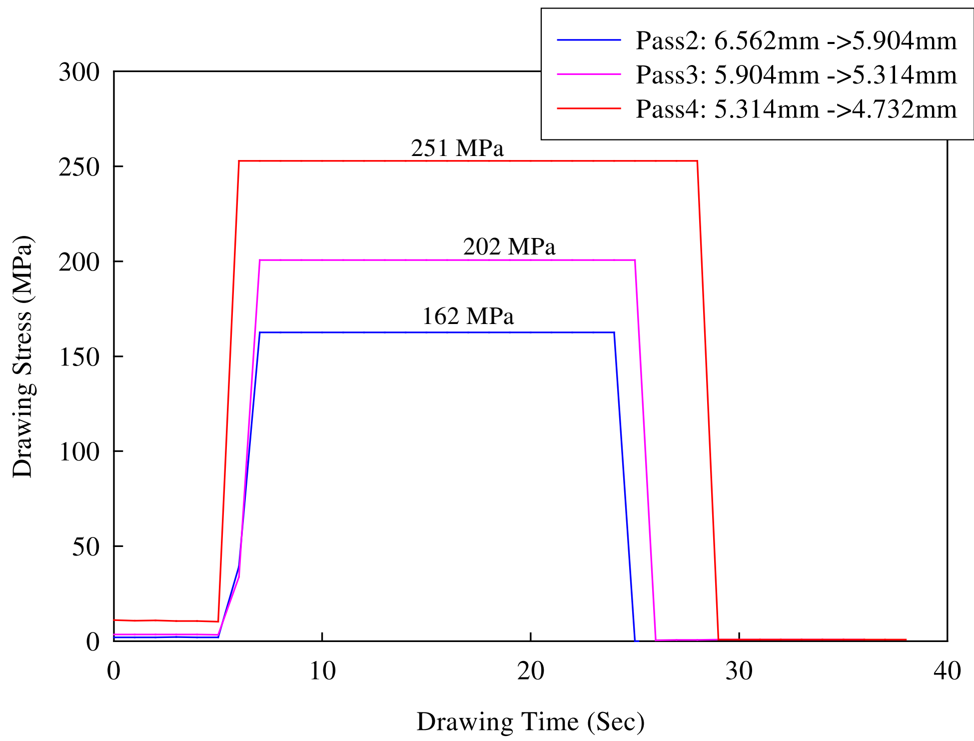

Figure 7.2 Drawing stress curves for different passes recorded in the experiment

The drawing force is obviously a function of area reduction, of die angle, of friction and of the wire material strength. Figure 7.3 shows the drawing stress required for steady-state drawing under a few area reductions against given die angles. According to this plot, there exists an optimal die angle for the same area reduction which requires the least drawing force. The reason for this is as follows: with smaller die angles, the contact area between the die and billet is larger, which causes higher friction losses, while with larger die angles, the loss increases due to increase of the redundant work which is caused by the non-uniform deformation. Furthermore, the optimal die angles are different corresponding to the various area reductions. For example, in this plot, the optimal die is between 8 and 10 degrees when the area reduction is 20% while it is between 12 and 14 degrees when the area reduction is about 35%.

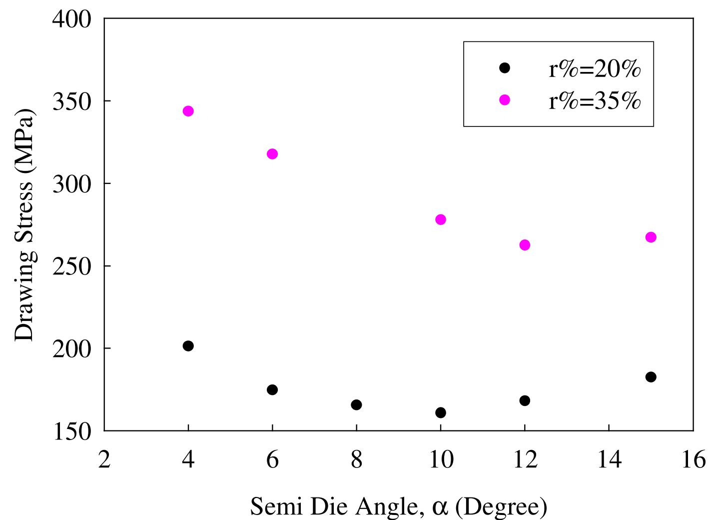

Figure 7.3 Drawing stress change with die angle and area reduction

7.2 Stress and Strain Distribution

Central burst, surface fracture and tensile failure are the main defects occurring in the drawing process which are mostly dependent on the stress and strain states in the billet during the drawing process. Proper selection of drawing parameters creates optimized stress and strain state in the billet which leads to a good quality wire product. Generally, a compressive stress state and uniform strain distribution are helpful for the successful drawing of wires whereas the fracture frequently initiates at the tensile stress area. In order to display the effect of the main drawing parameters on the stress and strain distributions, two characteristic series of nodes were monitored, one is along the central axis starting from the die entrance, and the other is along the radial direction out of the die exit. The reason to monitor the central axis is to display the feasibilities of central burst occurrence under different conditions, and the reason for monitoring the section at the die exit is to analyze the surface defects and tensile fracture. The two sets of position are shown in Figure 7.4, which is the contour of axial stresses distribution for the drawing of bi-metallic material with area reduction, r%, equals to 20% and half die angle, α equals to 6 degree. The stresses and strain distribution along the central axis and radial direction were plotted. The main parameters covered in this study are area reduction, die angle, drawing speed, Friction between the billet and die, interfacial bonding level and thickness of the sleeve.

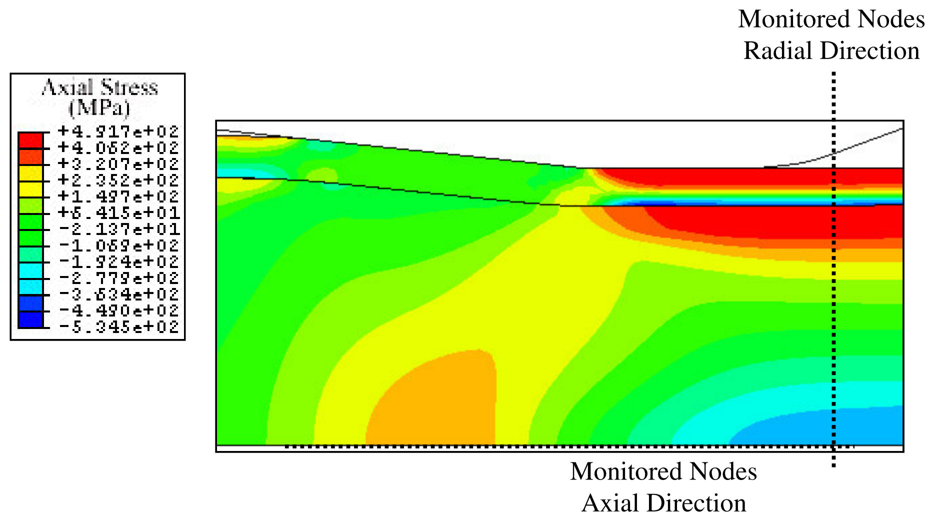

Figure 7.4 Axial Stresses Distribution showing the two sets of monitored nodes: Axial and radial direction, (r%=20%, α=6°).

7.2.1 Area Reduction and Die Angle

Area reduction and die angle are the two main parameters affecting the drawing process. Learned from the previous study of drawing mono-metallic material, higher area reduction and smaller die angle result in more uniform deformation, thereby better drawing conditions. However, the higher area reduction indicates higher deformation requiring the higher drawing stress. The smaller die angle also increases the friction loss and thereby may increase the drawing force. The higher drawing stress will be a disaster for the drawing process when it is larger than the yield stress of the weaker drawn component. Hence, this is a trade-off process. A limit for area reduction exists for certain materials. Similar conditions happen for the drawing of bi-metallic and multi-metallic materials. Figure 6.5 shows the effect of area reduction and die angle on the accumulated strain distribution along the monitored nodes. The horizontal axis of the graph represents the normalized radial distance from the center of the wire, denoted by 0, to the outer surface, represented by 1, along the monitored nodes. For the drawn wire, the strain increases from the central axis to the outer surface of the wire. At the interface, the strain is not continuous, with larger gap in higher die angles and lower area reduction. Higher area reduction generates a much more uniform strain distribution which is important for the uniformity of the final product. However, a drawing limit exists for the area reduction due to the maximum drawing stress the materials could stand.

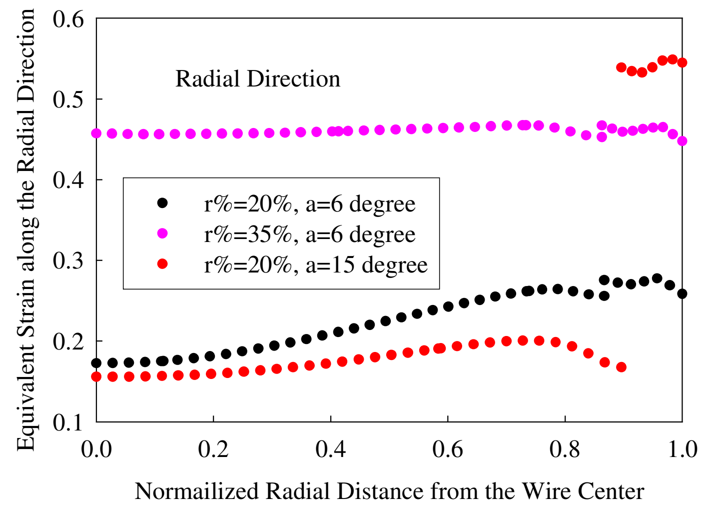

Figure 7.5 Equivalent Strain Distribution along the radial direction in the drawn wire under different area reduction and die angles.

A number of studies have been carried out to determine the effect of high hydrostatic stress on the failure of ductile materials. These studies have found that the ductility

increases with hydrostatic pressure. The typical results were summarized in Pugh's work at various hydrostatic pressures. The tensile hydrostatic stress may initiate the nucleation of voids and promote the spread of defects during the deformation process. Hence, in this analysis of drawing process, the hydrostatic stress and axial stress were selected as the characteristic stresses to display the effect of process parameters. In the drawing process, central burst are tend to occur at the central tensile axial stress and hydrostatic stress area when they are above certain values. Figure 7.6 shows the effect of die angle and area reduction on the distribution of axial stress and hydrostatic stress along the central axis. Too low area reduction results in non-uniform deformation along the cross section, and create bigger tensile axial stress in the center of the deformation area and even more tensile hydrostatic stress, which is similar with the effect of increasing die angles, the axial tensile stress in the center turns bigger, and the hydrostatic stress turns tensile, and the magnitude is bigger.

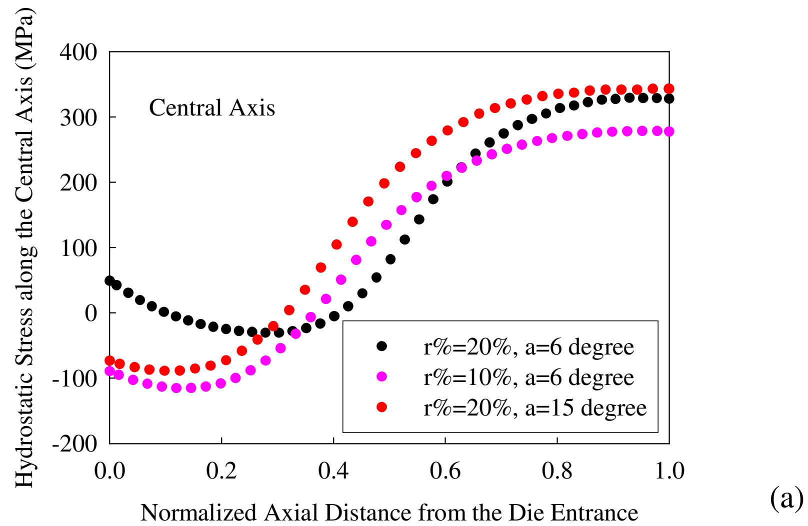

(a)

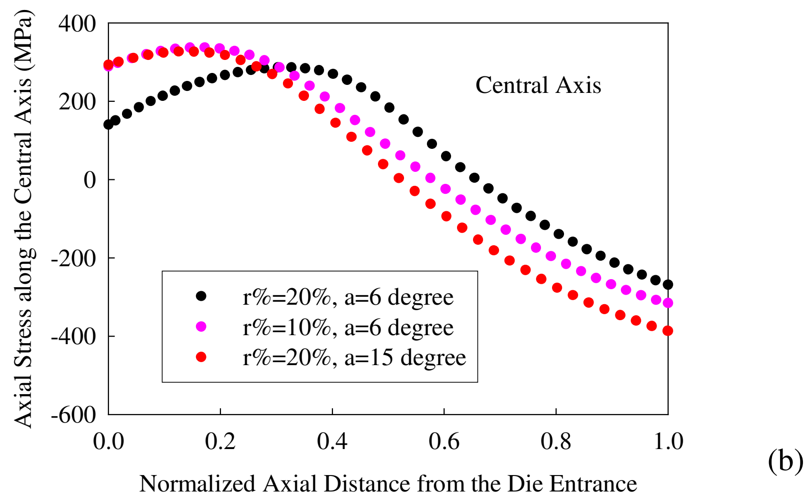

(b)

Figure 7.6 Hydrostatic Stress and Axial stress distributions along the central axis direction under different area reduction and die angles. (a) hydrostatic stress (minus denotes tensile and plus denotes compressive); (b) Axial Stress (minus denotes compressive and plus denotes tensile).

To determine the likelihood of defect occurring on the wire surface owing to the drawing force exceeding the materials plastic limit, the von mises equivalent stress and axial stress along the radial direction out of the die exit were selected and plotted as shown in figure 6.7. The axial stress varies from compressive along the center axis of the wire to tensile at the outside diameter. The largest tensile axial stress and largest Mises equivalent stress all occur in the sleeve surface at the interface, which indicates that the most possible starting point of tensile failure is on the outer-side surface. This tensile failure is generally due to the application of too large area reduction.

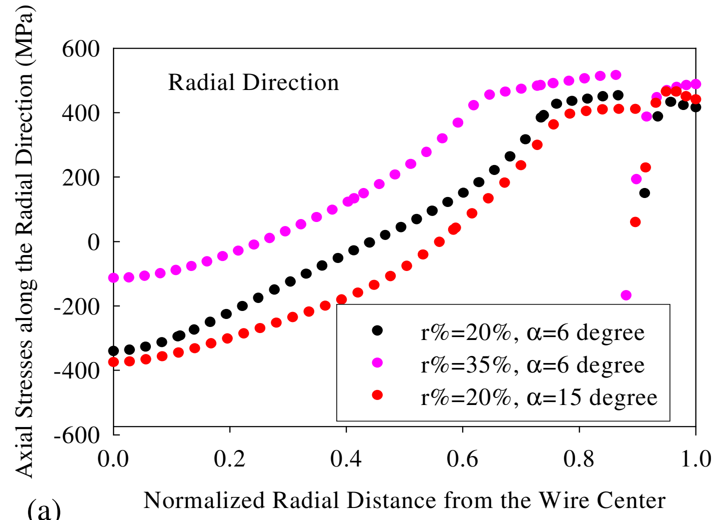

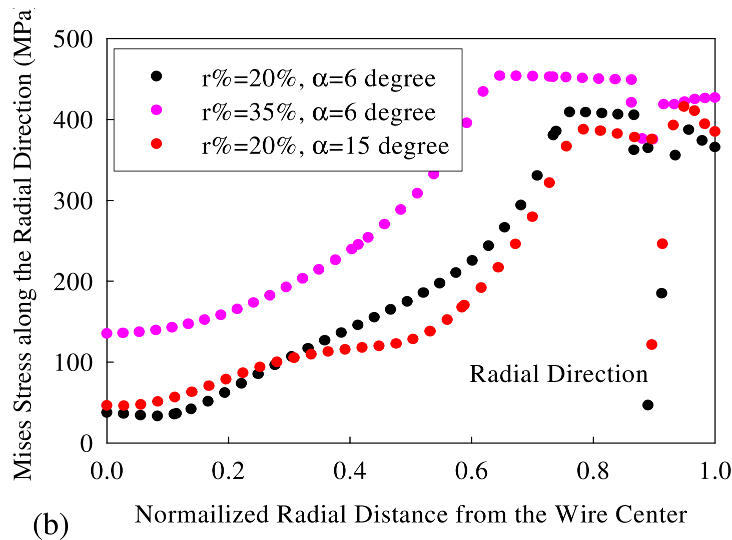

Figure 7.7 Mises Equivalent Stresses and Axial Stresses Distribution along radial direction under different area reduction and die angles. (a) Axial stress (minus denotes compressive and plus denotes tensile); (b) Mises Equivalent Stress.

7.2.2 Drawing Speed

Drawing speeds depend on the material and the cross-sectional area of the wire. They may be as low as 0.01m/s for heavy sections, to as high as 50m/s for very fine wire. For the drawing of multiple-component wires, there are two obvious influences of drawing speed: (1) a lower speed is helpful for maintaining a well lubricated condition, thereby reducing the friction loss and drawing force; (2) temperature could rise substantially at high drawing speeds, which may promote the unwanted reaction between the different components, thereby reduce the ductility of the composite. In this calculation, two drawing speeds, 75 mm/s and 750 mm/s, were used to display the effect of drawing speed. Figure 7.8 and figure 7.9 show the influence of drawing speed on the distribution of characteristic stresses along the radial and axial directions. A higher speed results in the increase of tensile axial stress and hydrostatic stress in the center which may promote the occurrence of central burst. However, if the drawing speed is maintained at a lower level, the change of speed would not lead to much difference for the drawing process. In the regular multifilamentary wire drawing, 75mm/s was usually used as the drawing speed.

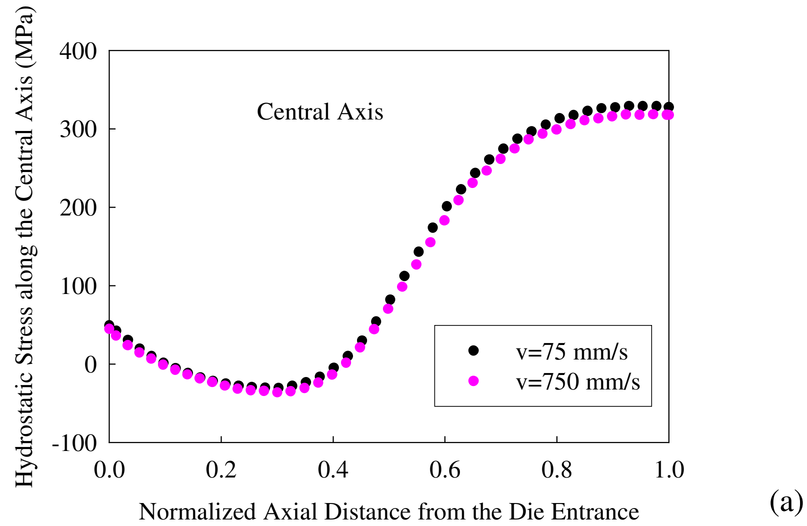

(a)

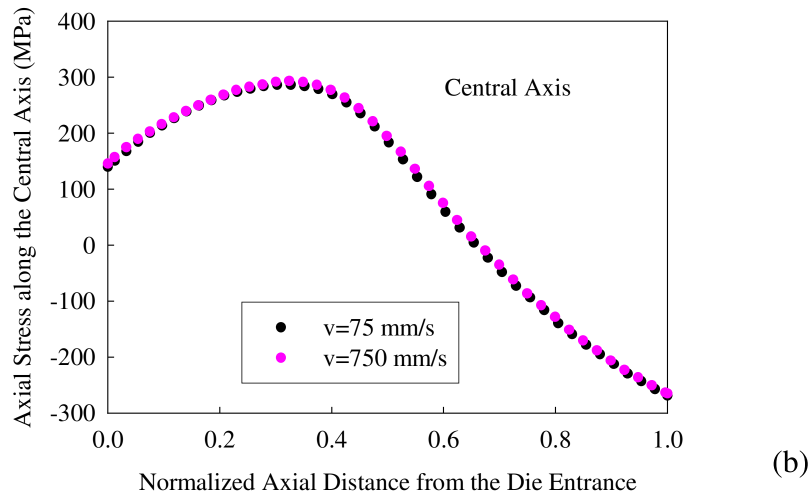

(b)

Figure 7.8 Hydrostatic Stress and Axial stress distributions along the central axis direction under different drawing speed when r%=20%, α=6°. (a) hydrostatic stress (minus denotes tensile and plus denotes compressive); (b) Axial Stress (minus denotes compressive and plus denotes tensile).

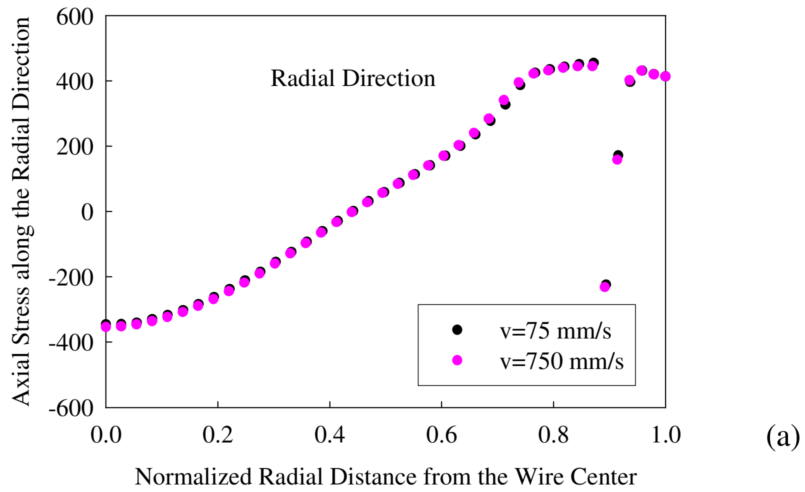

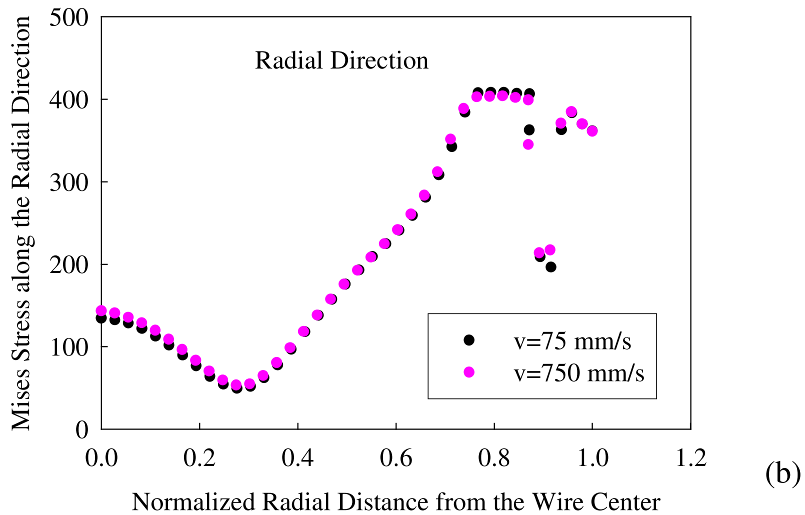

Figure 7.9 Mises Equivalent Stresses and Axial Stresses Distribution along radial direction under different drawing speed when r%=20%, α=6°. (a) Axial stress (minus denotes compressive and plus denotes tensile); (b) Mises Equivalent Stress.

7.2.3 Friction between Die and Billet

Friction is unavoidable in the drawing process. Whenever the wire and the die are in contact and relative motion, a resistance to this motion arises. Too much friction can result in tool distortion, loss of dimensional control, inferior surface finish and aggravated non-homogeneity of metal flow, and high required drawing stress. Figure 6.10 recorded the change of drawing stress during the drawing process by changing the friction coefficient. An improved lubrication condition would reduce the drawing stress largely and thus reduces and even avoids the tensile failure.

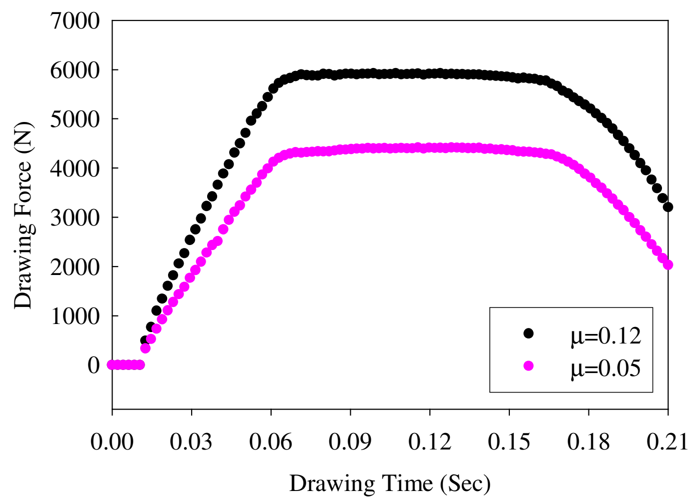

Figure 7.10 Drawing stress under different drawing speed when r%=20%, α=6°.

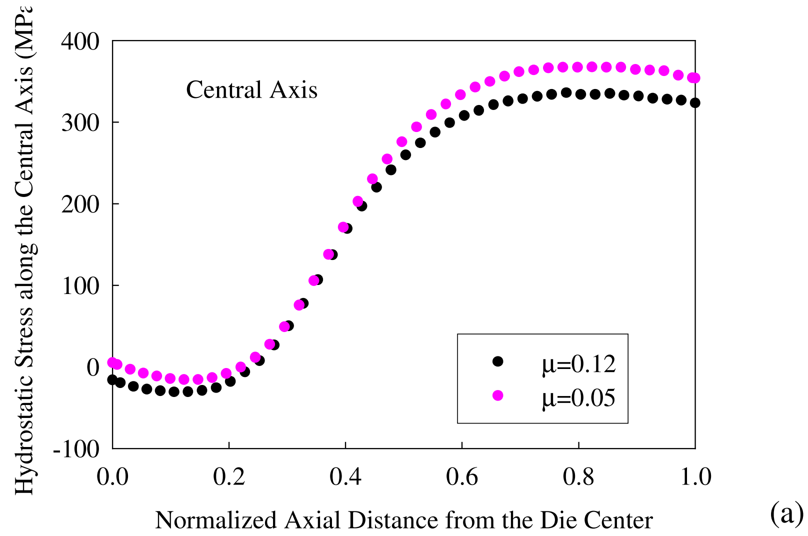

(a)

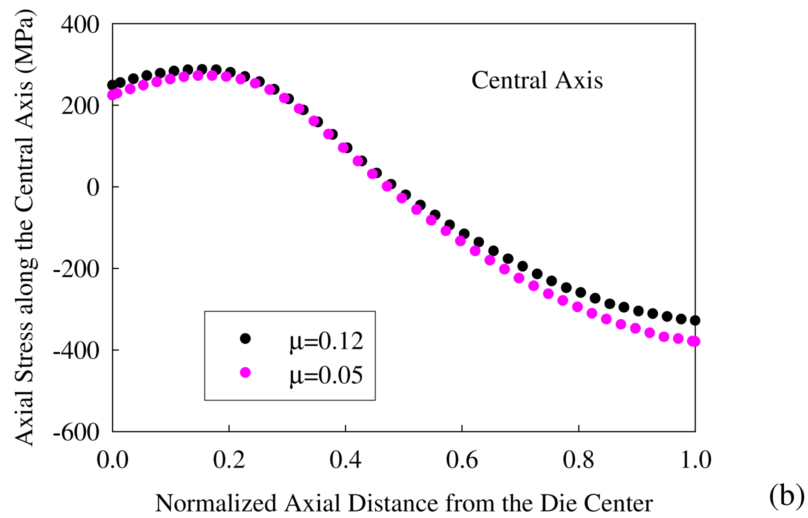

(b)

Figure 7.11 Hydrostatic Stress and Axial stress distributions along the central axis direction under different friction when r%=20%, α=6°. (a) hydrostatic stress (minus denotes tensile and plus denotes compressive); (b) Axial Stress (minus denotes compressive and plus denotes tensile).

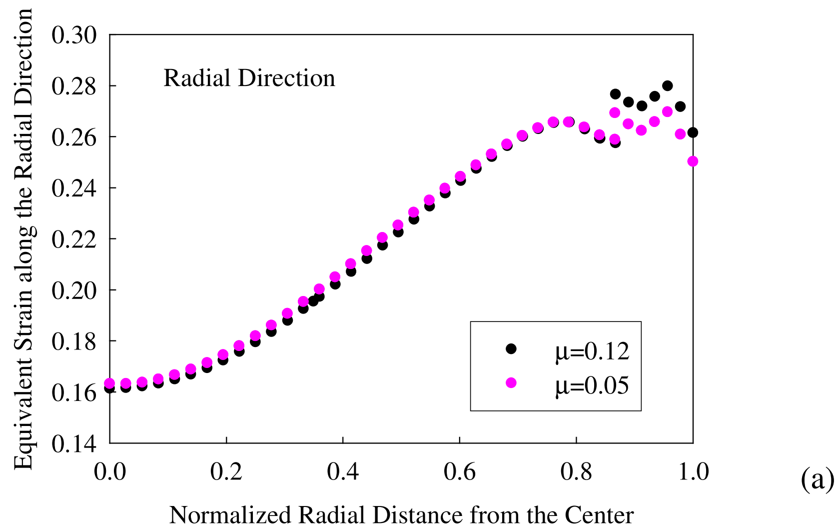

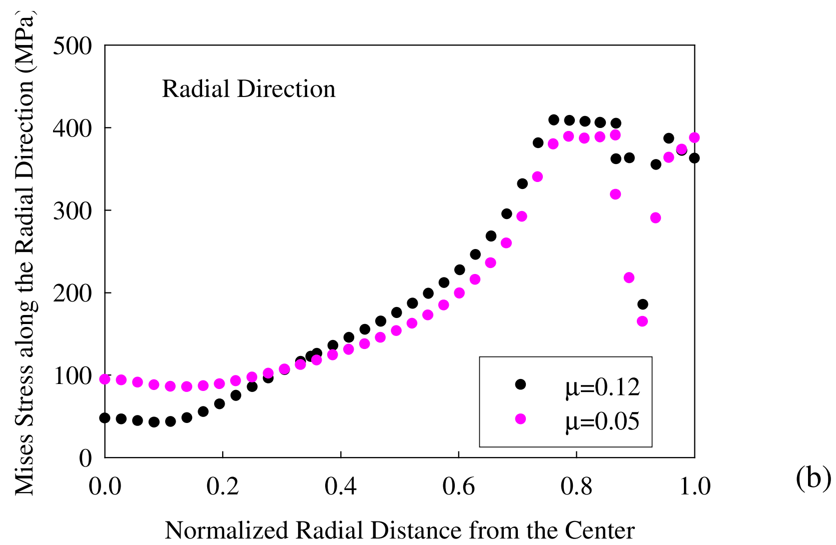

Figure 7.12 Equivalent Strain and Mises Equivalent Stresses along radial direction under different friction conditions when r%=20%, α=6°. (a) Equivalent Strain; (b) Mises Equivalent Stress.

The reduction in friction between the billet and die not only reduces the drawing force but also improve the stress and strain distribution in the drawn products. Shown from figure 7.11 and 7.12, more uniform strain distribution occurs along the radial direction especially in the sleeve. Less tensile hydrostatic stress and axial stress occur in the center under the deformation area which will reduce the possibility of central burst.

7.2.4 Interfacial Bonding

As predicted in the previous chapter, a certain level of bonding will be generated after a few passes of co-drawing. If we continue to draw these billets, our understanding of the influence of different levels of bonding on the subsequent drawing process becomes very important. In all the published work[4, 5], it is common to equate interface friction with bonding. However, friction is distinct from bonding. According to the classic Coulomb friction law, the resistance to the relative motion of contacting bodies depends on the normal pressure ($\tau = \mu N$, where N is the normal stress and μ is the friction coefficient), thus the increase of μ suggests a higher motion-resistance, and this increment of motion-resistance changes with the normal pressure, which is usually used as the parameter for bonding in the published work. However, for a truly bonded billet, a certain bond-stress exists between the contacting bodies independent of the normal pressure experienced in the deformation process. Hence, we assumed a fixed shear force, f_0, at the contact surface to represent the resistance to the relative motion of the contacted bodies. Hence, the total resistance to the relative motion of contacting bodies becomes $\tau = \mu N + f_0$. The aim of incorporating this into the FEM model is to represent the strength of the interfacial bond

so as to study the effect of this bonding level on the drawing process. We assumed that the fixed shear stress f_0 was 0, 100, 500 MPa and infinite (perfect bond) respectively. To realize this in the FEM model, a friction subroutine, “VFRIC”, was written using Fortran and put into the program to define the surface contact properties.

Fig 7.13 shows the slippage at the interface during drawing process. In the case with f_0=500 MPa, there is no interface slippage occurring between the interface which indicates the perfect bonding at the interface. The lower bonding level interface has larger slippage which indicates the effectiveness of our assumption. According to hydrostatic stress and axial stress distribution in Figure 7.14, the higher bonding level between the components results in the lower tensile axial stress and tensile hydrostatic stress in the center which will delay the occurrence of central burst. The bonding level has no much effect on the drawn wire except affecting the interfacial area.

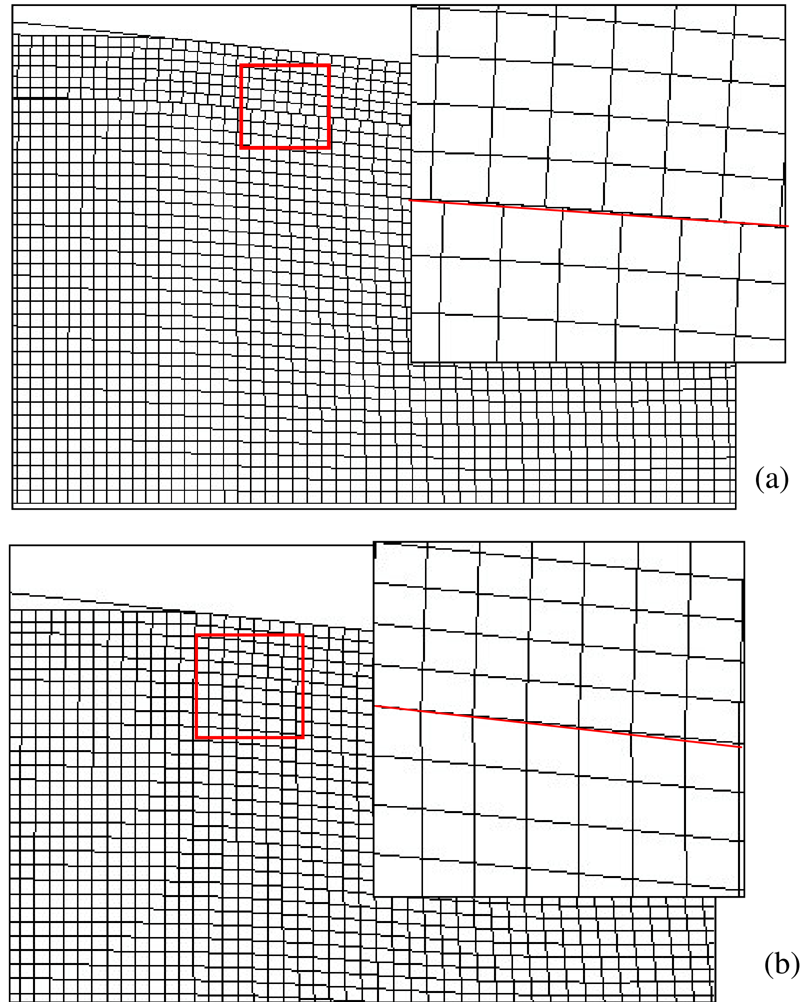

Figure 7.13 Interface slippage during the drawings with different bonding level (a) f_0=50 MPa; (b) f_0=500 MPa

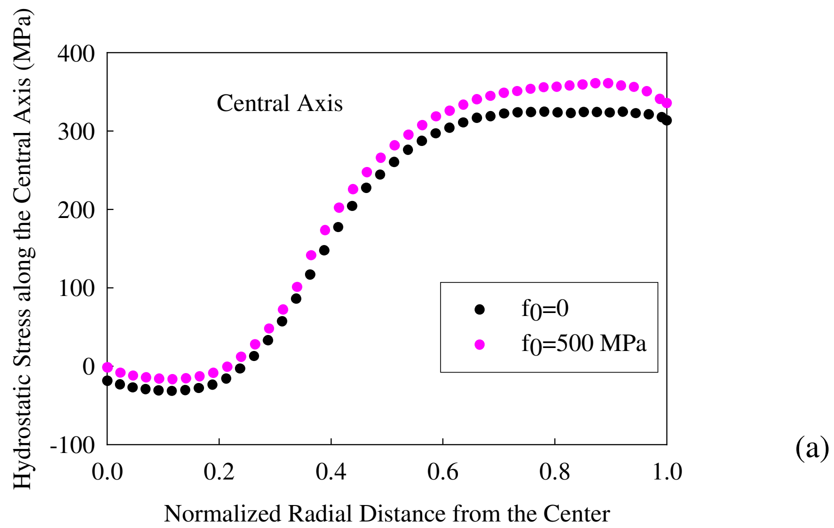

(a)

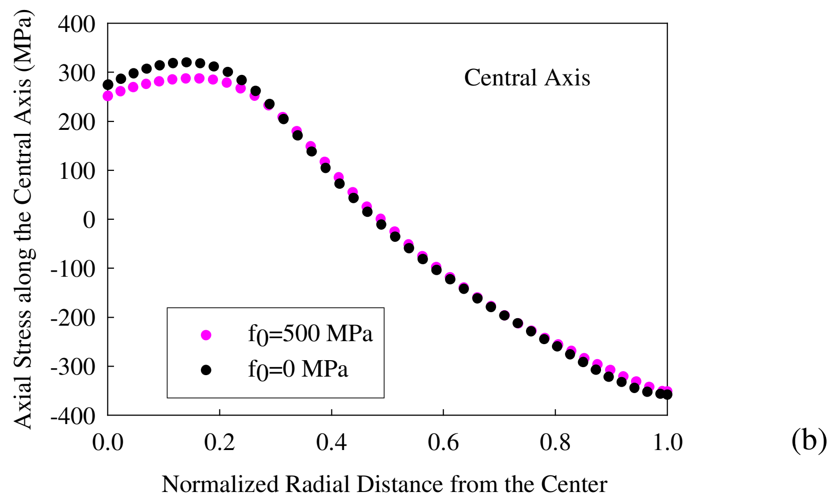

(b)

Figure 7.14 Hydrostatic Stress and Axial stress distributions along the central axis direction under different interfacial bonding conditions when r%=20%, α=6°. (a) hydrostatic stress (minus denotes tensile and plus denotes compressive); (b) Axial Stress (minus denotes compressive and plus denotes tensile).

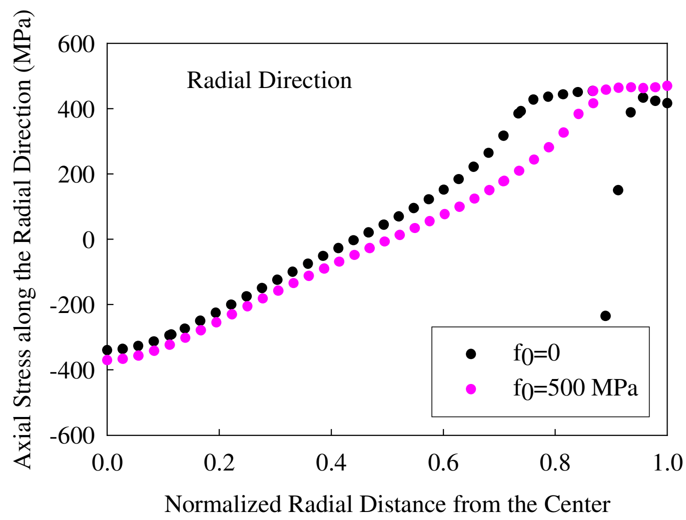

(a)

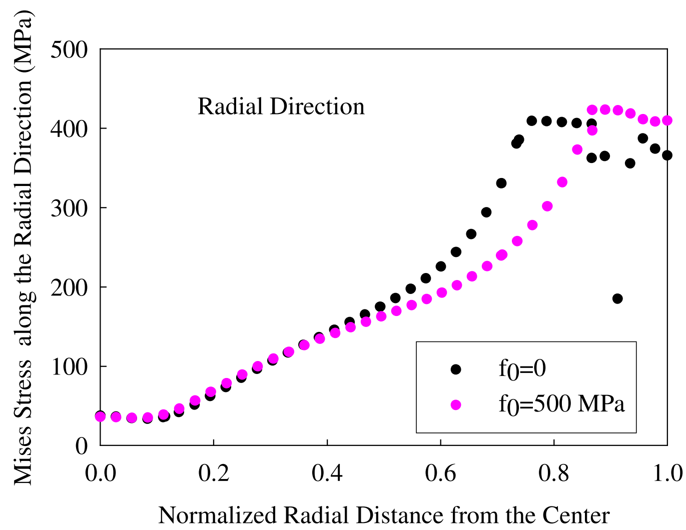

(b)

Figure 7.15 Equivalent Strain and Mises Equivalent Stresses along radial direction under different friction conditions when r%=20%, α=6°. (a) Equivalent Strain; (b) Mises Equivalent Stress.

7.2.5 Core Ratio and Cu Ratio

In the previous chapter, we have known that the thickness of Cu sleeve and the Cu between the filaments are important for the bonding generation. However, how do they affect the strain and stress distribution in the drawing process. Figure 7.16 ~ Figure 7.17 show the effect of two various core ratios in the drawing of two-component billet. Two core ratios were used in the billet assembly, one is 75% and the other is 60%. The thickness of the sleeve does not improve the uniformity of the final product, but it does decrease the central tensile axial stress and tensile hydrostatic stress which will reduce the possibility of occurrence of central burst.

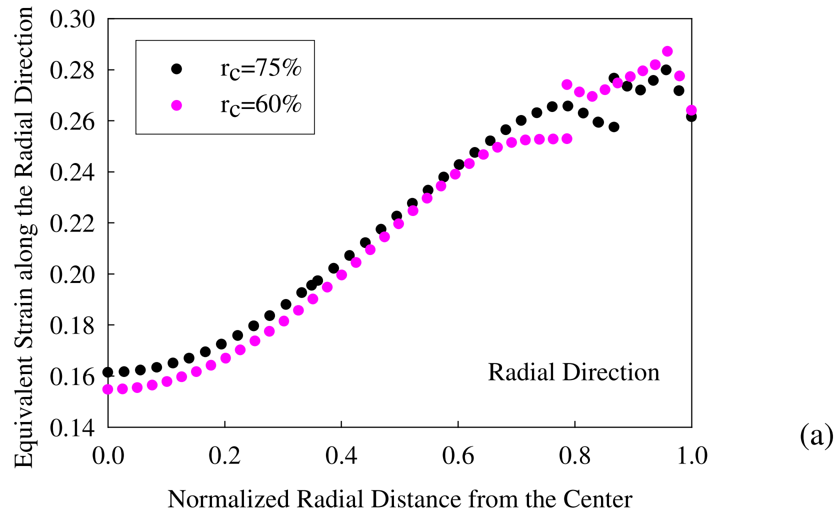

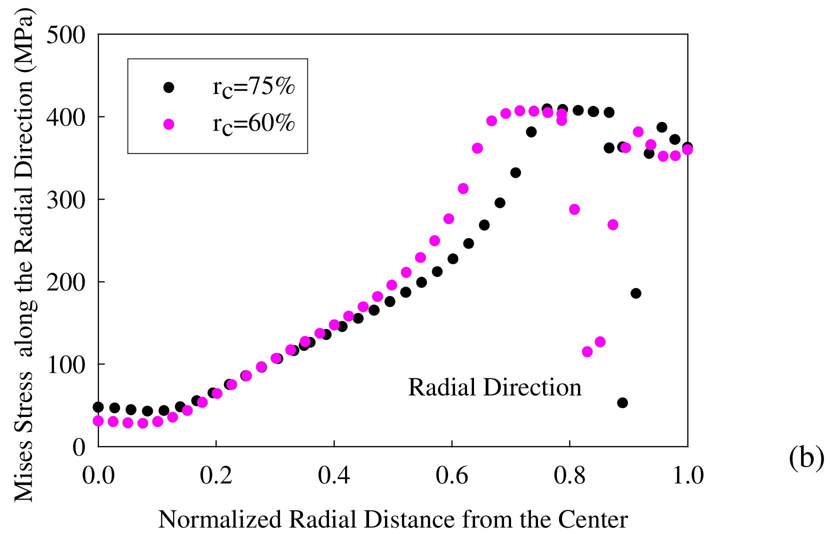

Figure 7.16 Equivalent Strain and Mises Equivalent Stresses along radial direction under different core ratios when r%=20%, α=6°. (a) Equivalent Strain; (b) Mises Equivalent Stress.

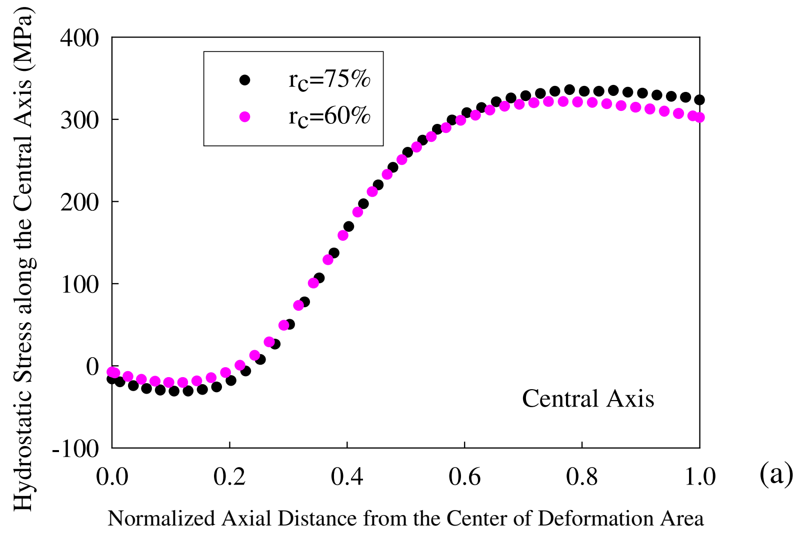

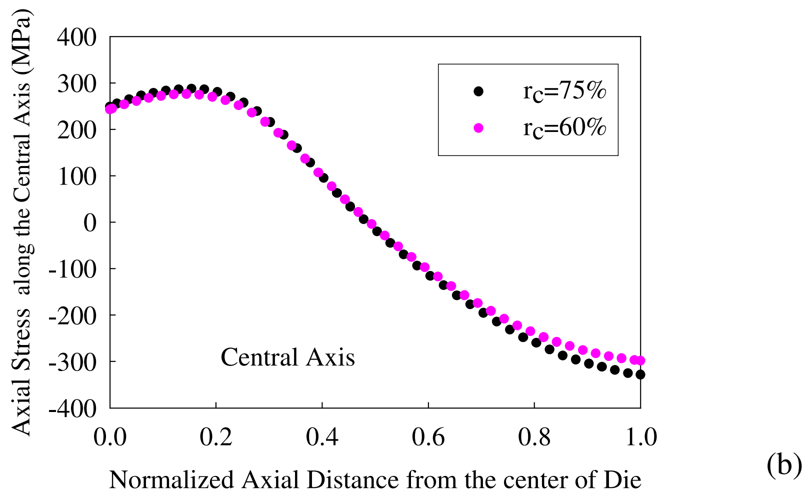

Figure 7.17 Hydrostatic Stress and Axial stress distributions along the central axis direction under different core ratios when r%=20%, α=6°. (a) hydrostatic stress (minus denotes tensile and plus denotes compressive); (b) Axial Stress (minus denotes compressive and plus denotes tensile).

7.2.6 Multiple Passes

In the published paper, the process of multiple-pass drawing process is usually analyzed as simple multiplying of single pass drawing. The reason for this seems to be the opinion that the problems concerning multiple-pass drawing do not differ considerably from those occurring in single-pass drawing. Such an understanding is not correct when considering residual stresses being created during drawing and the hardening of materials and so on. For example, in multiple-pass drawing, by applying the amount of deformation admissible in single-pass drawing, one can lead to significant lowering of final product quality as a result of internal bursting and tensile fracture. Moreover, in the previous published papers, main concerns are the values of the drawing stress, and no much focus is on the strain and stress distribution. In fact, is important to look for the possibility of taking into account of the non-uniformity of strain and stresses in individual passes in the multiple pass drawing. Such analysis is necessary considering the quality of final products and also the success of drawing process. In this section, the single pass and multi-pass drawing was simulated and compared. A wire with a diameter of 7.mm was drawn down to 5.094mm through two drawing schedules, one is through a 20% reduction pass, and the other is through two 10% reduction passes. These two conditions were calculated and compared. Figure 7.18 shows the strain distribution along the radial direction in the drawn wire out of die exit. The multiple-pass drawing separates the deformation into multiple passes with smaller pass area reduction which lead to the more non-uniform deformation in the products. Seen from the hydrostatic stress and axial

stress distributions along the central axis in figure 7.19, the much higher tensile stress occurred in the multiple-pass drawing process indicates that it is easier to generate central burst during the multiple-drawing. Hence, under the drawing limit, larger area reductions are always the choice for the successful drawing to avoid the central burst in the small area reduction multiple-drawing.

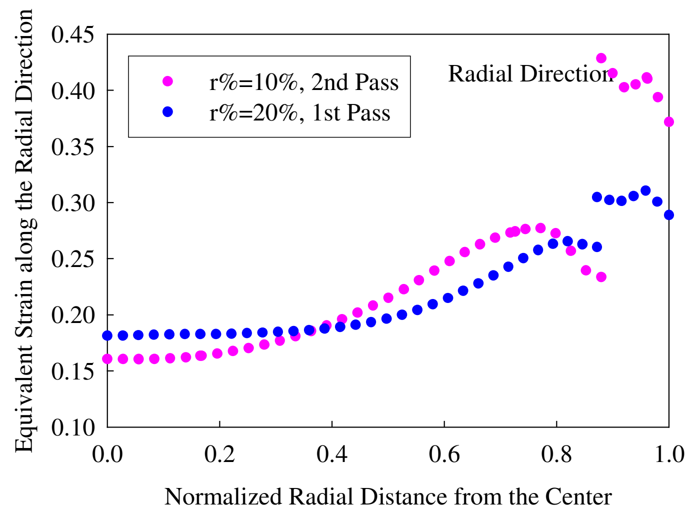

Figure 7.18 Equivalent Strain distributions along the radial direction in the drawn wire under different drawing schedules.

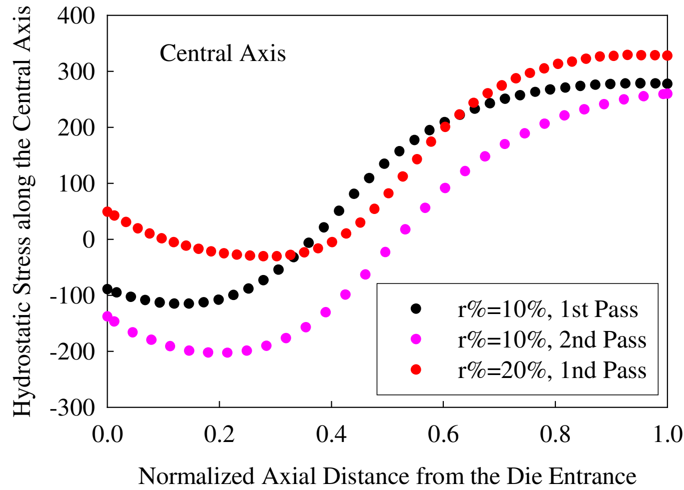

(a)

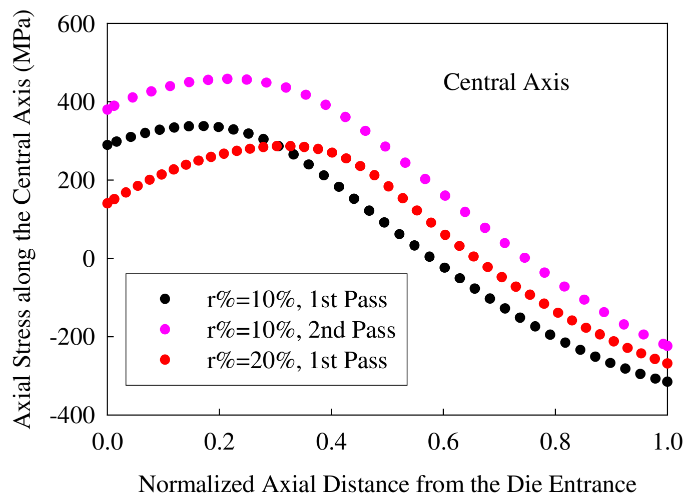

(b)

Figure 7.19 Hydrostatic Stress and Axial stress distributions along the central axis direction under different drawing schedules (a) hydrostatic stress (minus denotes tensile and plus denotes compressive); (b) Axial Stress (minus denotes compressive and plus denotes tensile).

7.3 Summary

In order to perform an optimized drawing process, we have to consider the following criteria: minimum drawing forces and energy consumption, uniform strain distribution inside the wire, minimum tensile stresses occurring in the deformation zone and minimum axial residual stresses in the drawn wire. Based on these criteria, the effect of the main drawing process parameters was analyzed by using the finite element modeling (FEM). Pass area reduction, die angle, friction between the die and billet, drawing speed and bonding level between the components all influence the stress and strain distribution in the wire, thereby affect the drawing process. Larger area reduction improves the uniformity of strain distribution and reduces the possibility of central burst, but it increases the required drawing stress which may result in the tensile failure out of the die exit. Larger die angle will reduce the friction loss due to the reduction of contact area, but it will increase the non-uniform deformation in the wire, thereby increases the redundant work required for the drawing process. These two effects result in the existence of optimal die angle which required the minimum drawing force. Friction is another important factor influencing the required drawing force. Worse lubrication condition increases the friction losses during drawing, and thereby increasing the required drawing force. Moreover, the higher friction degrades the non-homogeneous deformation conditions, and causes higher tensile stress in the center which may promote the central burst. Higher bonding level between the components results in a lower tensile stress in the central which is helpful for reducing the possibility of central burst. Higher drawing

speed increases the possibility of central burst, but there is no big difference under low drawing speed such as the general drawing speed used in the manufacture of complicated composite wire. The sleeve thickness also affects the drawing process. A thicker sleeve reduces the tensile stress in the center which will reduce the possibility of central burst. The drawing speed, bonding level between components and the thickness of sleeve have very little influence on the tensile failure. Multiple-pass drawing is commonly used in the wire manufacture, but the setup of drawing schedule is critical for the successful drawing. Under the drawing limit, a larger area reduction should be suggested for a successful drawing.

CHAPTER 8

8. CONCLUSION

Based on the condition of superconductor manufacture, this project is focused on the co-drawing process. The objective of this project is to get an understanding of the generation process of interfacial bonding during drawing process, to identify the bonding mechanism and investigate the effect of bonding on the later co-deformation. Due to the high cost and limitation of empirical trial-and-error approaches, Finite Element Method (FEM) was used to simulate the co-deformation process to investigate the effects of die angle, area reduction, the core ratio and the variation of bonding between components on the deformed geometry, stress distribution in the product and the details in the interface, and then combine the FEM simulation with a modified pressure bonding model to study the generation process of interfacial bonding between components.

Co-drawing of differently assembled billets has been performed to verify the simulation results. Additionally, SEM, EDS and TEM observations and mechanical testing has been conducted to investigate the generated inter-component bonding after co-extrusion and co-drawing. As a result, the effect of drawing parameters on the generation of inter-

component bonding strength and the influence of the interfacial bonding on the drawing conditions will be determined.

Reference:

[1] M. Shiomo, K. Mori, and K. Osakada, "Simulation of steady-state hydrostatic extrusion using rigid-palstic finite element method," *Japan insititute of mechnical science*, vol. 59, pp. 192-197, 1993.

[2] R. Sliwa, "A test determining the ability of different materials to undergo simultaneous plastic deformation to produce metal composites," *Materails science and engineering*, vol. A135, pp. 259-265, 1991.

[3] J. M. Alexander and C. S. Hartley, "On the Hydrostatic Extrusion of Copper-covered Aluminum Rods," presented at NEL/AIRAPT International Conference on Hydrostatic Extrusion, University of Stirling, UK, 1973.

[4] K. Osakada, M. Limb, and P. B. Mellor, "Hydrostatic Extrusion of Composite Rods with Hard Cores," *International Journal of Mechanical science*, vol. 15, pp. 291-307, 1973.

[5] B. Avitzur, R. Wu, S. Talbert, and Y. T. Chou, "An Analytical Approach to the Problem of Core Fracture during Extrusion of Bimetal Rods," *Journal of Engineering for Industry*, vol. 107, pp. 247-253, 1985.

[6] B. Avitzur, "Prevention of Filament Breaks during Drawing and Extrusion of Multifilamentary Wire," *Wire Journal International*, vol. 25, pp. 59-65, 1992.

[7] C. W. Wu and R. Q. Hsu, "Extrusion of Three-layer Composite Hexagonal Clad Rods," *Journal of Materials Processing Technology*, vol. 123, pp. 47-53, 2002.

[8] L. Lesik, H. Dyja, J. Pilarczyk, and S. Wiewiorowska, "Microhardness and Plastic Flow Investigation of Bimetallic Rod for Drawing," *Wire Journal International*, vol. 34, pp. 94-96, 2001.

[9] M. Ragab, A. Wifi, and G. Galal, "On the Deformation of Bimetal Wires by Drawing," *Journal of Materials Shaping Technology*, vol. 9, pp. 67-75, 1991.

[10] Z. Muskaiski, J. Pilarczyk, B. Golis, and S. Wiewiorowska, "Modeling the Drawing of Bimetallic Rods with Forge-2 Software," *Wire Journal International*, vol. 34, pp. 108-112, 2001.

[11] R. Lugosi and C. S. Hartley, "The Influence of Interfacial Shear Yeild Strength on the Deformation Mechanics of an Axi-symmetric Two Component System," presented at Fifth North American Metal Working Research Conference Proceedings, Dearborn, Mich., 1977.

[12] J. A. Parrell, M. B. Field, Y. Zhang, and S. Hong, "Nb3Sn conductor development for fusion and particle accelerator application," *Advanced Cryogenic Engineering (Materials)*, vol. 50B, pp. 369-375, 2004.

[13] T. Miyazaki, N. Matsukura, T. Miyatake, M. Shimada, K. Takabatake, K. Itoh, T. Kiyoshi, A. Sato, K. Inoue, and H. Wada, *Adv. Cryo. Eng. (Materials)*, vol. 44, 1998.
[14] J. D. Elen, C. A. M. v. Beijnen, and C. A. M. v. d. Klein, *IEEE Transactions on Magnetics*, vol. 13, pp. 470, 1977.
[15] E. Barzi, P. Limon, R. Yamada, and A. Zlobin, "Study of Nb3Sn strands for fermilab's high field dipole models," *IEEE Transactions on Applied Superconductivity*, vol. 11, pp. 3595-3598, 2001.
[16] B. A. Zeitlin, E. Gregory, T. Pyon, R. M. Scanlan, A. Polyanskii, and P. J. Lee, "Progress on the use of internal fins as barriers to reduce magnetization on high current density mono element internal Tin conductors (MEIT)," *Advances in Cryogenic Engineering*, vol. 50B, pp. 417-424, 2004.
[17] E. Gregory, E. Gulko, and T. Pyon, "Development of Nb3Sn Wires Made by the Internal-tin Process," *Advances in Cryogenic Engineering*, vol. 44B, pp. 903-909, 1998.
[18] R. M. Scanlan, "Conductor Development for High Energy Physics -- Plans and Status of the U.S. Program," *IEEE Transactions on Applied Superconductivity*, vol. 11, pp. 2150-2155, 2001.
[19] N. Inoue and M. Nishihara, *Hydrostatic extrusion -Theory and applications*, 1985.
[20] K. Osamura, "Composite superconductors." New York, 1994.
[21] E. W. Collings, *Applied superconductivity, Metallurgy, physics of Titanium alloys (vol.2)*, vol. 2, 1986.
[22] B. Avitzur, *Handbook of Metal-forming Processes*, 1983.
[23] L. S. Eil'man, "Nature of Metal Deformation during the Drawing of Bimetal Round Rods," *Tsvetnye Metally*, vol. 7, pp. 74-76, 1966.
[24] N. Given, "DIP Forming of Bimetallic Wire," *Iron Age*, vol. 198, pp. 46-47, 1966.
[25] B. Avitzur, "Analysis of central bursting defects in extrusion and wire drawing," *journal of engineering for industry*, vol. 90, pp. 79-91, 1968.
[26] B. Avitzur, *Metal forming: processes and analysis*, 1968.
[27] J. M. Story, B. Avitzur, and W. C. Hahn, "The effect of receiver pressure on the observed flow pattern in the hydrostatic extrusion of bi-metal rods," *Journal of engineering for industry, Transaction of the ASME*, pp. 909-913, 1976.
[28] T. Matsushita, Y. Yamaguchi, M. Noguchi, and M. Nishihara, "Hydrostatic extrusion of round and shaped tubes," *Journal of mechanical working technolody*, vol. 2, pp. 33-51, 1978.
[29] B. Avitzur, R. Wu, S. Talbert, and Y. T. Chou, "Criterion for the prevention of core fracture during extrusion of bimetal rods," *journal of engineering for industry*, vol. 104, pp. 293-304, 1982.
[30] B. Avitzur, R. Wu, S. Talbert, and Y. T. Chou, "Criterion for the prevention of sleeve fracture during extrusion of bimetal rods," *journal of engineering for industry*, vol. 108, pp. 205-212, 1986.
[31] B. Avitzur, J. F. Sculac, and Q. F. Liu, "Modeling of failure during metal forming processes," presented at Physical modelling of metalworking processes:

proceedings of a symposium sponsored by the TMS-AIME shaping and forming committee, Denver, Colorado,, 1987.
[32] A. T. Nagy, "Drawing of a Material Consisting of a Hard Core and a Soft Sleeve," *Journal of Mechanical Working Technology*, vol. 12, pp. 67-77, 1985.
[33] L. A. Pacheco and J. M. Alexander, "On the hydrostatic extrusion of copper-covered aluminum rods," presented at Numerical methods in industry forming process, Swansea, 1982.
[34] W. Zoerner, A. Austen, and B. Avitzur, "Hydrostatic extrusion of hard core clad rod," *Journal of basic engineering*, vol. 94, pp. 78-80, 1972.
[35] W. C. Oliver and W. D. Nix, "Effects of strain hardening in hydrostatic extrusion of axisymmetric bimetal rods," *Metals Technology*, pp. 75-76, 1981.
[36] W. Rasp and O. Paweiski, "The Forming Characteristics of Metallic Compound Materials Subjected to Bar-drawing," *Wire*, vol. 32, pp. 17-20, 1982.
[37] E. G. Smith, R. J. Fiorentino, E. W. Collings, and F. J. Jelinek, "Recent Advances in Hydrostatic Extrusion of Multifilament Nb_3Sn and NbTi Superconductors," *IEEE Transactions on Magnetics*, vol. 15, pp. 91-93, 1979.
[38] S. Alterovitz, J. A. Woollam, and E. W. Collings, "Critical current density in wire drawn and hysrostatically extruded Nb-Ti superconductors," *IEEE transactions of magnetics*, vol. 15, pp. 404-405, 1979.
[39] B. Chen, Q. Jin, G. Li, and F. Cao, "Nb-Ti superconducting materials produced by hydrostatic extrusion," *Rare Materials*, vol. 2, pp. 85-89, 1983.
[40] J. Q. Xu, W. Specking, F. Weiss, and R. Flukiger, "Development of internal-Tin diffusion multifilamentary Nb3Sn conductors including hydrostatic extrusion," *IEEE transactions on magnetics*, vol. 24, pp. 1127-1130, 1988.
[41] H. D. Pugh, "Hydrostatic extrusion," presented at Cu '86--Copper Tomorrow. Technology--Products--Research. Conference Proceedings,, Barga, Lucca, Italy, 10-12 Sept. 1986, 1986.
[42] B. Avitzur, "The production of bi-metal wires," *wire journal*, vol. 3, pp. 42-47, 1970.
[43] H. Tokuno and K. Ikeda, "Analysis of deformation in extrusion of composite rods," *Journal of materials processing technology*, vol. 26, pp. 323-335, 1991.
[44] R. Srinivasan, "Study of the hydrostatic co-extrusion of aluminum and copper," in *Materials science and engineering*: State university of New York at Stony Brook, 1983.
[45] M. Dehghani, "Computer simulation of hydrostatic co-extrusion of bi-metallic compounds," in *Agricultural and mechanical College*: The Louisiana state university, 1987.
[46] B. Avitzur, "Criteria for the Prevention of Filament and Wire Breaking during the Fabrication of Multifilamentary Composite Superconducting Wire," presented at IISSC, Atlanta, GA, 1991.
[47] B. Avitzur, "Prevention of filament breaks during drawing and extrusion of multifilamentary wire," presented at 61th annual convention, Wire association international, Atlanta, Georgia, 1991.

[48] X. Peng, M. D. Sumption, and E. W. Collings, "Finite Element Modeling of Hydrostatic Extrusion for Mono-Core Superconductor Billets," presented at Applied Superconductivity Conference, Houston, TX, USA, 2002.
[49] R. Sliwa, "Simultaneous Plastic Deformation of Composite Materials Containing Aluminum by Extrusion," presented at Fifth International Aluminum Extrusion Technology Seminar, Chicago, USA, 1992.
[50] R. Sliwa, "Plastic deformation of metal composite wire obtained in extrusion and drawing," presented at 49th International Congress on the Technology of Metals and Materials., Sao Paulo, Brazil, Oct. 1994, 1994.
[51] R. Sliwa, "Plastic zones in the extrusion of metal composite," *Journal of materials processing technology*, vol. 67, pp. 29-35, 1997.
[52] P. Montmitonnet, "Interface Adherence after Cold Backward-extrusion of a Bi-layered Plain Bearing," *Journal of Mechanical Working Technology*, vol. 11, pp. 23-36, 1985.
[53] N. Bay, "Mechanisms producing metallic bonds in cold welding," *Welding Journal*, vol. 62, pp. 137s-142s, 1983.
[54] N. Bay, "Cold welding, I. Characteristics, Bonding Mechanisms, Bond Strength," *Metal Construction*, vol. 18, pp. 369-372, 1986.
[55] L. F. Ciupik, "Mechanism of cold deformation bonding of metals during their simultaneous plastic flow," presented at Advanced technology of plasticity, Tokyo, Japan, 1984.
[56] C. S. Hartley, M. Dehghani, N. Lyer, A. T. Male, and W. R. Lovic, "Defects at Interface in Co-extruded Metals," presented at Computational Methods for Predicting Material Processing Defects, Amsterdam, Netherlands, 1987.
[57] N. Bay, "Cold Pressure Welding--a Theoretical Model for the Bond Strength," presented at The Joining of Metals: Practice and Performance., Coventry, UK, 1981.
[58] Babock, "Cold pressure welding," *wire industry*, vol. 53, pp. 822-823, 1986.
[59] N. Bay, "Cold Pressure Welding: Basic Parameters and Applications," presented at JOM-1 (Joining of Metals),, Helsingor, Denmark, 9-12 Aug., 1981.
[60] Anon, "Composite products manufactured through hot hydrostatic extrusion process," *Kobelco technology review*, vol. 1, pp. 47-48, 1987.
[61] N. Bay, C. Clemensen, and O. Juelstorp, "Bond strength in cold roll bonding," *Annals of the CIRP*, vol. 34, pp. 221-224, 1985.
[62] S. Mepsted, "Cold pressure welding," *Wire industry*, vol. 67, pp. 423-424, 2000.
[63] W. Wei and Q. N. Shi, "Bonding mechanism of Cu/Steel clad sheet in asynnetric rolling of bimetal," *Chinese journal of rare metals*, vol. 25, pp. 307-311, 2001.
[64] R. J. Schwensfeir, G. Trenkler, R. Delagi, and J. Forster, "Comparison of Bond in Roll-Bonded and Adhesively Bonded Aluminums," presented at Joining Technologies for the 1990s: Welding, Brazing, Soldering, Mechanical, Explosive, Solid-State, Adhesive, Hampton,, Virginia, USA, Oct. 1984, 1984.
[65] J. A. Cave and J. D. Williams, "Interface adherence after cold backward-extrusion of bi-layered plain bearing," *Journal of institute of metals*, vol. 101, pp. 203-207, 1973.

[66] I. Gutierrez, J. J. Urcola, J. M. Bilbao, and L. M. Villar, "Bonding by Hot Extrusion of Incoloy 825 and Duplex 2205 to Low Alloy Steel," *Materials Science and Technology*, vol. 7, pp. 761-769, 1991.
[67] B. Lopez, X. Gomez, J. Echeberria, I. Gutierrez, and J. J. Urcola, "Interface Analysis on Diffusion Bonded Bimetallic Composites," *Key engineering materials*, vol. 127-131, pp. 695-702, 1997.
[68] P. Mallesham and A. Dutta, "Diffusion welding-state of art," presented at Proceedings of the international conference on the joining of materials, Helsingr, Denmark, 1995.
[69] K. Nakasuji, K. Masuda, and C. Hayashi, "Development of manufacturing process of clad bar by rotary rolling," *ISIJ international*, vol. 37, pp. 899-905, 1997.
[70] P. Loewenstein and W. B. Tuffin, "Metallurgical Bonding of Dissimilar Metals by Co-extrusion," *Metals Engineering Quarterly*, vol. 4, pp. 26-31, 1964.
[71] R. L. O'Brien, "Welding Handbook," vol. 2: American Welding Society, 1991.
[72] E. R. Wallach, "Solid-state joining: techniques and applications," ***The Metallurgist and materials technologist***, vol. 16, pp. 71-76, 1984.
[73] W. B. Zhang, **N**, "Comparison between conventional and cross shear roll bonding of aluminium to mild steel," *Int. J. Joining Mater.*, vol. 6,, pp. 157-162,, 1994.
[74] X. K. Peng, G. Heness, and W. Y. Yeung, " Effect of Rolling Temperature on Interface and Bond Strength Development of Roll Bonded Copper/aluminium Laminates," *Journal of Materials Science*, vol. 34, pp. 277-281, 1999.
[75] J. A. Forster, S. Jha, and A. Amatruda, "The processing and evaluation of clad metals," *JOM*, vol. 45, pp. 35-38, 1993.
[76] X. Ji, Y. Dai, B. Zheng, L. Ye, and y. Mai, " Interface End Theory and Re-evaluation in Interfacial Strength Test Method," *Composite Interfaces*, vol. 10, pp. 567-580, 2003.
[77] B. Duncan and L. Crocker, "Review of Tests for Adhesion Strength," Teddington, Middlesex, UK, 2001.
[78] Y. Takahashi and K. Nishiguchi, "Determination of Optimum Process Conditions in Solid Phase Bonding by a Numerical Model," *Welding in the World*, vol. 27, pp. 100-113, 1989.
[79] Z. X. GUO and N. RIDLEY, " Modelling of Diffusion Bonding of Metals," *Materials Science and Technology*, vol. 3, pp. 945-953, 1987.
[80] Y. Takahashi, T. Koguchi, and K. Nishiguchi, "Modeling of Viscoplastic Adhering Process by A Finite Element Technique," *Journal of Engineering Materials and Technology*, vol. 115, pp. 151-155, 1993.
[81] C. S. Lee, H. Li, and R. S. Chandel, "Stimulation Model for the Vacuum-free Diffusion Bonding of Aluminium Metal-matrix Composite," *Journal of Materials Processing Technology*, vol. 89-90, pp. 344-349, 1999.
[82] A. Sluzakec and A. Sluzakec, " Solution of Thermal Problems in Friction Welding," *International Journal of Heat and Mass Transfer*, vol. 36, pp. 1583-1587, 1993.

[83] A. Francis and R. E. Craine, "On a Model for Frictioning Stage in Friction Welding of Thin Tubes," *International Journal of Heat and Mass Transfer*, vol. 28, pp. 1747-1755, 1985.
[84] A. Sluzalec, " Thermal Effects in Friction Welding," *International Journal of Mechanical Sciences*, vol. 32, pp. v, 1990.
[85] T. Kallgren, L. Z. Jin, and R. Sandstrdm, "Finite Element Modeling of Temperature Distribution in Friction Stir Weldin Porcess and its Influence on Distortion of Copper Canisters," presented at Scientific Basis for Nuclear Waste Management, Francisco, CA, USA,, 2004.
[86] A. Moal and E. Massoni, "Finite Element Simulation of the Inertia Welding of Two Similar Parts," *Engineering Computations*, vol. 12, pp. 497-512, 1995.
[87] A. Oberg, J. H. Schweitz, and H. Olofsson, "Computer Modeling of the Explosive Welding Process ." presented at 8th International Conference on High Energy Rate Fabrication, San Antonio, TE, 1984.
[88] V. M. Kornev and I. V. Yakovlev, "The Model of Wave Formation under Explosive Welding," presented at International Conference on Metallurgical Applications of Shock-wave and High-strain-rate Phenomena, Porland, OR, 1985.
[89] S. Q. Yang, Q. G. Dong, X. B. Tian, X. F. Wang, and Q. Wei, "Calculation and Measurement of Temperature Field in Joint of Ultrasonic Welding Polythene," *Transactions of the China Welding Institution*, vol. 16, pp. 172-178, 1995.
[90] C. Doumanidis and Y. Gao, "Mechanical Modeling of Ultrasonic Welding," *Welding Journal*, vol. 83, pp. 140S-146S, 2004.
[91] N. Bay, H. Bjerregaard, S. B. Petersen, and C. Santos, "Cross Shear Roll Bonding," *Journal of Materials Processing Technology*, vol. 45, pp. 1-6, 1994.
[92] K. J. B. Mcewan and D. R. Milner, "Pressure Welding of Dissimilar Metals," *British Welding*, vol. 9, pp. 406-420, 1962.